LUND UNIVERSITY

DYNAMIC DESIGN OF BRIDGES ON HIGH-SPEED RAILWAY LINES

Parametric Studies of Slab Bridges and Portal Frame Bridges

FELICIA NILSSON & FILIPPA DAHL

Structural Mechanics

Master's Dissertation

DEPARTMENT OF CONSTRUCTION SCIENCES

DIVISION OF STRUCTURAL MECHANICS

ISRN LUTVDG/TVSM--19/5236--SE (1-142) | ISSN 0281-6679

MASTER'S DISSERTATION

DYNAMIC DESIGN OF BRIDGES ON HIGH-SPEED RAILWAY LINES

Parametric Studies of Slab Bridges and Portal Frame Bridges

FELICIA NILSSON & FILIPPA DAHL

Supervisors: Professor **PER-ERIK AUSTRELL**, Division of Structural Mechanics, LTH
together with **KARL LUNDSTEDT**, MSc, and **JAN OLSSON**, MSc, Skanska Sverige AB.

Examiner: Professor **KENT PERSSON**, Division of Structural Mechanics, LTH.

Printed by V-husets tryckeri LTH, Lund, Sweden, July 2019 *(Pl)*.

For information, address:
Division of Structural Mechanics,
Faculty of Engineering LTH, Lund University, Box 118, SE-221 00 Lund, Sweden.
Homepage: www.byggmek.lth.se

Preface

As we are seeing the magnolia blossom for the fifth time in Lund, the time has come to conclude our five years as civil engineering students by writing this master dissertation. The work was initiated by Karl Lundstedt at Skanska Teknik, and was carried out in cooperation with the Division of Structural mechanics at LTH. We would like to thank our supervisors at the department of Bridge design at Skanska Teknik in Malmö: Karl Lundstedt and Jan Olsson. Thank you for all your help and support during the course of the work, for sharing your great industry expertise, and for providing us with necessary tools to complete the task. A depth of gratitude is also owed to our supervisor at LTH, Prof. Per Erik Austrell, for helping us sort out theoretical difficulties and for keeping our work on track. A special thanks is also addressed to Felicia's dear Canadian friend, Bardia Amir Poursaeid, for proofreading the entire thesis.

To our friends and family, thank you for being our cheerleaders through thick and thin. This accomplishment would never have been possible without you.

Lund, June 2019

Felicia Nilsson & Filippa Dahl

Abstract

In recent years, high-speed railway has been on the upswing in the public debate, as Swedish authorities have affirmed the plans of a high-speed corridor connecting Stockholm, Gothenburg and Malmö. The track speed limit is not fully determined, but will be in the range of 250-320 km/h. At these higher speed levels, it is harder to ensure traffic safety and passenger comfort, and dynamic analyses of the included bridges are required. Substantial research has already been published on the subject of high-speed railway dynamics; yet, there are still areas that need further investigation to understand the behaviour of bridges that undergo this type of loading.

In this thesis, parametric studies were performed on a three-spanned slab bridge and on a portal frame bridge. The main objective was to investigate how the response of the bridges changed when the train speed, the span length and the cross-section height were varied. The analyses were executed in BRIGADE/Plus and the response was primarily evaluated in terms of vertical accelerations of the bridge deck. However, verifications of vertical deflection, torsion, rotation at bearings, and section forces, were also covered in the study. Previous research has shown that the representation of the boundary between the foundation and the surrounding soil is a critical part of the modelling. In the major part of this study, the conventional method using fixed boundary condition was adopted in all DOFs except for those representing the rotation around the in-plane axes, where linear elastic rotational springs were inserted. A slightly more realistic approach with an increased Young's modulus of the soil and an additional spring in the vertical DOF, was also evaluated. In addition, a minor literature study of more comprehensive works on the topic of Soil-Structure Interaction (SSI), was conducted.

The results suggest that none of the bridges in the study meet the dynamic design requirements for a track speed interval of 250-350 km/h. Furthermore, an increase in cross-sectional height seems to be an efficient way of reducing the maximum accelerations, whereas an enlargement of the span length may drastically increase the response. A 10 % increase in span length can increase the acceleration by a factor 2 for the slab bridge, and by a factor 3 for the portal frame bridge. It has also been shown that using fixed boundary conditions at the soil-structure interface can yield non-conservative results. For the frame bridges of different span lengths, the accelerations were significantly larger for the case with vertical springs; however, no such trend was able to be identified for the slab bridges. In contrast to the existing body of research, the acceleration was not the decisive parameter in all aspects of this study. The section forces, and particularly the choice of dynamic enhancement factor, were critical for the shorter bridges in the track speed interval 125-250 km/h.

Keywords: High-speed railway bridges, bridge-train resonance, structural dynamics, modal dynamics, time stepping, soil-structure interaction, finite element method, BRIGADE/Plus

Sammanfattning

Sedan myndigheterna fastställt planerna på en höghastighetskorridor som ska knyta samman Stockholm, Göteborg och Malmö, har intresset för höghastighetståg ökat hos såväl allmänhet som forskare. Hastighetsbegränsningen på banan är ännu inte satt, men den kommer vara inom intervallet 250-320 km/h. Eftersom det är svårare att garantera trafiksäkerhet och passagerarkomfort vid dessa högre hastigheter, krävs dynamiska analyser av de ingående broarna. Även om det redan har genomförts avsevärd forskning på ämnet dynamik på järnvägsbroar för höghastighetståg, finns det flera områden som behöver utredas vidare för att förstå broarnas beteende.

I det här examensarbetet utfördes parameterstudier på en plattbro som spänner över tre fack och en plattrambro. Huvudsyftet var att utreda hur broarnas respons förändras när tåghastigheten, spännvidden och tvärsnittshöjden varieras. Analyserna genomfördes i BRIGADE/Plus och responsen utvärderades primärt i form av brodäckets vertikala acceleration. Verifiering av vertikal deformation, vridning, rotation kring lagerpunkter och snittkrafter inkluderades också i studien. Tidigare forskning har visat att modelleringen av gränsen mellan brofundamentet och omkringliggande jord är en kritisk del i dimensioneringsprocessen. I den större delen av arbetet användes den konventionella metoden med fixa upplagsvillkor i alla frihetsgrader förutom de som motsvarar rotation kring axlarna i planet, där linjärelastiska fjädrar applicerades. Ett något mer realistiskt angreppssätt med en ökad elasticitetsmodul för jorden och en ytterligare fjäder i den vertikala frihetsgraden utvärderades också. Dessutom utfördes en mindre litteraturstudie av mer omfattande arbeten om Jord-Struktur Interaktion (SSI).

Resultaten tyder på att ingen av broarna i studien uppfyller dimensioneringskraven för ett banhastighetsintervall på 250-350 km/h. Vidare verkar en ökning av tvärsnittshöjden vara ett effektivt sätt att minska den maximala accelerationen, medan en förstoring av spännvidden drastiskt kan öka responsen. Accelerationen kan öka med en faktor 2 för plattbron och en faktor 3 för rambron, när spännvidden ökas med 10 %. Arbetet har också visat att användandet av fixa upplagsvillkor vid gränsen mellan jord och bro kan ge icke-konservativa resultat. För plattrambroar med olika spännvidder var accelerationerna avsevärt större för fallet med vertikala fjädrar. Dock kunde någon sådan trend inte identifieras för plattbroarna. I motsats till befintlig forskning var accelerationen inte den storhet som styrde alla aspekter av den dynamiska dimensioneringen. Snittkrafterna, och i synnerhet valet av dynamisk förstoringsfaktor, var kritiska för de kortare broarna i banhastighetsintervallet 125-250 km/h.

Sökord: höghastighetståg, järnvägsbro, bro-tåg resonans, strukturdynamik, modal dynamik, tidsstegning, jord-struktur interaktion, finita elementmetoden, BRIGADE/Plus

Abbreviations

Abbrevation	Description
FEM	The Finite Element Method
FFT	Fast Fourier Transform
HSLM	High Speed Load Model
MDOF	Multi-degree-of-freedom
SDOF	Single-degree-of-freedom
SSI	Soil-structure interaction

Table of contents

1 Introduction

When a bridge is subjected to highly dynamic actions, such as the passage of high-speed trains, the acceleration of the bridge deck is often the governing parameter in the design [1]. Therefore, by gaining knowledge about when these accelerations are kept below certain threshold values, the efficiency of bridge designs could be assessed already in the initial phase of a project. This was done through performing dynamic analyses on two different types of concrete bridges that are commonly used on the Swedish railway network: a three-spanned slab bridge and a portal frame bridge. For each bridge type, three parameters that were assumed to be decisive for the dynamic response were varied: train speed, span length and cross-section height. Of course there are several other requirements to consider in a dynamic design, in excess of the accelerations. In accordance with [2], the dynamic effects were also evaluated in terms of displacements, torsion, rotation at bearings and section forces. However, in this thesis, these requirements were not the main focus.

Further, to avoid designing bridges with unnecessary large dimensions, it is important that the conventional methods used in modeling, to a reasonable degree of accuracy represent the true behavior of the bridge structure. One aspect that has recently been up for debate is the modeling of the boundary between the foundation and the surrounding soil, referred to as *Soil-Structure Interaction* (SSI). Today's industry practice involves using fixed boundary conditions, which according to recent research may be a non-conservative assumption. This subject was primarily covered as a short literature study, accompanied by very simple attempts of better resembling the interface between foundation and soil.

The dynamic analyses were executed using the computer software BRIGADE/Plus. In the following sections, general background information on the topic, along with the aim and the limitations of the thesis work, are presented.

1.1 Background

By definition, high-speed railway is a railway designed for a track speed of at least 250 km/h (or 200 km/h for upgrade of existing rails). In Sweden, high-speed railway have been a subject of public debate ever since the 1990's. The advocators allege that this upgrade is crucial to truly challenge the aircraft industry and to decrease the strain on the current rail system. In contrast, the adversaries argue that Sweden is too sparsely populated, and thus, only a small amount of the population would benefit from such an investment. In addition, considering that Sweden's high-speed railway infrastructure is decades behind other parts of Europe, this means of transport might be outdated before it is even in place.

According to the current plans, the intended high-speed railway network will stretch from Stockholm to Gothenburg, and from Stockholm to Malmö. The first construction phase is the so-called East Link between Järna and Linköping. This lane and the other parts of the corridor is visualized in Figure 1.1. The East Link, scheduled to be opened to service in 2033, will constitute of 160 km double-tracked railway and include 200 bridges. Originally, the track speed limit was set to 320 km/h; however, due to a lack of funding, it will most likely be reduced to 250 km/h [3]. The shortage in financial assets implies that the final choice of speed not only is uncertain on the East Link, but also along the remaining parts of the corridor. For that reason, the dynamic response in this thesis was both evaluated for track speeds up to 250 and 350 km/h, respectively.

Figure 1.1: Planned stretch of the high-speed railway corridor in Sweden highlighted in yellow [4]. Järna is located at the north end of the yellow line.

Over the last few years, there has been an increased interest in this field among researchers, as authorities have expressed their ambitions of having a high-speed railway corridor in Sweden in the near future. To the authors knowledge, the existing body of research primarily focuses on track speeds below 300 km/h; however, there are relatively few studies that deal with higher speeds. At several locations in Europe, high-speed trains already operate at the speed of 350 km/h, and therefore it is not unlikely that this eventually will be a reality in Sweden as well. At higher speeds, the accelerations of the bridge become larger. This ultimately requires a more elaborate dynamic analysis, since the risk of reaching the resonance frequencies increases.

1.2 Objective

The purpose of this Master's thesis is to study the effect of different parameters on the dynamic response of bridges, when subjected to high-speed train loading. By doing so, the critical parameter(s), and the aspects of the design process that must be given extra attention and thought, may be identified. As a result, the work can yield a first indication of which design alternative constitutes the most efficient option to withstand the dynamic loading.

The main aim is to answer the questions found in the list that follows.

- How, and to what extent, do the geometrical parameters varied in this study (span length and cross-section height) affect the dynamic response of bridges?
- Which design criterion governs the dynamic design? (acceleration, deflection, torsion, rotation at bearings or section forces)
- How does the dynamic response change when the track speed is increased?
- For which speeds do the railway bridges covered in this study meet the design requirements regarding dynamics?
- Does the conventional method used to model the boundary between the foundation and the surrounding soil yield moderately conservative results?

1.3 Limitations

The limitations of this study are provided below.

- Only load effects origin from the railway traffic are considered; in other words, a complete design is not performed. The considered loads are the dead weight of the bridge and the components that cause an inertia load on the bridge deck (e.g. ballast). The loads that fall outside of the framework include temperature loads, earth pressure, and acceleration/breaking forces.
- Non-linearities emerging from earth pressure or low temperatures affecting the bridge's stiffness are assumed to be neglectable, i.e. linear statics and linear dynamics are used.
- Interaction between the train and the rails is disregarded. This is a conservative assumption since the interaction tends to decrease the maximum response at resonance [5].
- The trains' impact on the bridges' eigenfrequencies is not considered. However, since the mass of the train is small compared to the mass of the bridge structure, this effect is assumed to be negligible.
- The material damping of the concrete affects the dynamic response of the bridge; however, the sensitivity of this parameter is not investigated in this study.
- Co-oscillating soil masses overlaying the substructure of the bridge are disregarded.
- Fatigue is not regarded.

2 Governing Theory

In this chapter, relevant theory and design requirements regarding dynamic analyses are described.

2.1 The Finite Element Method

The Finite Element Method (FEM) is a numerical method for solving partial differential equations that cannot be solved analytically, and can be used for problems in one, two and three dimensions. The FEM is used in various applications, ranging from heat- and groundwater flow to torsion of bars and elastic analyses of plates. The main principle of the FEM is that the structure is divided into smaller parts: *finite elements*. An approximation of how the variable of interest varies within each element is formed, referred to as *shape functions*. The elements are then assembled into a global element mesh; thus, the variable's variance over the whole structure is obtained. By reducing the size of each element, the approximate FE-solution should converge to the exact solution. More profound information about FEM can be found in [6]; however, a brief summary of some key aspects according to this source is provided below.

Although the methodology of compiling the FE-formulation of a one-, two- or three-dimensional problem in general terms is similar, the information below is primarily targeted to the elements used to model the bridges in this study: three-dimensional plane stress-and-plate elements. Initially, an equilibrium equation for an infinite part of the body is formed (Figure 2.1). This expression differs depending on whether the loading is static or dynamic. All loads are dynamic by nature; however, if the action is applied with a very low speed, the analysis can be considered as static. In other words, the inertia effects described by Newton's second law, can be neglected. Since dynamic analyses are the central theme of this paper, the dynamic formulation is used

$$\tilde{\boldsymbol{\nabla}}^{\boldsymbol{T}}\boldsymbol{\sigma} + \boldsymbol{b} = \rho\ddot{\mathbf{u}} \tag{2.1}$$

where $\tilde{\boldsymbol{\nabla}}^{\boldsymbol{T}}\boldsymbol{\sigma}$ describes the stress state in all directions caused by external loading, $\boldsymbol{b}$ is the gravity load and $\rho\ddot{\mathbf{u}}$ is the inertial force per unit volume (zero for the static case).

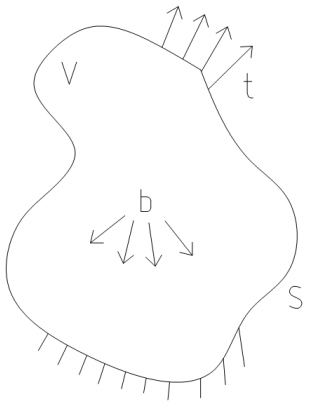

Figure 2.1: Free body diagram for an infinite part of a three-dimensional body, where b is a body force and t is an external force acting on the surface S of the body.

Due to the difficulty in approximating the variation of derivatives, it is considered advantageous that the sought variable is of the lowest possible order. For that reason, the equilibrium equation is integrated over the region. In addition, Equation 2.1 is multiplied by an arbitrary weight function in order to minimize the residual. There are multiple ways of choosing the weight function, with a common one being the Galerkin method. This method is a so-called weighted residual method, meaning that the average residual should be zero and that the weights are chosen accordingly.

$$\int_V \boldsymbol{v}^{\boldsymbol{T}} \tilde{\boldsymbol{\nabla}}^{\boldsymbol{T}} \boldsymbol{\sigma} \; dV + \int_V \boldsymbol{v}^{\boldsymbol{T}} \boldsymbol{b} \; dV = \int_V \boldsymbol{v}^{\boldsymbol{T}} \rho \ddot{\mathbf{u}} \; dV \tag{2.2}$$

To reach the FE-formulation presented in Equation 2.4, an approximation of the variation of the variable itself also has to be introduced. This approximation consists of nodal values of each element (which can either be known or unknown), multiplied by the shape functions, that describes the variation of the variable within the elements. Furthermore, a constitutive relation, known as the generalized Hooke's law, is used to express the stresses in terms of displacements and stiffnesses

$$\boldsymbol{\sigma} = \boldsymbol{D} \cdot \boldsymbol{\varepsilon} \; ; \; \boldsymbol{\varepsilon} = \tilde{\boldsymbol{\nabla}}^{\boldsymbol{T}} \boldsymbol{u} \; . \tag{2.3}$$

The FE-formulation of an undamped three-dimensional body exhibiting linear dynamics is

$$\mathbf{M\ddot{u}} + \mathbf{Ku} = \mathbf{f} \tag{2.4}$$

where

$$\mathbf{M} = \int_V \mathbf{N^T} \rho \mathbf{N} dV$$

is the mass matrix,

$$\mathbf{K} = \int_V \mathbf{B^T D B} dV$$

is the stiffness of the body, and

$$\mathbf{f} = \int_{Sh} \mathbf{N^T h} dS + \int_{Sg} \mathbf{N^T t} dS + \int_V \mathbf{N^T b} dV$$

is the applied surface force, the reaction forces and the body forces, respectively.

In the expression for $\mathbf{K}$, the variable $\mathbf{B}$ represents the derivative of the shape functions, which are denoted by $\mathbf{N}$. The force vector $\mathbf{f}$ includes both a known surface force, $\mathbf{h}$, on the part of the surface (S_h) where the boundary conditions are unknown, and an unknown surface force, $\mathbf{t}$, on a part of the surface (S_g) where the boundary conditions are known.

2.2 Shell Theory

In this thesis, the bridges are modelled using shell elements. Since the bridges covered in the study have widths that are relatively large compared to their lengths, the use of beam elements is not appropriate. A shell element, illustrated in Figure 2.2, is a combination of a plate element and a plane stress element.

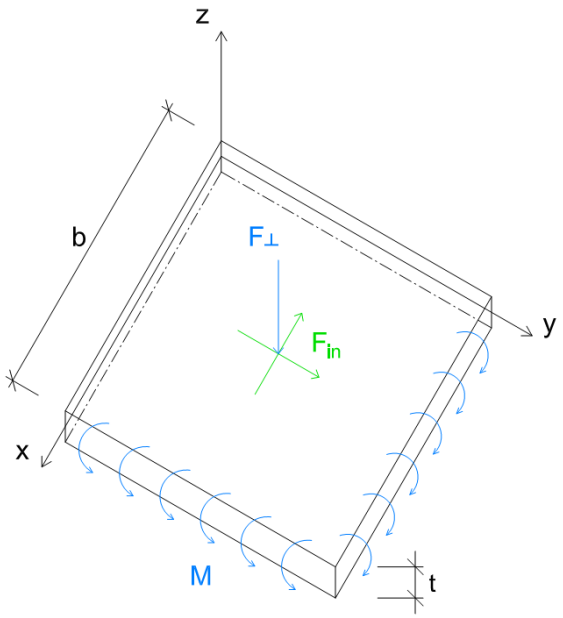

Figure 2.2: A principle drawing of a shell element, where the forces and moments highlighted in blue origins from plate actions and the forces highlighted in green origins from membrane actions.

A plate is a three-dimensional element, analogous to a beam, where the applied actions are mainly withstood by bending moments and shear forces. It is a structure where the in-plane dimensions are much greater than the out-of-plane dimension. In addition, a plate is only loaded by forces normal to its plane and moments around the in-plane axes (Figure 2.2). The Kirchhoff's plate theory is utilized in BRIGADE/Plus. This theory can be described as the equivalent to the Bernoulli-Euler beam theory, where plane sections remain plane and perpendicular to the beam axis under loading. In contrast to the loading of a plate element, plane stress elements are loaded by axial forces in the in-plane directions; thus, these elements can simplified be said to resemble a "three-dimensional" bar. The analogy of plane stress elements and bars, and plates and beams, respectively, is visualized in Figure 2.3.

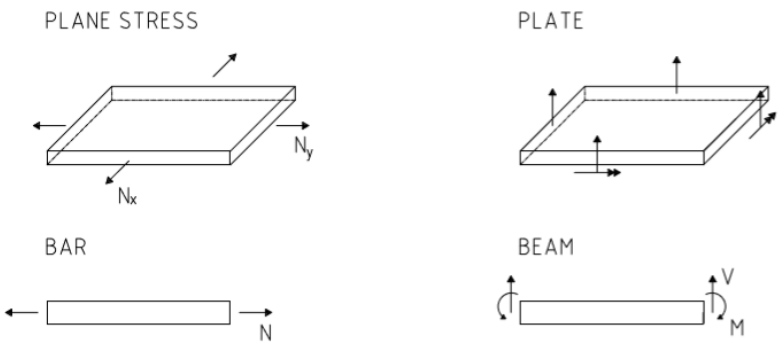

Figure 2.3: Loading of plane stress elements, plate elements, bars and beams.

For both the plate element and the plane stress element, plane stress is applicable. This means that the stresses with a component in the out-of-plane direction are assumed to be negligible, an assumption which is normally appropriate for thin bodies subjected to in-plane loading. Although the forces acting on the plane are directed perpendicular to the in-plane coordinates, the stress in the loading direction is insignificant compared to the bending stresses. By utilizing the concept of plane stress, the original three-dimensional problem of plate elements and plane stress elements is reduced to two dimensions.

Provided that the shell's stiffness is independent of the out-of-plane coordinate, the FE-formulation of the plate element and the plane stress element can be computed separately [6]. By combining the two uncoupled equations, the FE-formulation of the shell element can be obtained.

2.3 Structural Dynamics

By definition, structural dynamics is the study of the behaviour of structures that undergoes dynamic loading. In the following sections, the essential theory on the topic of structural dynamics is covered.

2.3.1 Equation of motion

The foundation of all structural dynamics is the *equation of motion*, which describes the mass' response to loading as a function of time. The simplest form of a dynamic system is a *single-degree-of-freedom* (SDOF) system, in which the motion is only evaluated in one direction. An example of a SDOF system is visualized in Figure 2.4: a body with a mass m, a stiffness k, and a damping coefficient c, subjected to a transient load $p(t)$. By drawing a free body diagram and utilizing Newton's second law, a force equilibrium along the x-axis can be formed

$$p(t) - f_s - f_d = m\ddot{u} \tag{2.5}$$

where the spring force $f_s = ku$ (lateral stiffness times displacement), the damping force $f_d = c\dot{u}$ (damping coefficient times velocity) and $\ddot{u}$ is the acceleration.

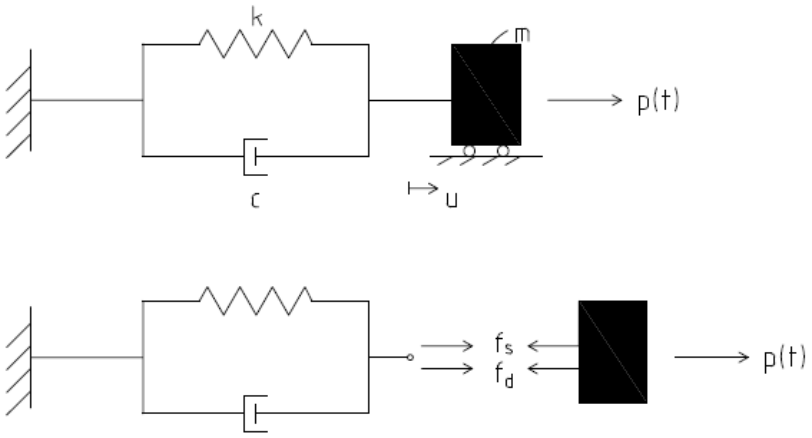

Figure 2.4: A representation of a SDOF system with damping.

A rearrangement of the terms in Equation 2.5, yields the equation of motion for a SDOF system

$$m\ddot{u} + c\dot{u} + ku = p(t)\ . \tag{2.6}$$

The corresponding equation for a *multi-degree-of-freedom* (MDOF) system is

$$\mathbf{M\ddot{u}} + \mathbf{C\dot{u}} + \mathbf{Ku} = \mathbf{f} \tag{2.7}$$

where the included variables now are vectors and matrices instead of scalars. This is the FE-formulation of a damped system (compare with the undamped formulation presented in Equation 2.4).

2.3.2 Eigenfrequencies and eigenmodes

By disturbing a system from its equilibrium state, e.g. by applying a load, a vibrating motion is induced. This motion is highly amplified if the frequency of the applied load coincides with the so-called *eigenfrequency* or the *natural circular frequency* of the system, a phenomenon referred to as resonance. When the system is at resonance, it has a particular mode shape that is often described as an *eigenmode*. The number of eigenmodes (and eigenfrequencies) of a system is the same as the number of DOFs; however, the eigenmodes associated with the lowest frequencies excite at a lower energy level, and is therefore more likely to occur. The values of the eigenfrequencies are unique for every system, and are dependent on the material properties: that are, mass and stiffness.

The expression for the natural circular frequency can be derived from the equation of motion by prescribing the force to zero (i.e. the system is in free vibration). Depending on whether damping is present or not, the expression differs slightly. The concept of damping is more elaborately described in Section 2.3.5.

Equation 2.8 shows the equation of motion for an undamped MDOF system that undergoes free vibration.

$$\mathbf{M\ddot{u} + Ku = 0} \tag{2.8}$$

In order to determine the natural circular frequency, a trial solution for the unknown variables $\mathbf{u}$ and $\ddot{\mathbf{u}}$ has to be chosen. Proven by Fourier, all wave motions can be expressed as a sum of sine and cosine functions; therefore, an appropriate choice of trial function is either a sine, cosine, or a sum of the two. For simplicity, a basic sine function is used in this derivation:

$$\mathbf{u_i(t)} = A_i sin(\omega_i t)\mathbf{\Phi_i} \tag{2.9}$$

$$\mathbf{\ddot{u}_i(t)} = -A_i \omega_i^2 sin(\omega_i t)\mathbf{\Phi_i} \tag{2.10}$$

where A is the amplitude, t is the time, ω is the angular frequency and $\mathbf{\Phi}$ is a vector describing the mode shape. To illustrate the concept of $\mathbf{\Phi}$, a two-storey frame building with two degrees of freedom is used (Figure 2.5).

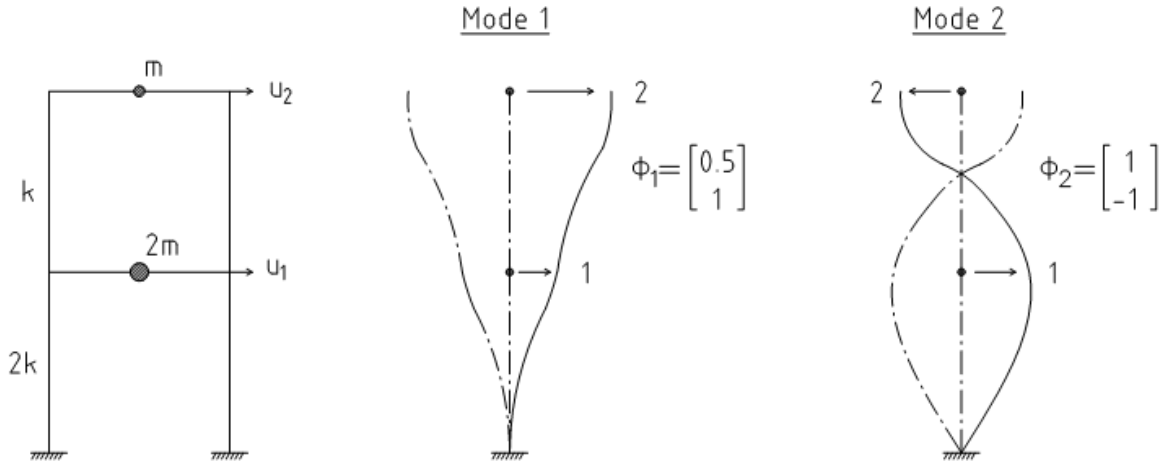

Figure 2.5: Mode shapes and mode vectors $\mathbf{\Phi_i}$ of a two-degree-of-freedom system.

By inserting Equation 2.9 and 2.10 into Equation 2.8, the equation of motion becomes

$$(\mathbf{K} - \boldsymbol{\omega}^2\mathbf{M})\mathbf{\Phi} \cdot \mathbf{A}sin\boldsymbol{\omega}t = \mathbf{0}$$

with

$$\boldsymbol{\omega} = \begin{bmatrix} \omega_1 \\ \omega_2 \\ \cdot \\ \cdot \\ \cdot \\ \omega_n \end{bmatrix} ; \ \mathbf{\Phi} = \begin{bmatrix} \begin{bmatrix} \\ \Phi_1 \\ \\ \end{bmatrix} & \begin{bmatrix} \\ \Phi_2 \\ \\ \end{bmatrix} & \cdots & \begin{bmatrix} \\ \Phi_n \\ \\ \end{bmatrix} \end{bmatrix} ; \ \mathbf{A} = \begin{bmatrix} A_1 \\ A_2 \\ \cdot \\ \cdot \\ \cdot \\ A_n \end{bmatrix} .$$

Since the displacement at resonance is non-zero, the $\mathbf{A}sin\omega t$-term cancels out:

$$(\mathbf{K} - \boldsymbol{\omega}^2\mathbf{M})\mathbf{\Phi} = \mathbf{0} \ . \tag{2.11}$$

This is an eigenvalue problem where the eigenvalues (i.e. the natural circular frequencies), are found from the determinant of $(\mathbf{K} - \boldsymbol{\omega}^2\mathbf{M})$, and will be in the form of

$$\omega_i = constant_i \cdot \sqrt{\frac{k}{m}} \tag{2.12}$$

where k is the stiffness and m is the mass of the system.

With the natural circular frequencies ω_1- ω_n known, the corresponding eigenvectors or

mode shapes can readily be obtained from Equation 2.11.

The equivalent formula for a damped system is presented in Equation 2.13, where ζ is the damping ratio, defined in Section 2.3.5. As can be seen, the value of the natural frequency diminishes slightly when damping is included.

$$\omega_{Di} = \omega_i \sqrt{1 - \zeta_i^2} \tag{2.13}$$

2.3.3 Modal dynamics

Performing dynamic analyses can be a very time-consuming task; however, by employing information about eigenfrequencies and eigenmodes, the analysis time can be drastically reduced. In this thesis, modal truncation is used. This is a reduction method where the modes that are not excited, i.e. do not contribute to the response, are ignored. In order to easily understand the theory of modal reduction, it is convenient to express the total response as the sum of the responses associated with each eigenmode, a concept referred to as modal expansion:

$$\mathbf{u}(t) = q_1(t)\Phi_1 + q_2(t)\Phi_2 + ... + q_N(t)\Phi_N = \sum_{i=1}^{N} q_i(t)\mathbf{\Phi}_i = \mathbf{q}_N(t)\mathbf{\Phi}_N \tag{2.14}$$

where $q_i = A_i cos\omega t + B_i sin\omega t$ for the undamped case.

Inserting Equation 2.14 in the equation of motion (Equation 2.7) and multiplying each term by the transpose of the mode vectors, yields

$$\mathbf{\Phi}_N^T \mathbf{M} \mathbf{\Phi}_N \ddot{\mathbf{q}}_N + \mathbf{\Phi}_N^T \mathbf{C} \mathbf{\Phi} \dot{\mathbf{q}}_N + \mathbf{\Phi}_N^T \mathbf{K} \mathbf{\Phi} \mathbf{q}_N = \mathbf{\Phi}_N^T \mathbf{P} \tag{2.15}$$

where the mass and the stiffness matrices are diagonalized. For the case with classical damping, the damping matrix is also diagonalized by $\mathbf{\Phi_N^T}$. The dimensions of each term in Equation 2.15 are

$$\mathbf{\Phi}_N^T \mathbf{M} \mathbf{\Phi}_N, \mathbf{\Phi}_N^T \mathbf{C} \mathbf{\Phi}_N \text{ and } \mathbf{\Phi}_N^T \mathbf{K} \mathbf{\Phi}_N \ : [N \times N] \tag{2.16}$$

$$\mathbf{q}_N \text{ and } \mathbf{\Phi}_N^T \mathbf{P} : [N \times 1] \tag{2.17}$$

In general, the number of DOFs of a system is several thousands, which means that the $N \times N$ matrices becomes immense and computationally costly to solve. However, as mentioned in the beginning of this section, the size of the equation system can be reduced if modal truncation is used. The basis of modal truncation is that an eigenvalue analysis is executed, from which the eigenmodes 1 to J that have an impact on the response, are extracted. As a rule of thumb, J is significantly smaller than the total number of eigenmodes, N. The corresponding expression of the equation of motion for the J lowest eigenmodes is

$$\mathbf{\Phi}_J^T \mathbf{M} \mathbf{\Phi}_J \ddot{\mathbf{q}}_J + \mathbf{\Phi}_J^T \mathbf{C} \mathbf{\Phi} \dot{\mathbf{q}}_J + \mathbf{\Phi}_J^T \mathbf{K} \mathbf{\Phi} \mathbf{q}_J = \mathbf{\Phi}_J^T \mathbf{P} \tag{2.18}$$

with

$$\mathbf{\Phi}_J^T \mathbf{M} \mathbf{\Phi}_J, \mathbf{\Phi}_J^T \mathbf{C} \mathbf{\Phi}_J \text{ and } \mathbf{\Phi}_J^T \mathbf{K} \mathbf{\Phi}_J \ : [J \times J] \tag{2.19}$$

$$\mathbf{q}_N \text{ and } \mathbf{\Phi}_N^T \mathbf{P} : [J \times 1] \tag{2.20}$$

In this work, Equation 2.18 is solved iteratively using time stepping, which is the topic of the next section. Note that the equation also can be solved from a steady state analysis.

2.3.4 Time stepping

Unless otherwise stated, equations and theory in this section are retrieved from [7].

When dealing with transient loading, the equation of motion becomes more complicated to solve as the response varies at every infinite point in time. A way of handling this issue is to divide the time into smaller time steps, Δt, and then approximate the variation of the response within each step. There are numerous types of time-stepping procedures, which generally can be divided into two categories: implicit methods and explicit methods. Explicit methods are appropriate for highly dynamic events, e.g. earthquakes and car crashes, involving large inertial forces and non-linearities such as contact conditions. In this thesis, however, linear models are used, and therefore implicit integration is a more suitable choice.

Common for both methods is that initial conditions (i.e. displacements and velocities at time zero) need to be known in order to begin the time-stepping. If modal dynamics is used, the initial values expressed in modal form are computed from the modal expansion. Equation 2.14 is multiplied by the transpose of the mode vector of the first eigenmode and the mass matrix. This is done to utilize the orthogonality properties of the mode vectors, which cancel out all terms in the sum except for i=j (where j here denotes the first eigenmode, but can also express an arbitrary mode). This yields

$$\mathbf{\Phi}_j^T \mathbf{M} \mathbf{u} = \sum_{i=1}^{N} \left(\mathbf{\Phi}_j^T \mathbf{M} \mathbf{\Phi}_i \right) \mathbf{q_i} = \left(\mathbf{\Phi}_j^T \mathbf{M} \mathbf{\Phi}_j \right) \mathbf{q_j}$$

and ergo

$$\mathbf{q_j} = \frac{\mathbf{\Phi}_j^T \mathbf{M} \mathbf{u}}{\mathbf{\Phi}_j^T \mathbf{M} \mathbf{\Phi}_j}; \quad \dot{\mathbf{q}}_\mathbf{j} = \frac{\mathbf{\Phi}_j^T \mathbf{M} \dot{\mathbf{u}}}{\mathbf{\Phi}_j^T \mathbf{M} \mathbf{\Phi}_j} \ .$$

For implicit methods, the equation of motion must be solved at every time increment. This implies that the mass, damping and stiffness matrices have to be inverted, which is very computationally expensive. Nevertheless, the time steps can be relatively large since implicit methods can be made unconditionally stable (with the right choice of input parameters). A method is said to be stable when time increment used is not generating large, rapidly growing errors which will cause the response to increase rapidly. Contrary to the implicit method, the explicit method is only conditionally stable and smaller time increments are needed in order to fulfill the stability requirement. Although the increments are smaller in the explicit method, the computational time for each time step is significantly shorter, since equilibrium is only checked at the beginning of the time stepping. In addition, the mass, damping and stiffness are stored in vectors, as opposed to matrices in the implicit case, which is also a time-reducing factor [8].

Both the implicit and the explicit methods are based on finite difference methods, meaning that the derivatives (velocity and acceleration) of the sought variable (displacement) are approximated. For explicit methods, the central difference method is often used, in which only information about the system at the current time is needed to determine the response at the next time step. This characteristic is what distinguishes an explicit method from an implicit one, where future, unknown responses also are included in the equation of motion at time $i+1$. In an implicit method, the variation of the acceleration is approximated, and the most common way to assume this variation is by using the Newmark family of methods, described by Equation 2.21 and 2.22. The parameters γ and β describe how the acceleration varies within a time step, and further also governs the stability of the solution.

$$\dot{u}_{i+1} = \dot{u}_i + \left[(1-\gamma)\, \Delta t \right] \ddot{u}_i + (\gamma \Delta t)\, \ddot{u}_{i+1} \tag{2.21}$$

$$u_{i+1} = u_i + (\Delta t \dot{u}_i) + \left[\left(\frac{1}{2} - \beta \right) (\Delta t)^2 \right] \ddot{u}_i + \left[\beta\, (\Delta t)^2 \right] \ddot{u}_{i+1} \tag{2.22}$$

where u is the displacement, $\dot{u}$ is the velocity and $\ddot{u}$ is the acceleration.

The equation of motion at time $i+1$ is presented in Equation 2.23. Inserting the Newmark equations (Equation 2.21 and 2.22), yields an expression where the unknown acceleration, u_{i+1}, is included. Consequently, iterations are necessary in order to solve the equation of motion, which is computationally expensive.

$$m\ddot{u}_{i+1} + c\dot{u}_{i+1} + ku_{i+1} = p_{i+1} \tag{2.23}$$

What differentiates methods within the Newmark family from each other is how γ and β are chosen. One branch of the Newmark family, the Hilber-Hughes-Taylor time integration, is implemented by default in BRIGADE/Plus. This method uses

$$\gamma = \frac{1-2\alpha}{2} \; ; \; \beta = \frac{(1-\alpha)^2}{4} \; ,$$

and is unconditionally stable if α is chosen to a value between $-\frac{1}{3}$ and 0 [9].

As has been emphasized in this section, implicit integration is a very time-consuming operation. To reduce the computational time, modal reduction, described in Section 2.3.3, can be utilized. A prerequisite for modal reduction is that the model should be linear, which further justifies the choice of implicit time-integration.

2.3.5 Damping

Damping is a material and a structural property that, by energy-dissipating mechanisms, reduces the oscillations from, for example, a train passage. The sources of damping are numerous, including friction between material particles, opening and closing of concrete cracks, friction in bearings and damping properties of the surrounding soil and foundation. Due to the difficulty in accounting for all the damping mechanisms simultaneously, damping is usually greatly simplified and idealized in physical models. For railway bridges, the Kelvin-Voigt model has proven to be a good representation of the damping [10]. This model consists of a so-called viscous damper, connected in parallel to an elastic spring (Figure 2.6). Viscous damping can broadly be described as the rate-dependent resistance between a structure that is submerged in a liquid, and the enclosing liquid.

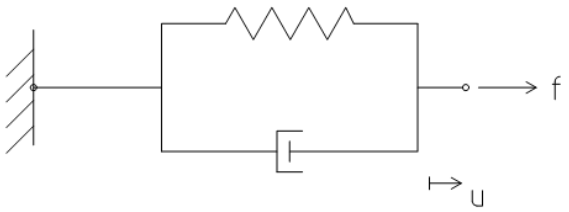

Figure 2.6: The Kelvin-Voight model: an elastic spring with the stiffness k and a viscous damper with the damping constant c.

Moreover, the damping constant in a viscous model, c, can be related to the velocity as stated in Equation 2.5. A more common measure of the damping, however, is the damping ratio, ζ, which is related to c according to

$$\zeta = \frac{c}{2m\omega_n} \ . \tag{2.24}$$

Among different methods in determining the damping ratio, the *Half-power bandwidth method* belongs to the more frequently used ones. The fundamental principle of this method is that the width of the resonance peaks is used to compute the values of ζ: the wider the peak, the higher the damping. Due to time constraints, a simpler approach described in Eurocode [5] was used in this thesis. These values of the damping ratio are only dependent on the span length and on the material of the bridge, and can be obtained from Table 2.2.

Damping can be applied at either a structural, or at a material level. Material damping is more complicated since it requires a material model. For linearly dynamic problems, structural damping can be used, meaning that the damping matrix is constructed directly from the values of the damping ratio. Furthermore, modal damping can be adopted if modal dynamics is utilized. This is a type of structural damping, where the damping ratios are applied directly at the eigenmodes. The different modes can have different damping; however, since evaluating the impact of the damping is beyond the scope of this work, the same value of the damping ratio was chosen for all modes.

2.4 Soil Dynamics

It is well established within the field of geotechnics that the behaviour of soil during deformation is nonlinear. The properties governing the dynamic behaviour of the soil are the shear modulus, representing the stiffness, and the damping ratio, expressing the structural and geometrical damping. These properties are both dependent on the frequency of the loading and on the amplitude of the shear strain [11]. For vibrations of lower frequencies, such as wind and wave loading, the static stiffness (i.e. the stiffness at frequency zero) is adequate to describe the dynamic stiffness [11]. Although the material properties of the soil changes slightly at higher frequencies, the frequency-dependency of soil is not very prominent. On the contrary, the amplitude-dependency of the dynamic stiffness and damping can be considerable. The dynamic stiffness of the soil tends to decrease with increasing strain amplitude, and has its lowest values around resonance peaks. As can be seen in Figure 2.7, the opposite behavior applies for the damping. Of course the actual values of the stiffness ratio and shear strain, as well as the slope of the lines, varies depending on the aggregate size, the effective confining stress etc.; however, the general behaviour is the same.

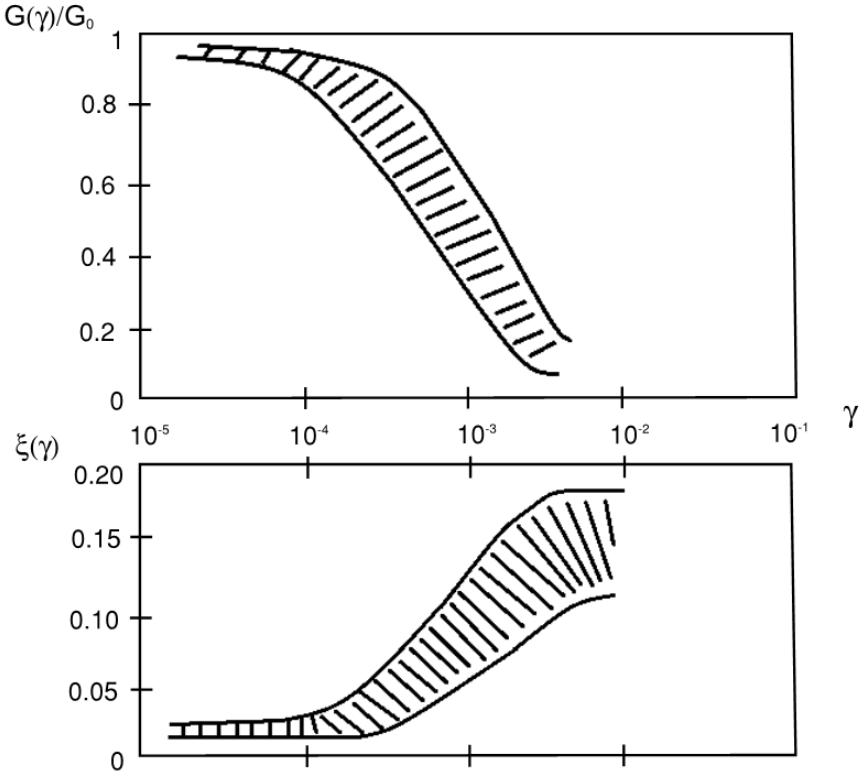

Figure 2.7: Principle behaviour of a soil's shear modulus and damping ratio as a function of amplitude (shear strain) inspired by [11] (page 202). G_0 refers to the initial shear modulus and G is the actual shear modulus, dependent on the level of shear strain.

The structural damping can be derived from the hysteretic stress-strain curve, which describes the time lag between the applied action (stress), and the response of the soil (strain) [12]. In Figure 2.8, the ellipse represents one loading cycle, and the area within the ellipse symbolizes the corresponding energy loss, originating from inelastic behaviour of the soil. Another source of damping relevant for soils is geometrical damping. This type of damping arises when applying a harmonic loading, causing vibrations that induce wave motions in the soil. The dissipation of these waves is often referred to as geometrical (or radiation) damping. Both structural and geometrical damping are included in the so-called dynamic stiffness function, which is described later on in this section.

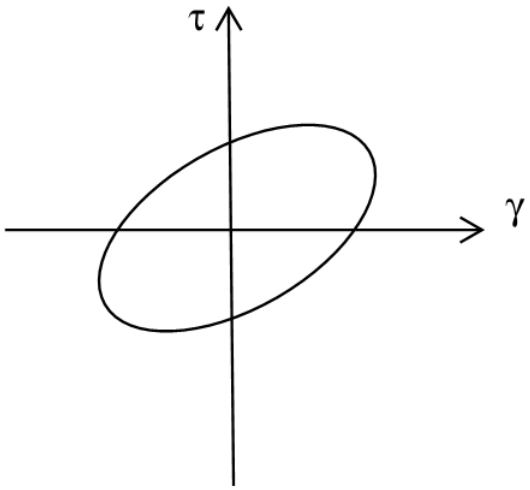

Figure 2.8: Principle shape of a soil's hysteretic stress-strain curve inspired by [12] (page 21)

The level of shear strain is not only important to determine the value of the shear modulus and the damping ratio, but also for choosing a suitable material model. According to [13], railway-induced vibrations usually yield relatively small strains in the soil material. At these strain levels, in the order of 10^{-3} and 10^{-4}, a linear viscoelastic model has proven to be adequate to represent the deformation behaviour [12]. These models consist of springs and dashpots, expressing the stiffness and the damping characteristics of the material. The linear viscoelastic model most widely used in engineering practice is the Kelvin-Voight model, described in Section 2.3.5.

2.4.1 Soil-structure interaction

In the previous section, the deformation properties of the soil is presented as an isolated phenomenon, whereas in reality, the response of the soil is dependent on the response of the structure and vice versa. This interaction is referred to as SSI, and is the topic of this section. As mentioned in the introduction of the thesis, it is not obvious if and when the effect of SSI should be taken into consideration in a dynamic analysis, in order to obtain moderately conservative results. Although analyses of high-speed railway bridges have been performed for many years, there are no actual rules or guidelines in the standards on how to deal with SSI. Instead, the industry has developed its own approach: to neglect the effect of SSI, and to use fixed boundary conditions to represent the interface between the foundation and the subsoil. The need of including SSI probably arose when the track speed increased to such levels, that it became difficult to keep the deck acceleration within allowable limits. With the belief that the fixed boundary conditions are an overly conservative assumption, a more accurate representation with an elastic ground model would give more beneficial results. However, recent research has shown that the results are not consistent, and that understanding the nature of SSI is not the easiest of tasks. Beneath, a brief description of how to incorporate SSI in a dynamic analysis is provided, followed by an excerpt of results obtained from different studies of SSI.

The dynamic stiffness, often referred to as the impedance, expresses the resistance of a soil that undergoes harmonic loading. The impedance is a function of frequency that origins from the force-over-displacement ratio. For the case with steady-state dynamics, it is convenient to use the complex notation

$$\chi_z = K_z(\omega) + i\omega C_z(\omega) \tag{2.25}$$

where the real part, $K_z(\omega)$, corresponds to the stiffness and the imaginary part, $C_z(\omega)$ represents the damping characteristics [14]. Equation 2.25 is valid for the vertical DOF; however, the impedance in the other DOFs can be computed analogously. The equation of motion then becomes

$$[-\omega^2\mathbf{M} + i\omega\mathbf{C}(\omega) + \mathbf{K}(\omega)]\mathbf{u}^*(\omega) = \mathbf{f}^*(\omega) \ ,$$

which, for steady-state dynamics, can be solved directly in the frequency domain for every frequency of interest. With the displacements known, the impedance can readily be calculated, and inserted as boundary conditions at the interface between the structure and the soil. In this type of analysis, a large-scale model of the soil is required, which numerically in a FE-model implies a massive amount of DOFs, and thus, a lot of computational capacity. The computational work is, however, much limited due to the

use of steady-state dynamics.

For an analysis of highly transient loadings, such as high-speed trains, it becomes more difficult to compute the impedance functions. One possible method is to apply an operator that transforms the load from the time domain to the frequency domain, e.g. a *Fourier Transform* or a *Laplace Transform*, and thus dissolves the transient load into its different frequency components. This can be a challenging task due to the complexity of the train-configuration, and additionally there might be a phase lag between the frequency components that is hard to take into account. Another approach is to abandon the concept of steady-state and impedance functions, and to solve the dynamic problem directly in the time domain using time-stepping. In order to include the SSI in such an analysis, a complete model of the surrounding soil, the foundations and the abutments, as well as the bridge structure, is necessary. This would require an enormous amount of computational capacity, and would therefore be difficult to implement in engineering practice.

The results from a minor literature study covering the works of [13], [15] & [16] are presented in the list below. Unless otherwise stated, the information applies for portal frame bridges on shallow foundations. The soil is modelled in a three-dimensional space with finite elements, and both steady-state dynamics and time stepping procedures are used to compute the dynamic response. The soil profiles, the distance to the bedrock, and the presence of ground water may vary among the reports. Note that the information is only based on a small number of analyses, being mostly purely theoretical. More comprehensive research on the subject is necessary to fully understand the concept of SSI, and to validate the results of the current studies.

- Neglecting the backfill soil may be a conservative assumption. The backfill soil increases the stiffness of the system, and thus also the natural frequency and the track speed at which resonance occurs. In addition, the energy-dissipating mechanisms of the soil could lower the amplitude of the maximum response of the bridge.

- Including SSI increases the global damping of the structure; thus, lower accelerations at resonance peaks can be obtained. The mentioned effect is larger for soils with a lower elastic modulus.

- The global stiffness of the structure decreases when SSI is taken into account. This effect is more evident at higher frequencies. Further, a lower stiffness leads to a lower value of the natural frequency, and thereby also a lower critical track speed.

- SSI tend to have a greater impact on short and stiff bridges.

- Using fixed boundary conditions results in an underestimation of the vertical acceleration of the bridge deck.
- Fixing the vertical DOF and modeling the other DOFs with linear elastic springs, yield half the value of the deck acceleration compared to the case where also the vertical DOF is modelled as a spring.
- For a portal frame bridge, a frequency-independent representation of SSI, obtained from impedance functions when the frequency is zero, has proven to give conservative results compared to that of the frequency-dependent equivalent (as well as the modeling with fixed boundary conditions). For a simply supported slab bridge, impedance functions at the frequency of the first bending mode yield satisfactory results.

2.5 Design Requirements According to Eurocode

The following is based on Section 6 in [5] and Appendix A2 in [17].

The train speed governs whether a dynamic analysis of the bridge is required or not. For track speeds of 200 km/h or less, only a static analysis is needed, and the dynamic effect is taken into account by multiplying the static load with a dynamic load factor, ϕ. The dynamic load factor does not consider the resonance effects, i.e. that the response can be highly amplified near resonance peaks. Therefore, for track speeds exceeding 200 km/h, a dynamic analysis must be performed. At these higher speed levels, a comparative static analysis should also be conducted, in order to determine the most unfavourable case that will dictate the design.

Below, the appropriate load models and other parameters to consider for the static and the dynamic analysis, respectively, are described.

2.5.1 Static analysis

Load model LM71 and load model SW/0 represent the vertical loading caused by railway traffic in a static analysis; however, load model SW/0 is only of interest for continuous bridges. The two static load models are visualized in Figures 2.9 and 2.10.

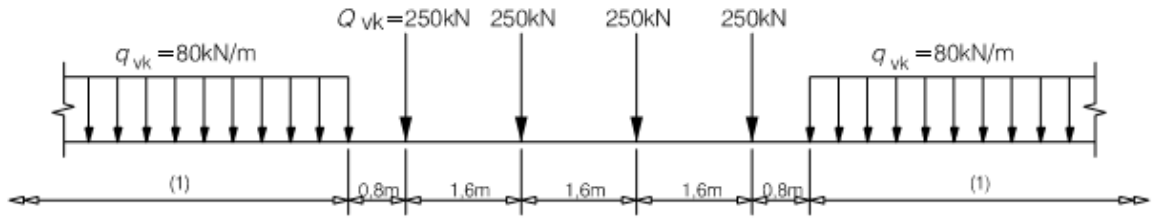

Figure 2.9: Load model LM71. The length (1) is infinite.

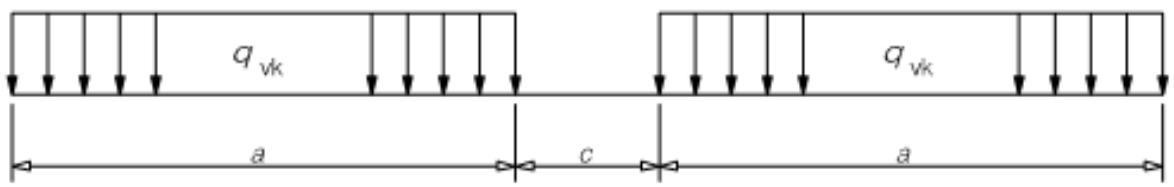

Figure 2.10: Load model SW/0, where $q_{vk} = 133kN/m$, $a = 15m$ and $c = 5.3m$.

The characteristic values from static analyses with load model LM71 and load model SW/0 should be multiplied by the dynamic load factor (ϕ) and also a second factor,

denoted by α (Equation 2.26). This factor accounts for whether the rail traffic is heavier or lighter than normal rail traffic. For most bridge applications, including the bridges in this study, an α-value of 1.33 is chosen.

$$\alpha \cdot \phi \cdot (LM71) \tag{2.26}$$

or

$$\alpha \cdot \phi \cdot (SW/0)$$

As stated in [18], the dynamic load factor can be taken as the value for carefully maintained tracks

$$\phi = \phi_2 = \frac{1.44}{\sqrt{L_\phi} - 0.2} + 0.82 \tag{2.27}$$

where the determinant length, L_ϕ, is dependent on the bridge type, and is obtained from Table 2.1.

Table 2.1: Determinant length, L_ϕ, for different bridge types.

Slab bridge	$L_\phi = k \cdot L_m$ $L_m = \frac{1}{n} \cdot (L_1 + L_2 + ... + L_n)$; where L_i is in [m] and n is the number of spans n | 2 3 4 k | 1.2 1.3 1.4 1.5
Frame bridge	Can be considered as a continuous slab bridge with three spans

For track speeds exceeding 200 km/h, the results obtained from Equation 2.26 should be compared with those of a static analysis of the *High-Speed Load Model* (HSLM), further described in Section 2.5.2, multiplied by a different set of dynamic amplification factors (Equation 2.28). Alternatively, the response of analyses with LM71 and SW/0 multiplied by α and ϕ can be compared directly with that of the dynamic analysis of HSLM (where the dynamic magnification is, of course, already accounted for). Note that a complete dynamic analysis has to be performed in excess of the static comparison at this speed level.

$$(1 + \varphi'_{dyn} + \varphi''/2) \cdot (HSLM) \tag{2.28}$$

The dynamic enhancement factor, φ'_{dyn}, is

$$\varphi'_{dyn} = max \left| \frac{y_{dyn}}{y_{stat}} \right| - 1 \tag{2.29}$$

where $max \left| y_{dyn} \right|$ and $max \left| y_{stat} \right|$ are the maximum dynamic response and the maximum static response of the load model HSLM, respectively, measured in terms of parameters such as deflection at a specific point of the bridge deck.

A second amplification factor, φ'', accounts for track irregularities and vehicle imperfections

$$\varphi'' = \frac{\alpha}{100} \left[56e^{-\left(\frac{L_\phi}{10}\right)^2} + 50 \left(\frac{L_\phi n_0}{80} - 1 \right) e^{-\left(\frac{L_\phi}{20}\right)^2} \right] \tag{2.30}$$

where

n_0 is the first natural bending frequency (in Hz) of the bridge loaded by permanent actions,

L_ϕ is the determinant length according to Table 2.1

$\alpha = \begin{cases} \frac{v}{22} \text{ if } v \leq 22 \ m/s \\ 1 \text{ if } v > 22 \ m/s \end{cases}$; v is the maximum allowable track speed.

Briefly, for track speeds higher than 200 km/h, load effects such as acceleration, deflection, torsion, rotation at bearings, are computed in the dynamic analysis described in the next section, and compared with threshold values specified in the standards. However, the section forces are evaluated by comparing Equation 2.26 and 2.28. The section forces are considered as acceptable if Equation 2.28 yields a lower value than Equation 2.26.

2.5.2 Dynamic analysis

For a dynamic analysis, the HSLM should be used. This load model consists of two different universal trains: HSLM-A and HSLM-B (Figures 2.11 and 2.12). HSLM-B constitutes of a number of evenly spaced, moving point loads, and is applicable for simply supported bridges with a span up to 7 m. HSLM-A, containing 10 trains (A1-A10) with varying number of coaches, coach lengths, bogie axle spacings and point load magnitudes, should be used in all other cases.

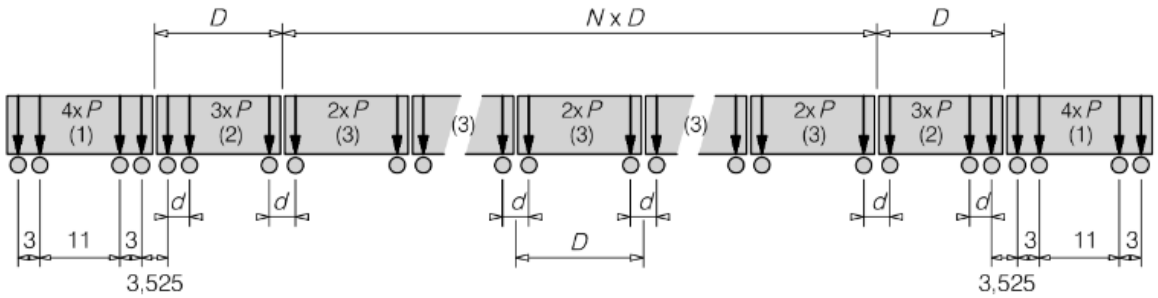

Figure 2.11: HSLM-A. The number of coaches (N), the length of the coaches (D), the spacing between the bogies axles (d) and the point load magnitude (P), are different for the trains A1-A10. The exact values can be found on page 78 in [5].

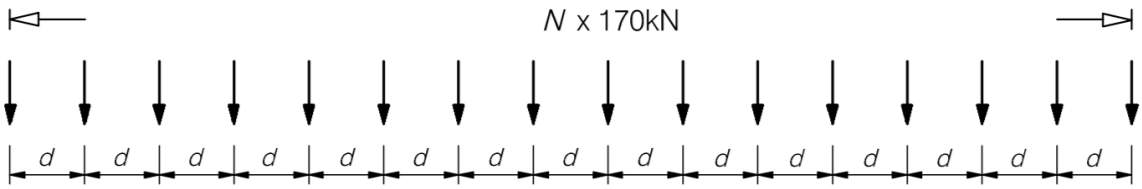

Figure 2.12: HSLM-B. The number of point loads (N) and the distance between the loads (d) depend on the span length.

The maximum frequency considered in the analysis should be chosen according to the expression below.

$$f_0 = max \begin{cases} 30 \text{ Hz} \\ 1.5 \cdot \text{The frequency of the first bending mode} \\ \text{The frequency of the third bending mode} \end{cases}$$

The maximum allowable acceleration of a bridge's superstructure that ensures traffic safety is 3.5 m/s^2 for a ballasted track. This threshold value is derived from the occurrence of ballast instability, i.e. when the ballast begins to behave non-linearly, multiplied by a safety factor. Hence, the acceleration limit does not account for the capacity of the bridge itself.

The bridge should be designed for a speed that is 1.2 times greater than the maximum allowable track speed. Furthermore, not only the bridge's response to the maximum speed, but also to a series of increasing speeds up to the design value, should be evaluated. This is because resonance can occur at speeds lower than the design value.

Regarding the mass of the structure, two different estimations should be used in the analysis: a lower estimation to obtain the highest possible acceleration of the superstructure according to Newton's second law; and a higher estimation to obtain the lowest speed at which resonance will occur.

The natural frequency (as well as the speed at which resonance occurs) is likely to be overestimated if the stiffens of the bridge is overestimated; therefore, a lower bound estimation of the stiffness should be used.

Eurocode specifies standard values of the damping ratio to be used for bridges of different materials and span lengths. The values for reinforced concrete bridges are shown in Table 2.2.

Table 2.2: Values of the damping ratio for reinforced concrete bridges (Table 6.6 in [5]).

Bridge Material	ζ Lower limit of percentage of critical damping [%]	
	Span $L < 20m$	Span $L \geq 20m$
Reinforced concrete	$\zeta = 1,5 + 0,125\,(20 - L)$	$\zeta = 1,5$

3 Method of Analysis and Important Modeling Aspects

Below, the general procedure for the analyses is described. As mentioned in the beginning of this report, the acceleration is often decisive for the design; however, it is not certain for which types of bridges, and under which preconditions, this assumption may apply. There are several other design criteria that could be critical, including deflection and torsion of the bridge deck, and rotation at bearings. Therefore, supplementary analyses of these quantities were performed, in excess of the evaluation of the acceleration. In bridge engineering, the design approach is often to determine the bridge's dimensions and the necessary amount of reinforcement from a static analysis. To account for the dynamic amplification, the static results are multiplied by the dynamic load factor (ϕ), described in Section 2.5.1. This factor normally overestimates the dynamic enhancement; thus, the corresponding dynamic analysis will provide results within allowable limits and the from-a-static-analysis computed dimensions do not have to be altered. To investigate whether this design approach is true for the different bridge types, section moments and shear forces were extracted and compared using Equation 2.26 and 2.28.

In the first analysis, Analysis 1, two different bridge types were studied: a three-spanned slab bridge (Analysis 1A) and a portal frame bridge (Analysis 1B). For each bridge type, several parameter studies were performed. In Analysis 2, the boundary conditions used in Analysis 1 were modified to obtain a more realistic representation of the interface between the foundation slabs and the subsoil. This was done for both bridges with original measures of span length and cross-section height, which from now on will be referred to as thickness.

The dynamic analyses were performed in BRIGADE/Plus (version 6.2-7), a three-dimensional finite element program for analysis of bridges developed by Scanscot Technology. It can be described as an extension of ABAQUS, where design codes are implemented and where transient loads can have not only varying magnitude, but also varying positions in time. The universal trains HSLM, LM71 and SW/0 are all predefined in BRIGADE/Plus; thus, it is a suitable tool for studying train passages. Since all bridge types considered have a span length larger than 7 m, the HSLM-B trains were not used. Furthermore, BRIGADE/Plus is limited to implicit time integration, and the operator that is implemented by default in the software is of the Newmark family of methods.

3.1 Analysis 1 - Parametric Studies of Different Bridge Designs

The first analysis primarily covered the parameter studies (i)-(iii) listed below, with the response evaluated in terms of vertical accelerations of the bridge deck.

(i) Parametric study of span length.

(ii) Parametric study of design speed.

(iii) Parametric study of thickness.

For the bridges with different span lengths, the response was also analyzed in other quantities than the acceleration. More detailed information about these procedures and the design requirements used can be found in Appendix E.

(iv) Vertical deformation.

(v) Torsion.

(vi) Rotation at bearings.

(vii) Section forces (i.e moments and shear forces).

Furthermore, two additional studies were performed.

(viii) An investigation of a potential resemblance between the frequency of the train loading and those of the bridges' dominating eigenfrequencies.

(ix) A comparison of the results obtained from bridge models with varying size of output region.

The methodology used in the parametric studies (i), (ii), and (iii), is briefly outlined in the flowchart provided in Figure 3.1.

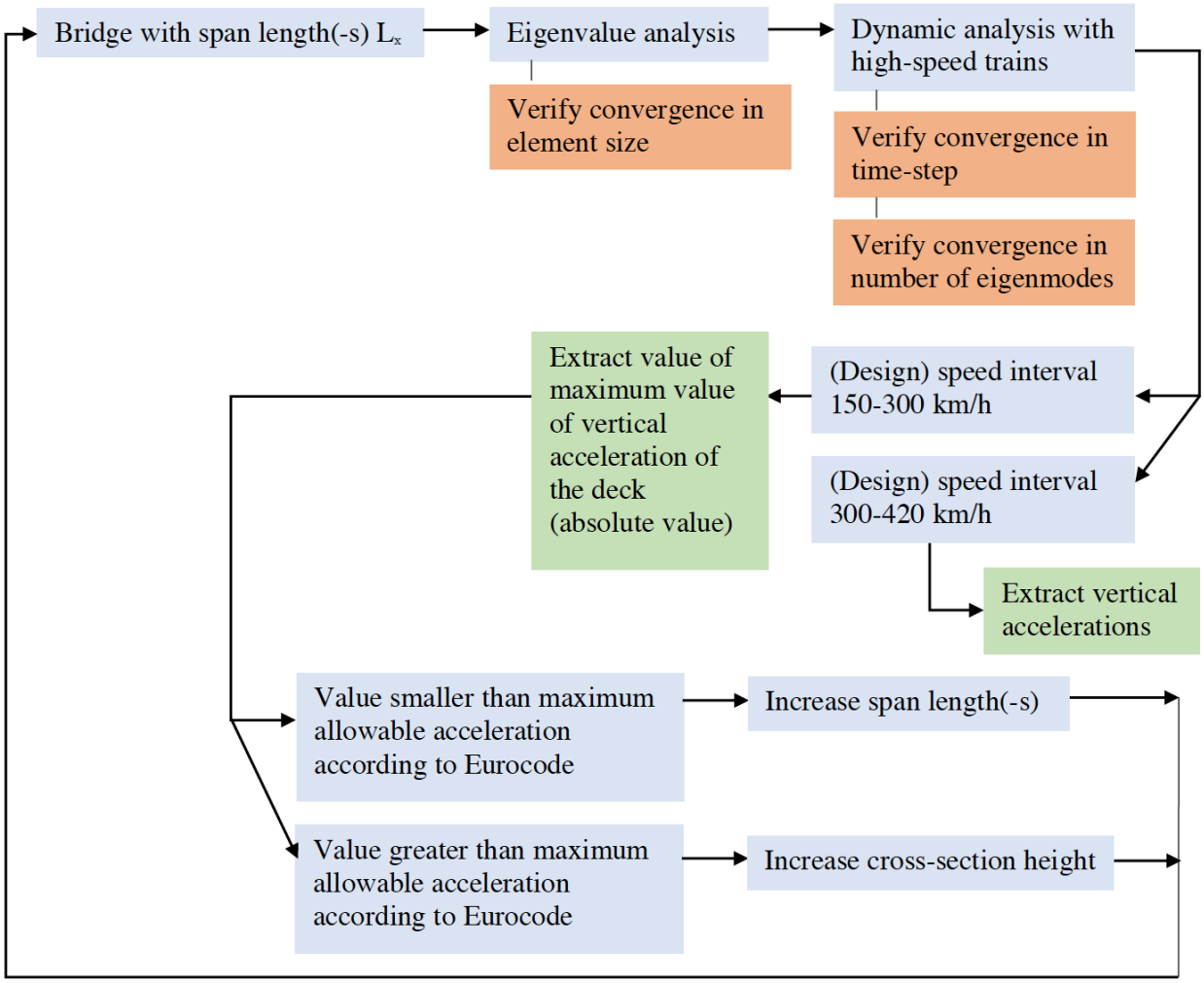

Figure 3.1: Flowchart describing the analysis procedure of parameter studies (i), (ii), and (iii).

Initially, an eigenvalue analysis was performed on a slab bridge (Analysis 1A), and on a frame bridge (Analysis 1B), respectively. The dimensions and the design of these two bridges are based on actual railway bridges that have recently been built. From the eigenvalue analysis, the number of modes needed to fulfill both the minimum requirement in Eurocode and convergence was extracted; hence, a dynamic analysis with modal reduction could be conducted. The response was evaluated for two speed intervals: 150-300 km/h (where the design value of 300 km/h corresponds to a track speed of 250 km/h); and 300-420 km/h (where the design value of 420 km/h corresponds to a track speed of 350 km/h). Since resonance effects and acceleration peaks may occur at speeds lower than the maximum value, a series of speeds up to the design value (and not only the design value) were included in the analysis. Generally, a speed increment of 10 km/h was used; however, the increment was reduced to 2.5 km/h around resonance peaks.

The lower track speed of 250 km/h is most likely to apply for the East Link; therefore, the lower associated design speed interval was used as a basis for the parametric study of span length and thickness. The higher speed interval was primarily used for comparison. First, the span length(-s) was increased until the maximum allowable acceleration was exceeded, while the thickness was kept constant. Then the thickness of the bridge, with spans that gave unacceptable high accelerations, was enlarged until the design requirements were fulfilled.

In agreement with the design requirements stated in Eurocode (Section 2.5.2), all bridges were analyzed with both a lower-bound and a higher-bound estimation of the mass. The mass was varied by using ballast with different densities, according to Section 3.1.1.

An integral part of an FE-analysis is that the convergence criterion is fulfilled. Convergence can refer to different concepts; however, the general definition is that the approximate solution should approach the exact solution when the parameter of interest is refined. In this thesis, the following types of convergence were considered.

- Convergence in element size, which was verified by comparing the value of the frequency of the highest mode regarded obtained from a model with a fine mesh with that of a model with a coarser mesh.
- Convergence in time step, meaning that the time increment should be small enough to fully capture the motion. This was validated by performing dynamic analyses with different sizes of the time increment, and comparing the time history of the response in one node.
- Convergence in number of eigenmodes, validated by comparing the results (here maximum and minimum accelerations) of a modal analysis including all modes with that of a fewer number of modes.

In the sequent sections, preconditions for Analysis 1 are presented and relevant modelling features in BRIGADE/Plus are commented upon. The figures are solely of the slab bridge, though are applicable for both bridge types. In Sections 3.1.3 and 3.1.4, the additional studies, denoted (viii) and (ix) (see page 30), are described.

3.1.1 Material properties

The tables that follows below displays chosen values of material properties of concrete, ballast and soil. The density of concrete is normally 2400 kg/m^3; however, to account for the heavier reinforcement, an equivalent density of 2500 kg/m^3 was chosen. Further, the foundation of the bridge was assumed to be resting on frictional soil, where the characteristic value of the Young's modulus, E_{50}, was used. This value corresponds to 50 % of the ultimate load, and is derived from a load duration substantially larger than that of a train passage.

Table 3.1: Material properties of concrete.

Material property	Value	Unit
Density	2500	kg/m^3
Poisson's ratio	0.2	-
Young's modulus	35	GPa

Table 3.2: Ballast densities.

Estimation	Density [kg/m^3]
Lower-bound	1700
Higher-bound	2000

Table 3.3: Material properties of frictional soil according to [19].

Material property	Value	Unit
Weight	22	kN/m^3
Young's modulus (Characteristic value)	30	MPa

3.1.2 Modelling procedure in BRIGADE/Plus

The bridge deck, the wings, and the end shields were modelled as shell elements in BRIGADE/Plus. The columns were modelled as beam elements. The edge beams were disregarded in the analysis. Considering the dynamic aspect of the design, this is a conservative assumption since the edge beams increase the stiffness of the bridge.

Loads from the ballast and the link plates were added as inertia in terms of non-structural mass, placed according to Figures 3.2 and 3.3, respectively. The values of the non-structural mass are calculated in Appendix B and are displayed in Tables 3.4-3.5.

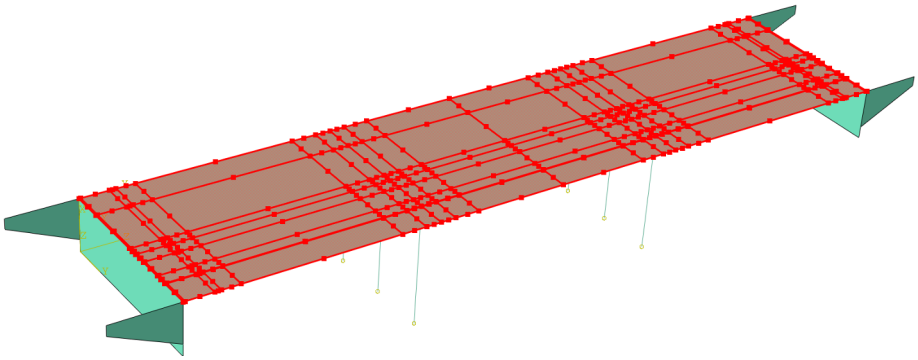

Figure 3.2: Distribution of the ballast (highlighted in red).

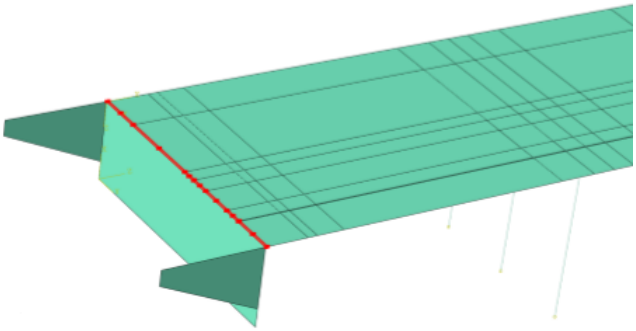

Figure 3.3: Distribution of the load from the link plate at the left end of the bridge over an area of $11.5 \cdot 0.1 m^2$ (highlighted in red).

Table 3.4: Values of the non-structural mass of the ballast.

Ballast density $\left[kg/m^3\right]$	Non-structural mass $\left[kg/m^2\right]$
1700	1020
2000	1200

Table 3.5: Values of the non-structural mass of the link plate.

Ballast density $\left[kg/m^3\right]$	Non-structural mass $\left[kg/m^2\right]$
1700	52519
2000	55671

Another important modelling feature is the connection between the columns and the slab foundations for the slab bridge, and the connection between the legs of the frame and the slab foundations for the portal frame bridge, respectively, shown in Figure 3.4. The underlying soil was disregarded, and the slab itself was assumed to prevent translation in all directions; thus, these DOFs were prescribed to zero. The rotational DOFs were modelled as rotational springs. Since it is difficult to determine the spring stiffness of each separate connection within a group of columns resting on the same slab, a group of columns was represented only with one rotational spring. In BRIGADE/Plus, this simplification is executed by inserting coupling constraints between each group of columns. The same methodology applies for the portal frame bridge: the rotational stiffness of the foundations slab was represented by a spring bed which can be condensed to one spring positioned in the midpoint of each slab with the use of coupling. The rotational spring stiffnesses in the x- and y-directions, presented in Table 3.6, were calculated according to Appendix B and C, and inserted as springs/dashpots in BRIGADE/Plus. Rotation around the z-axis was assumed to be restrained by the slab foundation.

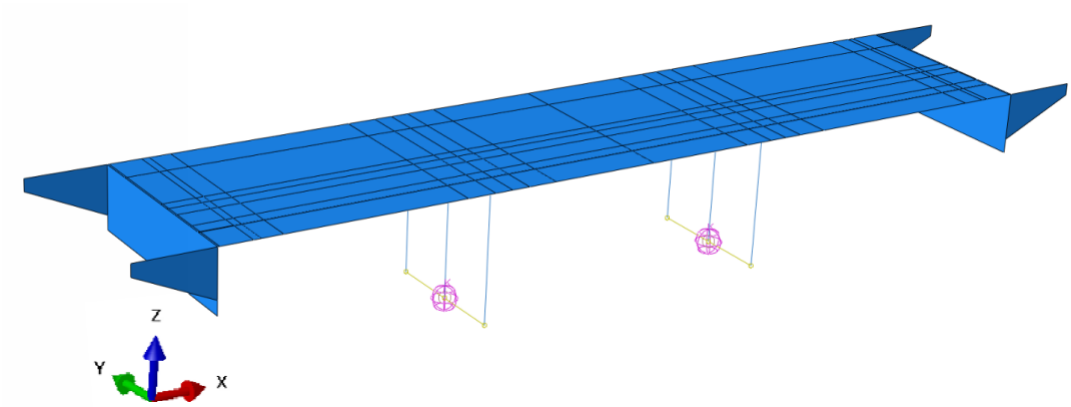

Figure 3.4: Connection between columns and slab foundation in BRIGADE/Plus. The coupling constraints and the rotational springs are displayed as yellow lines and purple circles, respectively.

Table 3.6: Values of the rotational spring stiffness of the slab foundation.

Axis	Spring stiffness $[GN/m/rad]$	
	Analysis 1A	Analysis 1B
x	5.88	4.06
y	2.10	1.25

At the ends of the slab bridge, the deck is supported by bearings that rests on shear walls. There is a set of three bearings at each end (Figure 3.12), and to avoid creating unrealistically large constraint forces, only the central one was modelled as a fixed bearing (in the y- and z-directions). The other two bearings were allowed to move in all directions except for the z-direction.

When assigning thicknesses to the model, the middle surface of each bridge component was used as a reference for the offset. This implies that there will be overlaying elements, i.e. an overestimation of both the mass and the stiffness at the inner corners at the ends of the deck (Figure 3.5). On the contrary, the mass and the stiffness were underestimated at the outer corners. Thus, the total effect of misplacing parts of the geometry was assumed to be negligible.

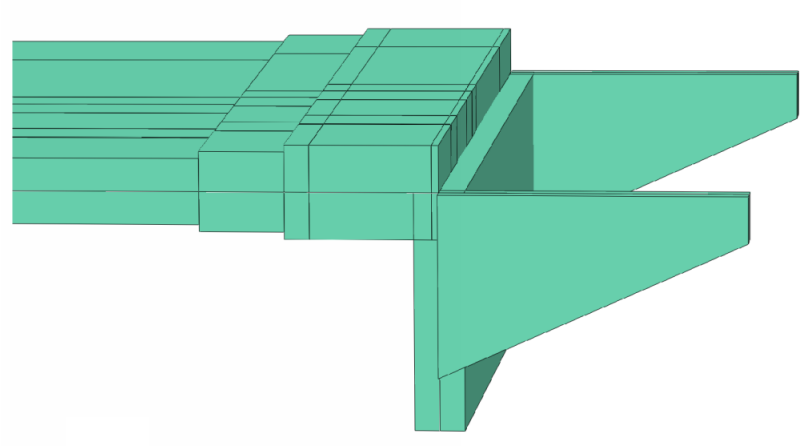

Figure 3.5: Rendered shell thicknesses at the end of the slab bridge.

According to the standards [17], only one track needs to be regarded in the analysis of a two-tracked railway bridge. Further, as mentioned in Section 2.5.2, the instability of the ballast governs the value of the maximum allowable acceleration. Ballast instability occurs underneath the tracks, and therefore, the output field can be limited to a smaller strip of the bridge's width, which is desirable since it reduces the analysis time. In addition, the geometry of the deck is symmetric in two planes; hence, only a strip at a quarter of the deck is an adequate output field (Figure 3.6).

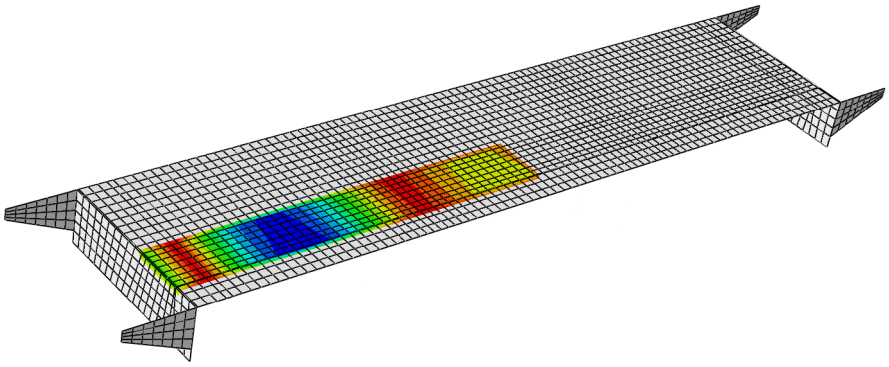

Figure 3.6: Output field in BRIGADE/Plus.

The distribution of the train loads over the rails and the sleepers according to [5] is illustrated in Figure 3.7. From the inclination ratio, the width considered in the analyses was determined as a value of 3200 mm.

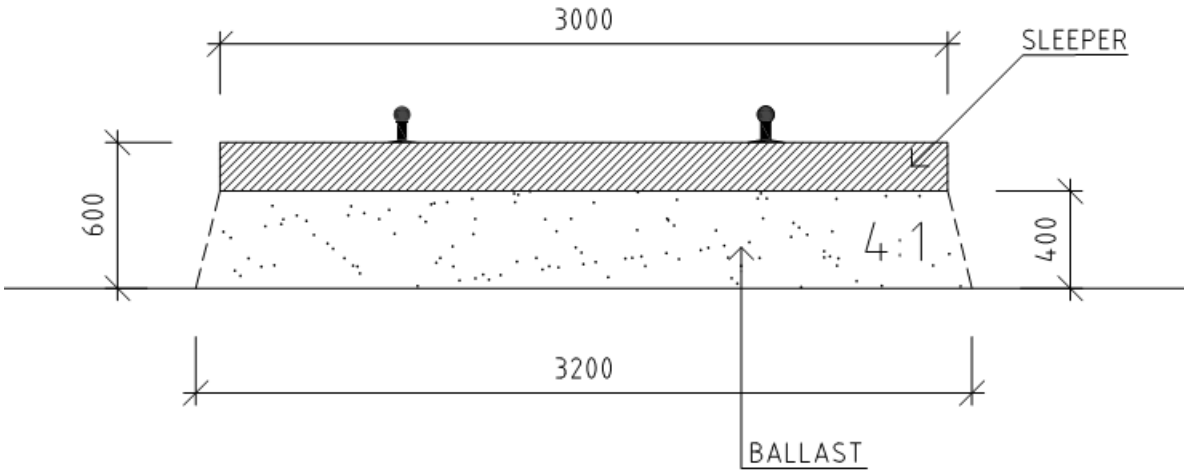

Figure 3.7: Analysis width.

3.1.3 Study of loading frequencies

As already emphasized, performing dynamic analyses with all HSLM-trains is a time-consuming task; thus, it would be beneficial if there was a way to readily assess which train and what speeds that will be critical for the response. The authors believed that if there was a resemblance in the loading frequency and the frequencies of the eigen-modes governing the response, these modes would be triggered, and the response would be amplified (and reach its maximum value). The loading frequencies were computed in a simplified manner, as the inverse of the coach length divided by the train speed. The coach lengths for HSLM A1-A10 are provided in Tables 3.7 [5]. Note that this was only a complementary study and that the graphs in Section 4 are not based on this approach.

Table 3.7: Coach lengths D for HSLM A1-A10. The distance D is defined in Figure 2.11.

HSLM-A	D [m]
1	18
2	19
3	20
4	21
5	22
6	23
7	24
8	25
9	26
10	27

The lowest bending modes proved to have the greatest impact on the response, as described in Appendix A. The frequencies of these eigenmodes were therefore compared with the calculated loading frequency for each train and at each speed level. Further, the critical scenario will most likely occur when the coach length is equal to the distance between the largest displacements within each span, obtained from the dominating mode shapes. This concept is illustrated in Figure 3.8. The distance between the displacement-peaks is dependent on the boundary conditions of the bridge deck, and were computed from the eigenvalue analysis.

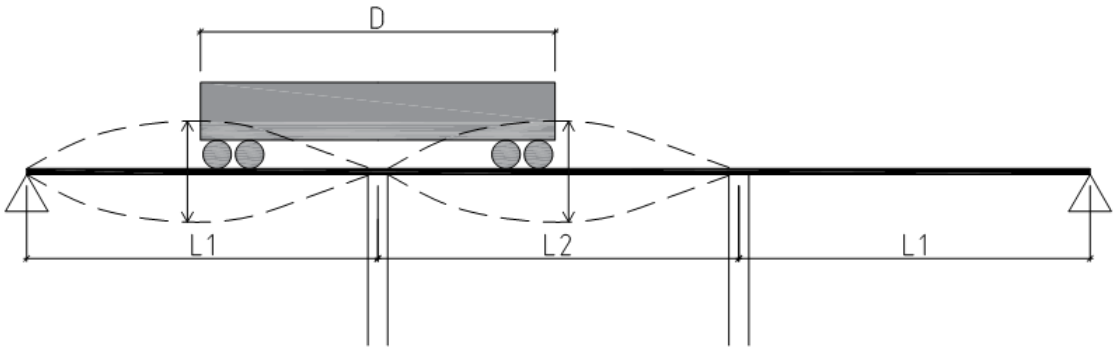

Figure 3.8: Coach length D along with span lengths L1 and L2 of the slab bridge. For the frame bridge, there is only one span, L1. The dashed lines show the deformed bridge deck.

3.1.4 Study of the size of the output region

Another point to consider is the size of the region where results are extracted. As it is only stated in Eurocode which value of acceleration that must not be exceeded, and not necessarily where on the bridge deck this value is referring to, a complementary analysis of the span length was performed on a larger region stretching to the longitudinal edge of the bridges (Figure 3.9 - compare with Figure 3.6).

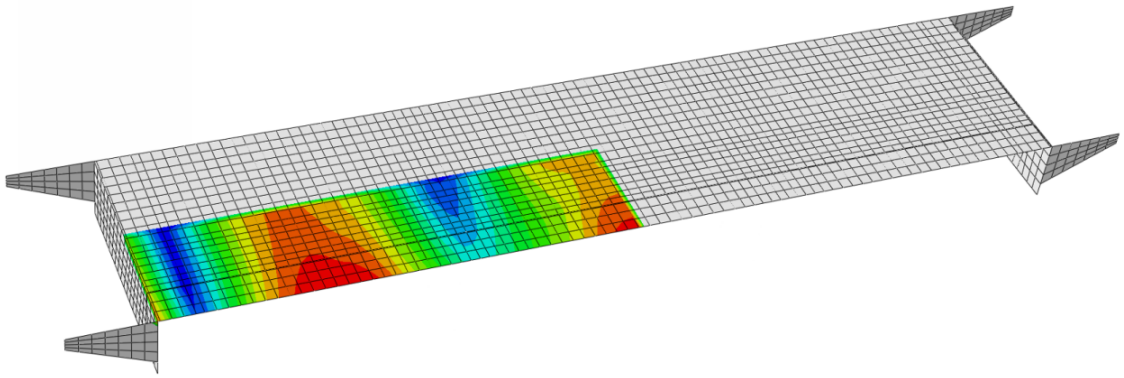

Figure 3.9: Wider output region.

3.2 Analysis 1A - Slab bridges

In analysis 1A, a three-spanned slab bridge, with a principle geometry according to Figure 3.10, was studied. Principal drawings of the slab bridge, along with relevant measures, are provided in Figures 3.10-3.12. As can be seen in the figures, the bridge has two sets of intermediate columns, which are attached to rectangular slab foundations. In addition, the bridge deck rests on bearings that allow for thermal expansion of the bridge. The end-shields and the wings prohibit the surrounding soil from sliding and also constitute a resistance against dynamic loading. As mentioned in Section 3.1.2, the edge beams, visualized in Figure 3.11, were disregarded in the analysis. Furthermore, to distribute the loads acting on the ends of the bridge, link plates are connected to the bridge deck.

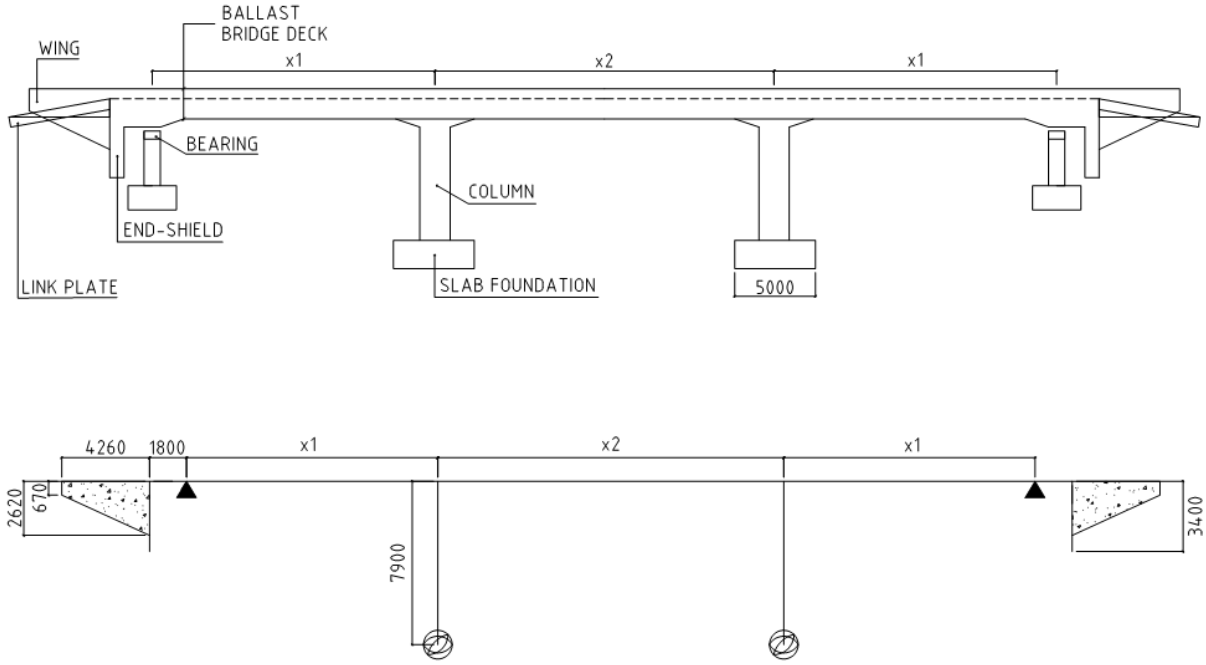

Figure 3.10: Elevation drawings of the slab bridge. The small triangles at the ends of the bridge deck in the lower figure symbolize the bearings and the moment springs represent the boundary conditions at the bottom of the columns.

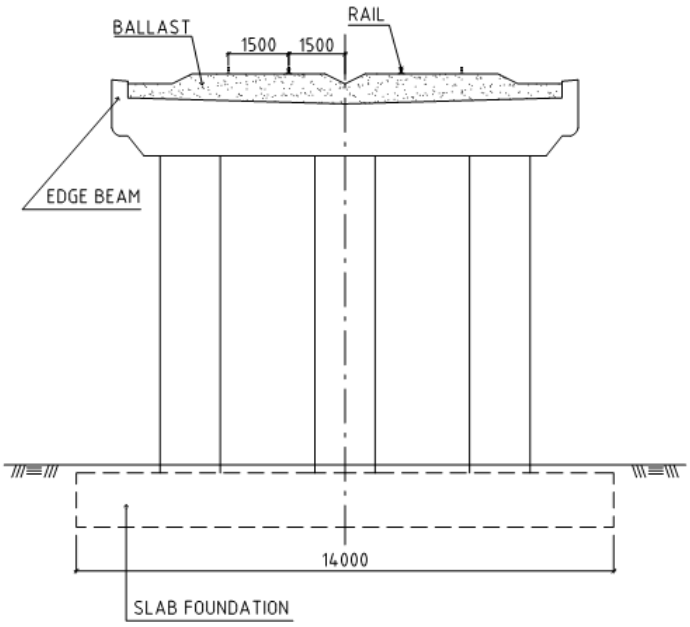

Figure 3.11: Sectional view of the slab bridge at the location of the columns.

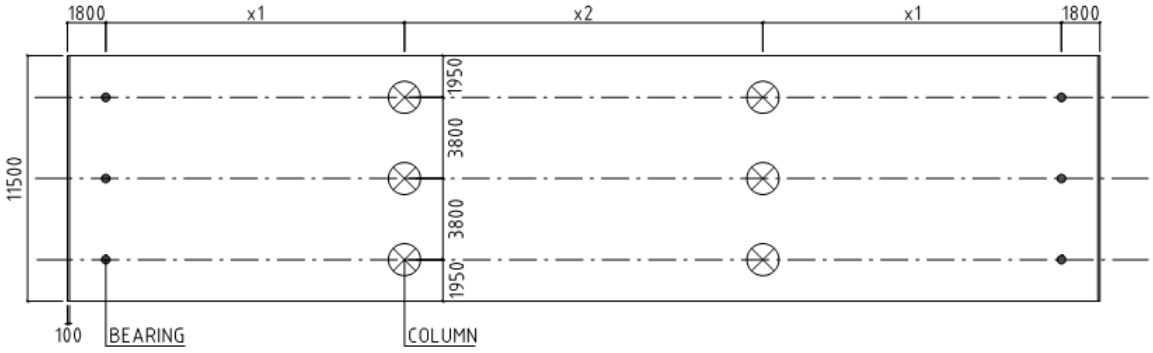

Figure 3.12: Top-view of the slab bridge.

To obtain an efficient design, the thickness of the bridge deck is not constant throughout the length; instead, the thickness is enlarged only at the sections where the moments are the greatest. The variance in thickness along the bridge is shown in Figure 3.13. The thicknesses of the different bridge elements are displayed in Table 3.8.

Table 3.8: (Original) thicknesses of different parts of the slab bridge. Here, the "thickness" of the columns refers to the diameter.

Bridge element	Thickness [m]
Deck t1	0.95
Deck t2	1.15
Deck t3	1.35
Wings	0.4
End shields	0.7
Columns	1.5

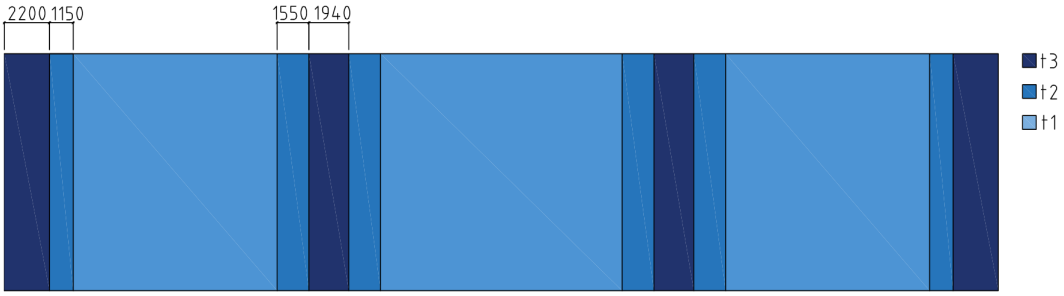

Figure 3.13: Deck thicknesses: t1; t2; and t3.

The span lengths used in the parametric study of span length are provided in Table 3.9. The value of the damping ratio for each bridge was derived from the equations in Table 2.2.

Table 3.9: Span lengths and corresponding damping ratios for the slab bridges. The enlargement factor refers to the increase in span length compared with the shortest bridge (S0).

Name of bridge	Span lengths $(x_1; x_2; x_1)$ [m]	Enlargement factor	Damping ratio [%]
S0	14.0; 16.8; 14.0	1	1.72
S1	15.4; 18.5; 15.4	1.1	1.60
S2	16.7; 20.0; 16.7	1.2	1.50
S3	18.4; 22.0; 18.4	1.3	1.50

3.3 Analysis 1B - Portal Frame Bridge

The simple geometry of the portal frame bridge used in Analysis 1B is visualized in Figure 3.14. Analogous with the slab bridge, the legs of the frame bridge rest on slab foundations, and further, there are also wings attached at the ends of the bridge deck. The loading from the link plate proved to have a minor impact on the results in Analysis 1A, and was therefore disregarded in this analysis. For longer spans (bridge S3 and S4), the portal frame bridge was assumed to be prestressed.

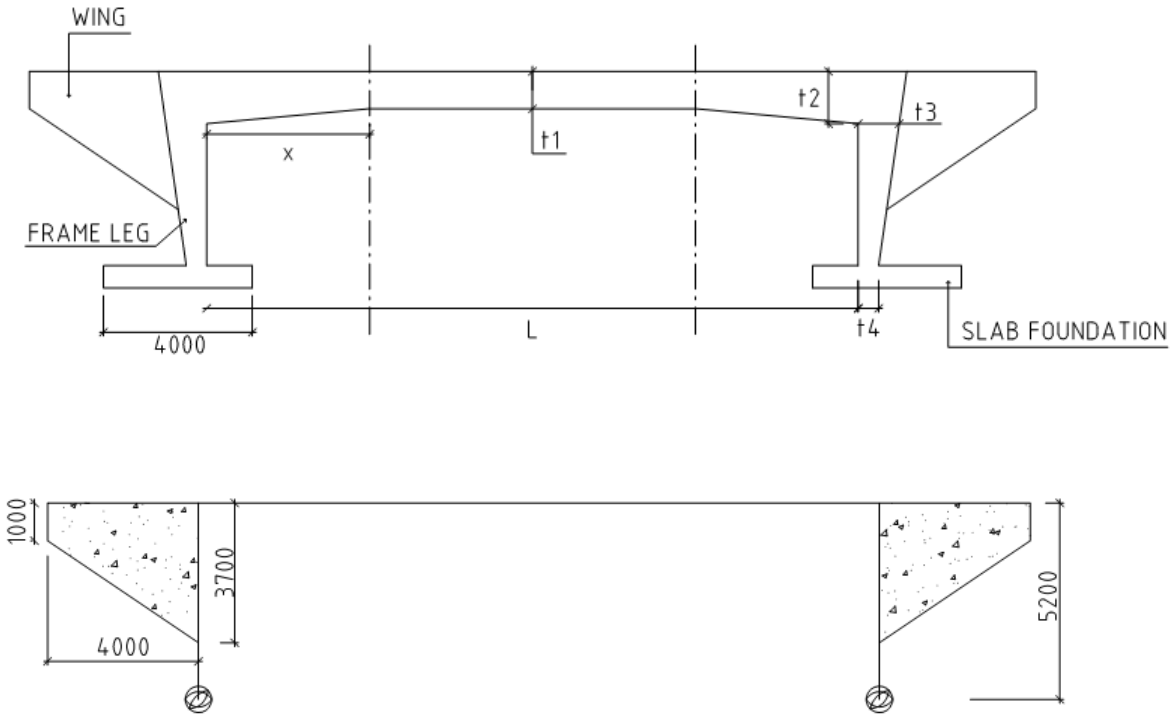

Figure 3.14: Elevation drawings of the portal frame bridge. The moment springs in the lower figure represent the boundary conditions at the bottom of the frame legs.

A sectional view of the portal frame bridge is provided in Figure 3.15. As can be seen, the width of the bridge and the placement of the tracks are similar to those of the slab bridge.

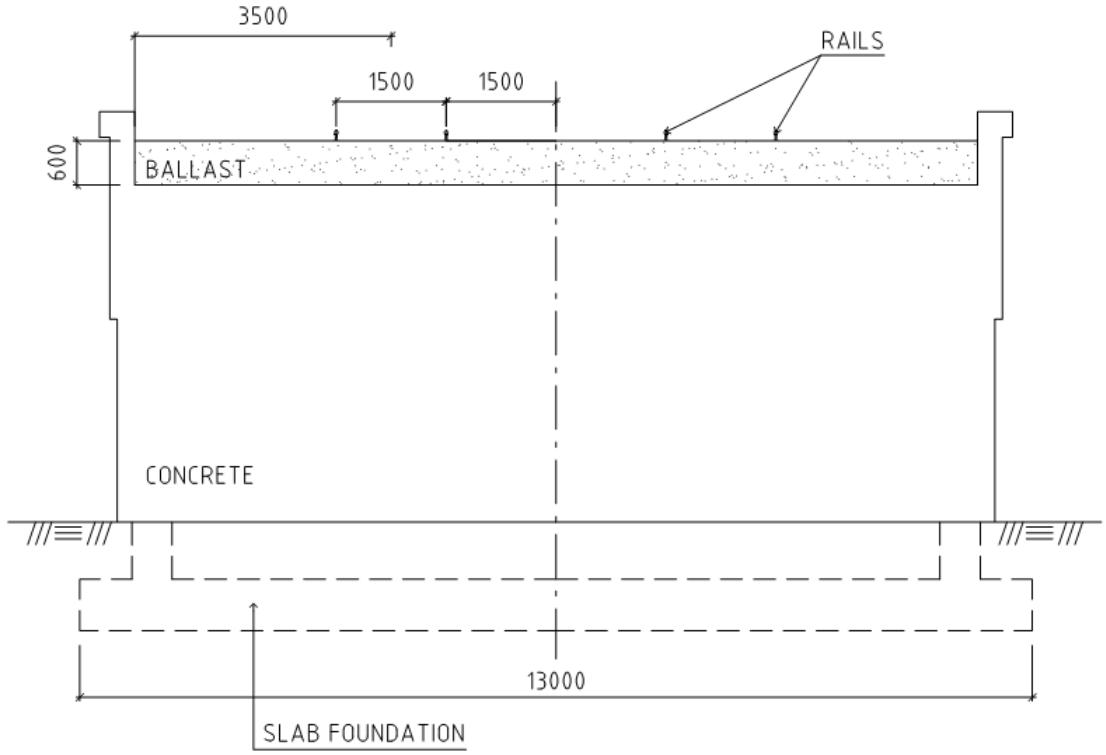

Figure 3.15: Sectional drawing of the portal frame bridge.

The thickness of the frame legs and the outer quarters of the bridge deck were assumed to be varying linearly. A constant thickness was adopted for the wings and the center part of the deck. The thicknesses of all bridge elements for the original bridge, S0, can be obtained from Table 3.10. The variance in thickness over the length and over the different bridge elements is visualized in Figure 3.16.

Table 3.10: (Original) thicknesses of different parts of the portal frame bridge.

Bridge element	Thickness [m]
t1	1.0
t2	1.4
t3	1.1
t4	0.55
Wings	0.4

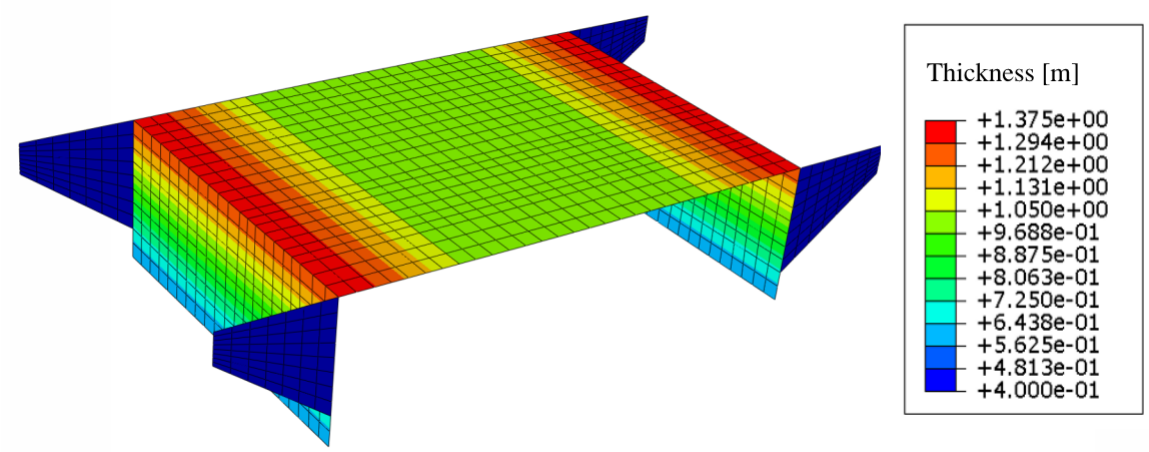

Figure 3.16: Colour plot of the thickness of the original frame bridge, S0.

In Table 3.11, the different span lengths used in the parametric study are displayed. The values of the damping ratios were obtained from the equations in Table 2.2.

Table 3.11: Span lengths, distances x (see Figure 3.14), and corresponding damping ratios for the portal frame bridges. The enlargement factor is referring to the increase in span length compared with the shortest bridge (S0).

Name of bridge	Span length (L) [m]	Distance x [m]	Enlargement factor	Damping ratio [%]
S0	17.5	4.4	1	1.67
S1	19.3	4.8	1.1	1.5
S2	21.0	5.3	1.2	1.5
S3	22.8	5.7	1.3	1.5
S4	24.5	6.2	1.4	1.5

3.4 Analysis 2 - Boundary Conditions at the Soil-Structure Interface

In Section 2.4.1, it was suggested that using fixed boundary conditions to model the boundary between the foundation slab and the subsoil may be non-conservative. To develop a complete three-dimensional FE-model of the surrounding soil is beyond the scope of this thesis; however, a simplified attempt was made, replacing the fixed vertical DOF with a linear elastic spring. The stiffness of the vertical springs was calculated according to [20] and is found in Appendix D. The rotational springs around the x- and y-axes used in Analysis 1, were retained in Analysis 2. The bridges covered in Analysis 2 were the slab bridge S0 and the portal frame bridge S0.

Further, the Young's modulus of the soil, presented in Table 3.3, is derived from long-term loading. The time of a train passage, however, is only a few seconds. It is well known that the Young's modulus tends to decrease with the load duration; therefore, it is likely that the actual stiffness of the soil subjected to train actions is much greater than the tabulated value. The increase in Young's modulus due to the shorter time duration might have a significant impact on the size of the response. This hypothesis was investigated for the S0-bridges, using a Young's modulus three times greater than E_{50}, both for the case with and without the vertical spring.

4 Results and Discussion

In this section, the results are followed directly by a discussion of each finding. Only the integral results are provided here: results of study (i)-(iii), synthesized results of study (iv)-(vii), and comments on the results of study (viii)-(ix) (for definition of the different studies, see Section 3.1). Study (ii), i.e. the parameter study of design speed, is incorporated in the results of study (i). Supplementary calculations, convergence studies, and more detailed information about the findings, can be found in the appendices. When referring to the absolute value of the peak acceleration (i.e. both negative and positive values), the term *maximum acceleration* is used. In situations where it is necessary to distinguish between the two, it is clearly specified what value that is associated with which acceleration. Furthermore, for simplicity, a linear variation is assumed between all measuring point in the graphs.

Worth noting is that no static verifications were performed (other than that of the section forces), i.e. all bridges except for the slab bridge S0 and the portal frame bridge S0 may have to be modified in reality to meet the static requirements. Such a modification (e.g. a thickness enlargement) probably changes the parameter study of the span length; however, this was not investigated.

4.1 Analysis 1A

The results from the analysis of the three-spanned slab bridges are presented in the graphs and tables below. The maximum accelerations almost exclusively appeared at the midpoint of the end span and the center span, denoted 1 and 2 in Figure 4.1. Therefore, the results of the parametric studies were extracted in these nodes. In the few cases where the location of the maximum vertical acceleration was not node 1 or 2, the deviation was considered negligible.

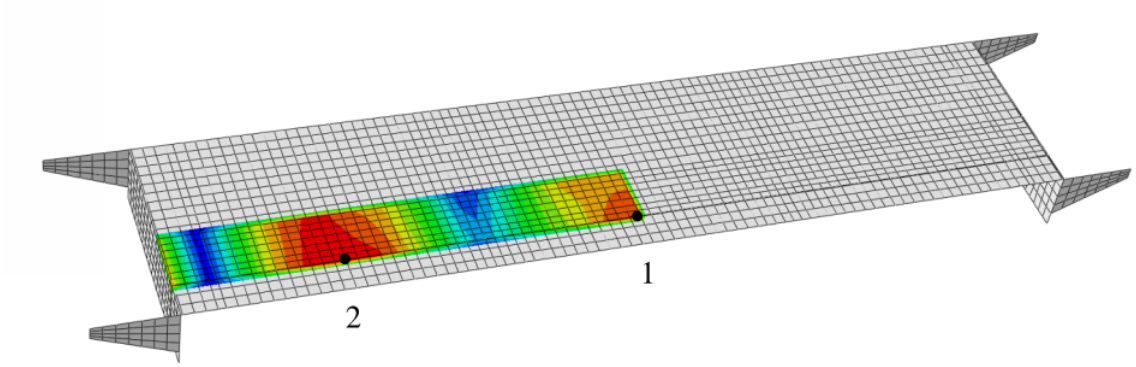

Figure 4.1: Deck output region according to Section 3.1.2.

4.1.1 Parametric study of span length (i)

The maximum acceleration of the bridge deck for the span lengths specified in Table 3.9 are provided in Figure 4.2. As can be seen, all bridges except for bridge S3 fulfill the requirement of maximum allowable acceleration when subjected to train loading with speeds in the interval 150-300 km/h. On the contrary, none of the bridges exhibit a maximum acceleration lower than 3.5 m/s^2 when the speed window is increased to 300-420 km/h. Noteworthy is also that the maximum acceleration of each speed interval is relatively constant up to bridge S2 (a magnification factor of 1.2). After this, critical point, the acceleration drastically increases. Although the breaking point is much more evident for the higher speed interval, the trend of the lower speed interval is similar. However, in practice it may be difficult to design bridges with span lengths of over 20 m (correspondent to bridge S2), without using a substantial amount of pretensioned tendons. Further, for both the lower and the higher speed interval, the density of the ballast does not seem to have a significant impact on the result. By applying a heavier ballast, the mass is increased by 115 tons in average for the slab bridges and 45 tons in average for the portal frame bridges, compared to the model with lighter ballast. Although these weight-increases are substantial, they only correspond to a 4 % change in total mass, which may explain the negligible difference in response.

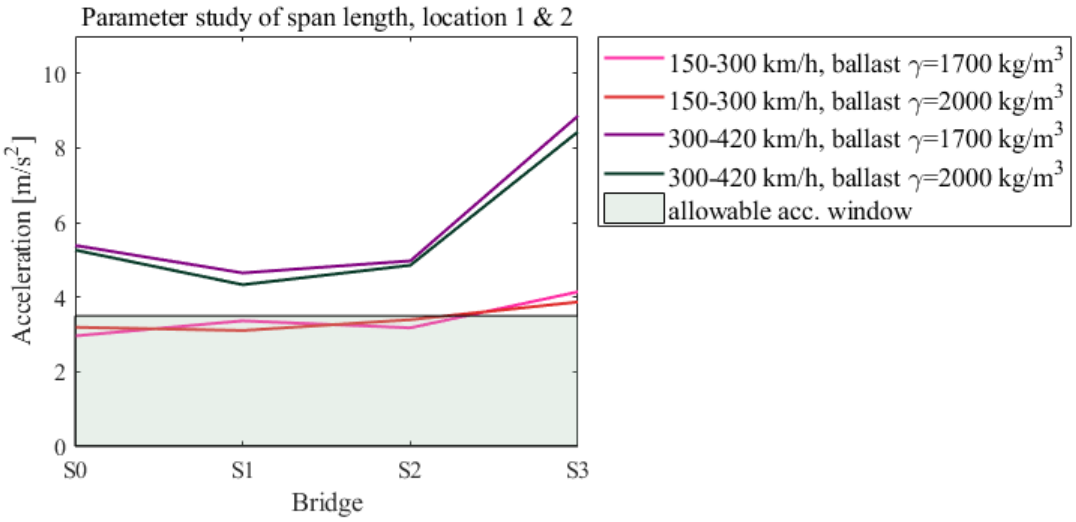

Figure 4.2: Maximum accelerations of the slab bridges with different span lengths.

Figures 4.3 and 4.4 show the variance in maximum vertical acceleration over the speed window. It is clear that the same location is not decisive for all bridges (location 1 for bridge S1 and S2, and location 2 for bridge S0 and S3). Further, the critical speed at which the acceleration limit is exceeded, appears to decrease with increasing span lengths. This might be because the frequency of the fundamental bending modes, which largely governs the response, also decrease with increasing span lengths, as the bridges become more slender (Tables A.1 and A.2 in Appendix A). The problem of keeping the acceleration within an acceptable limit for bridges S0-S2, should be manageable for a designer. By increasing the thickness and/or the amount of reinforcement, these bridges should be able to fulfill the design requirements. If a bridge with a length correspondent to that of bridge S3 is desired for train traffic with a track speed exceeding 300 km/h, a three-spanned slab bridge is not an appropriate choice of bridge design.

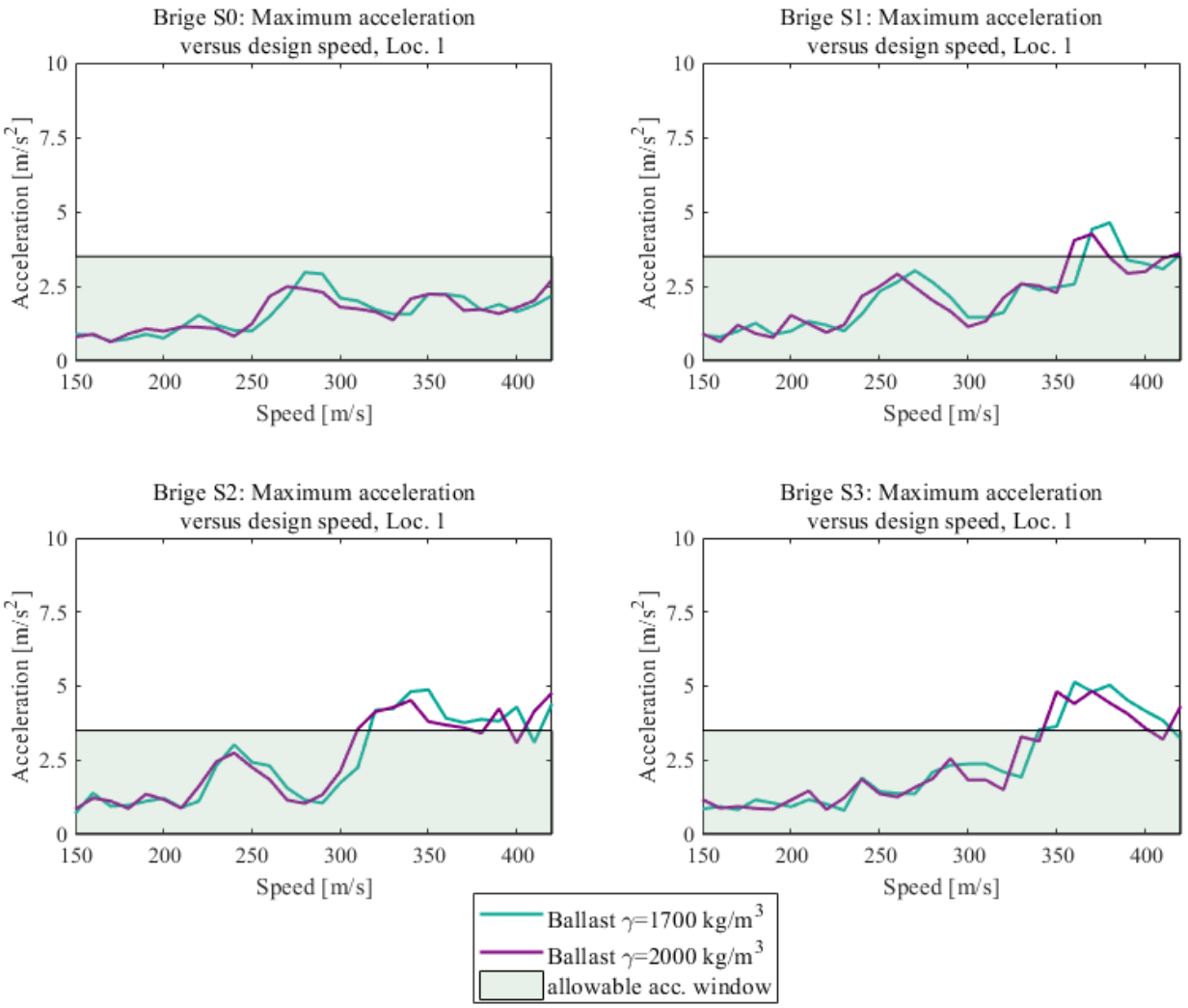

Figure 4.3: Maximum accelerations at different speed levels for the slab bridges at location 1.

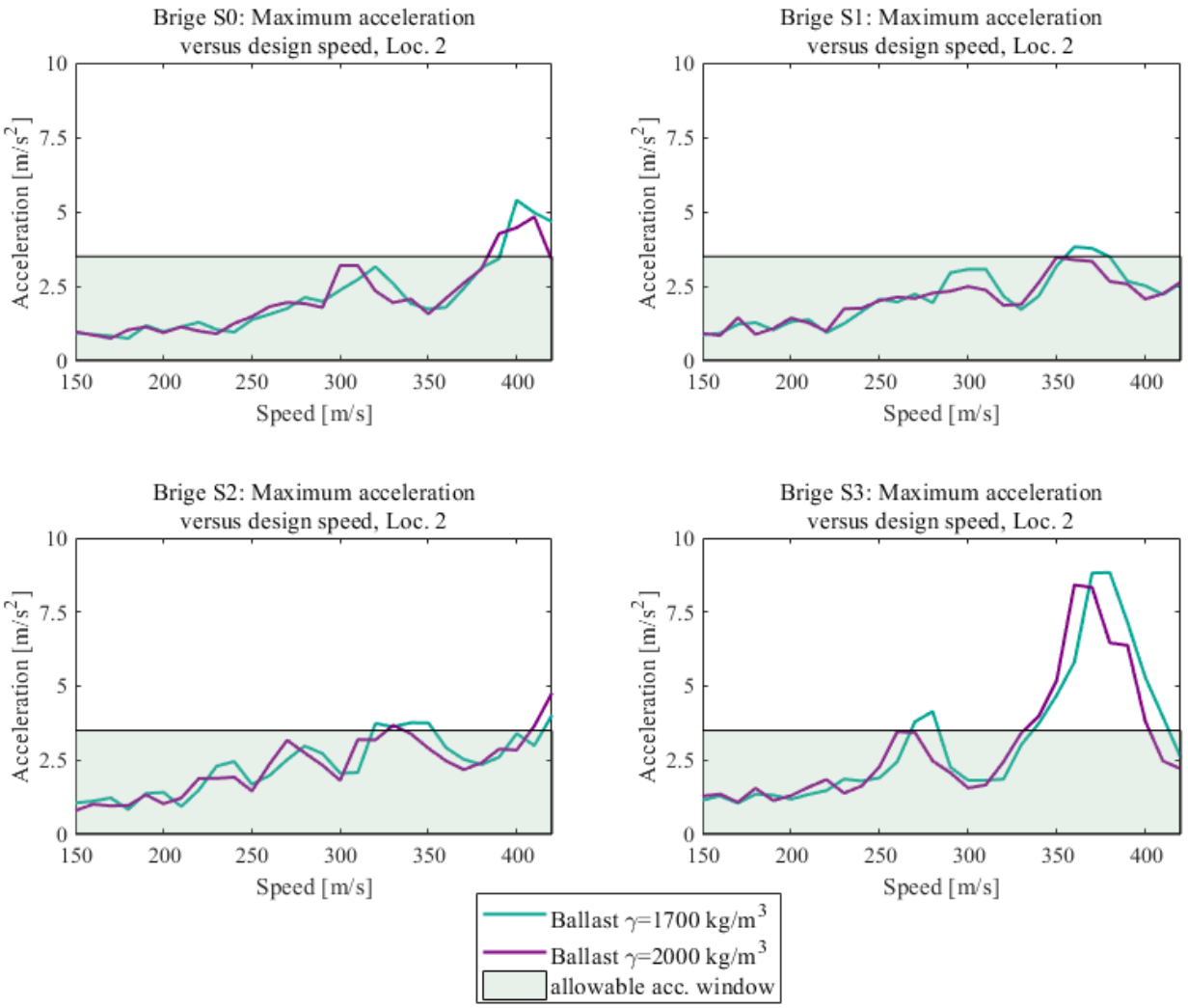

Figure 4.4: Maximum accelerations at different speed levels for the slab bridges at location 2.

4.1.2 Parametric study of thickness (iii)

As mentioned in Section 3.1, the thicknesses of the bridges S0, S1, S2 and S3, respectively, were enlarged until the maximum acceleration fell below 3.5 m/s^2. For the speed interval 150-300 km/h, a parametric study of the thickness only needed to be performed on S3, since all other bridges already met the requirements (Figure 4.2). For speeds of 300-420 km/h, a parametric study was necessary for all bridges.

The plots of maximum acceleration versus thickness are displayed in Figure 4.5. For the lower speed interval, it is demonstrated that only a 10% increase in thickness is sufficient to fulfill the design requirements (5% for the heavier ballast). Having in mind that the span length has been enlarged by approximately 30%, the thickness increase can be considered as rather small. The objective of enlarging the cross-section height of the bridge deck is to increase the stiffness and thereby also the natural frequencies and the critical train speed. However, a side effect of increasing the thickness is often that the mass is increased as well, counteracting the effect of the greater stiffness. As the increase in thickness proved to have a clear, positive impact on the result, it is suggested that the stiffness increases more relative to the mass when the cross-section is enlarged.

For the higher speed interval, there are odd breaking points in the graphs at which the slope changes significantly (as opposed to the lower speed interval where the response seemed to be decreasing linearly). This inconsistency may be due to the difference in which trains that are critical for the different thicknesses. For bridge S2 however, the same train is decisive for all thicknesses (Appendix G), which can explain why it exhibits a rather linear behavior. What is also striking about the results is that a greater enlargement is required for bridge S2 than bridge S3 to meet the allowable limit, which is further clarified in Figure 4.6. The authors found no simple explanation to this outcome.

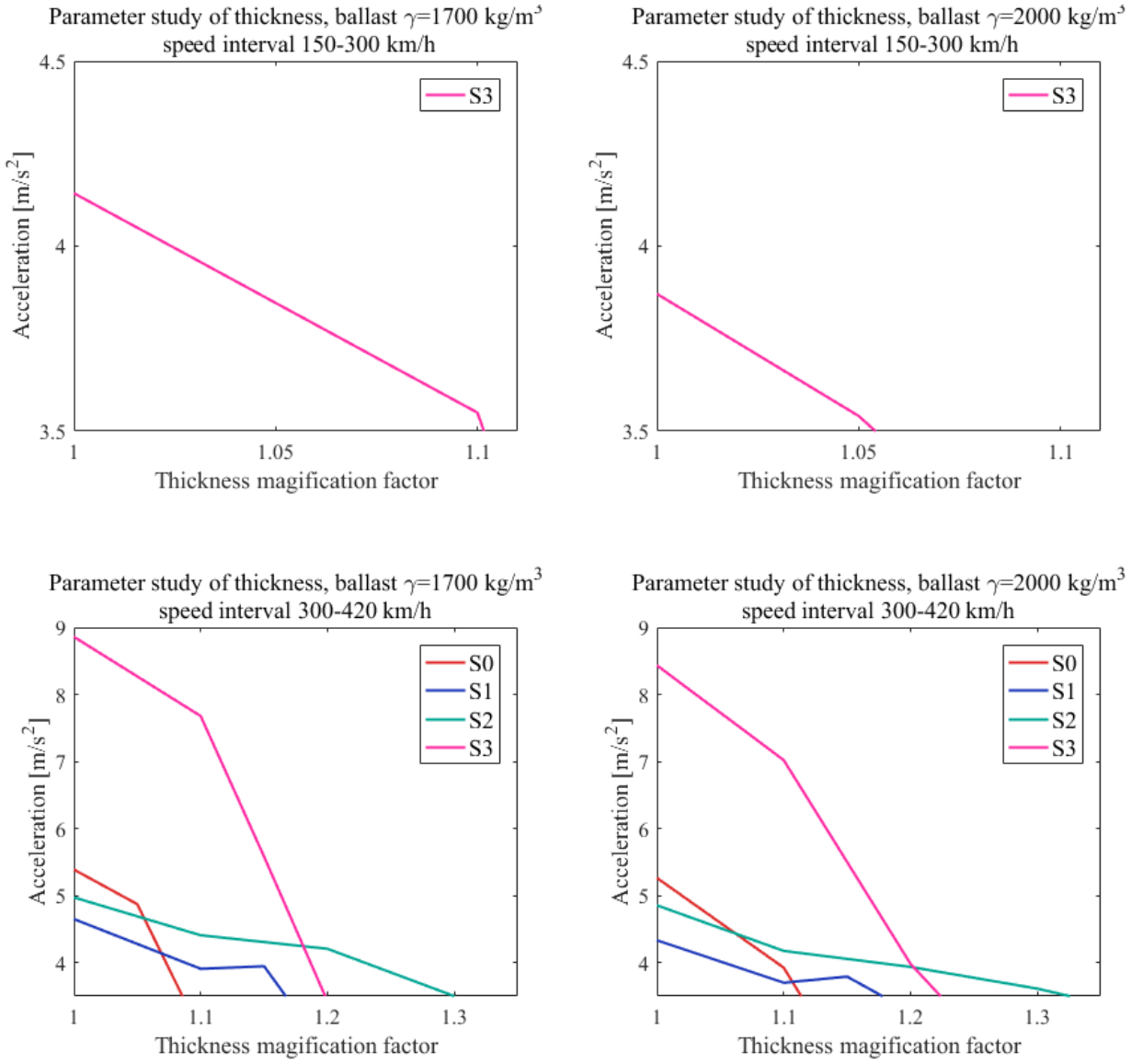

Figure 4.5: Maximum vertical acceleration of the bridge deck as a function of the thickness.

Figure 4.6 shows the needed enlargement in thickness (compared to the values specified in Table 3.8) to keep the accelerations within allowable limits. As can be seen, for span lengths up to the value of bridge S2, the thickness increases linearly with the span length. However, for the longest bridge, the required increase is smaller than what would be expected if bridge S3 had followed the same trend as the shorter bridges. It should be noted that the thickness of all bridges (except for bridge S0) will be enlarged in reality to fulfill the static requirements, i.e. the thickness increase is not only due to dynamics.

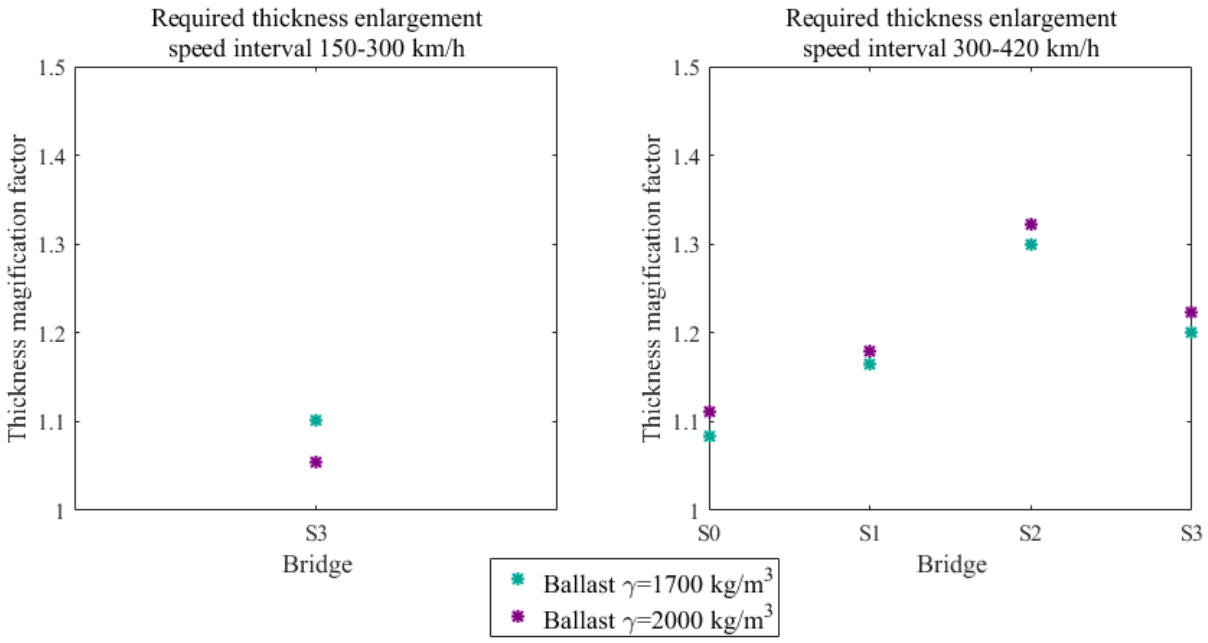

Figure 4.6: Required thickness enlargement for the slab bridges with different span lengths.

4.1.3 Deformation, torsion and rotation at bearings ((iv),(v),(vi)

Figures 4.7-4.9 below display the deformation at midspan, the relative torsion over the output width, and the angle of rotation at bearings. All three quantities are related to threshold values specified in the standards (for further description, see Appendix E).

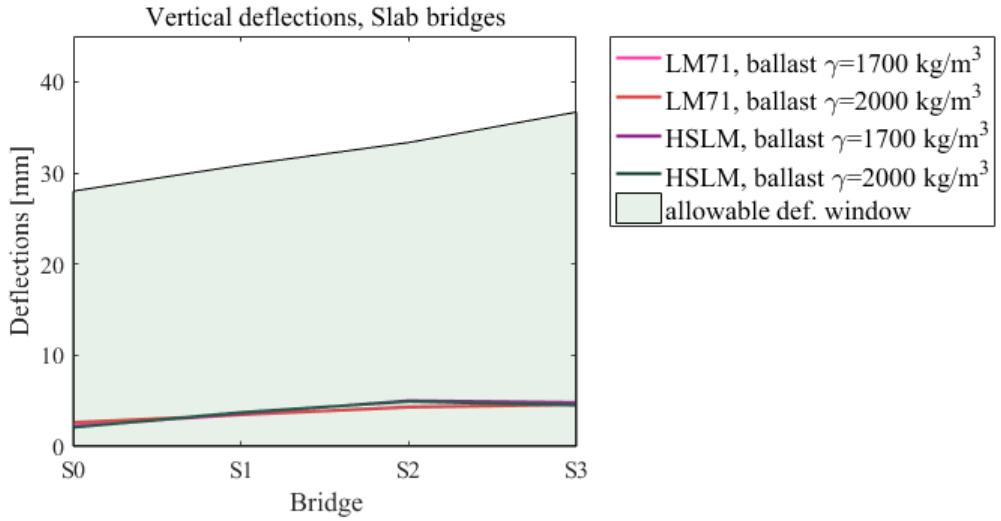

Figure 4.7: Deflections of the slab bridges with different span lengths.

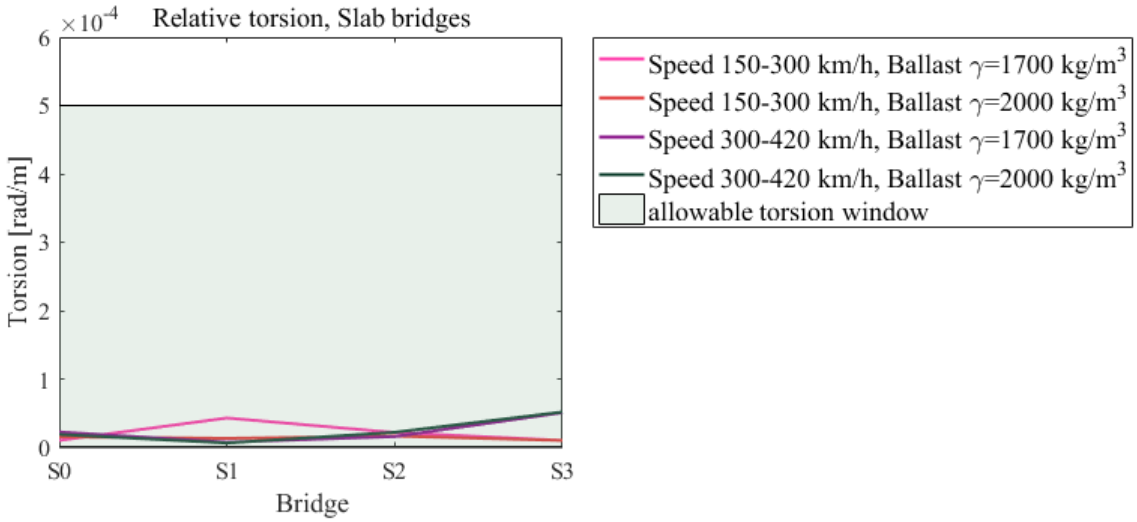

Figure 4.8: Maximum relative torsion of the slab bridges with different span lengths.

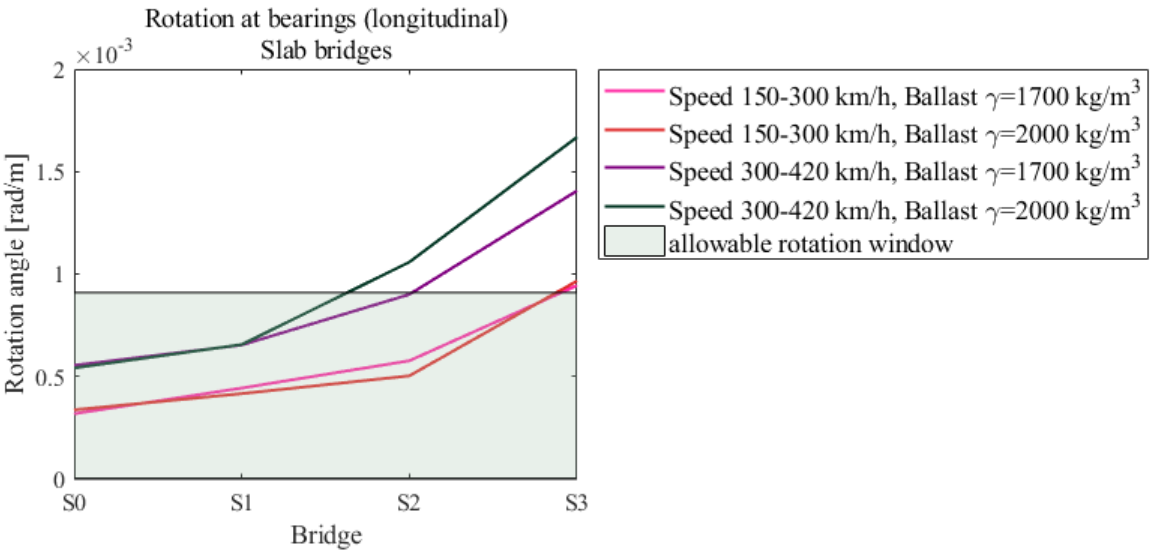

Figure 4.9: Maximum rotation angle of the slab bridges with different span lengths.

As can be seen, the torsion around the x-axis as well as the vertical deflection, are far below the maximum allowable limit for all span lengths. However, the rotational angle at the section of the bearings is acceptable for all bridges except for the one with longest spans (S2 and S3). It should be noted that the static demands most likely will require a thickness enlargement of the longer bridges; therefore, the large rotational angles may be a fictive problem.

4.1.4 Section forces (vii)

The design moments and shear forces for the slab bridges with a ballast density of 1700 kg/m^3 are provided in Figure 4.10. Corresponding graphs of the heavier ballast, along with tabulated values of the different dynamic amplifications factors, can be found in Appendix E. This is the only aspect of the study where there is an apparent difference in results of the two ballast densities; however, the same general conclusions apply. Note that the support moments are shown in terms of absolute values in the graphs, and that the moments includes both the bending moment and the corresponding torsion moment. Since the ratio between the dynamic and the static response (φ'_{dyn}) depends on the speed, the design values of the section forces were computed separately for the two speed intervals. As described in Section 2.5.1, the criterion used for verification of the section forces was that the design value obtained from HSLM loading should be less than that of LM71 loading. The comments below are valid for both ballast densities.

All bridges meet the requirement (with the exception of bridge S0 with a ballast density of 1700 kg/m^3) when φ'_{dyn} of the lower speed interval is used. In contrast, only bridge S0 (ballast density 1700 kg/m^3) passes the section-force-verification when using φ'_{dyn} of the higher speed interval. It should be noted that the design values were obtained by applying the maximum dynamic enhancement factor on the maximum moment. However, this may yield an overestimation of the static HSLM response, since the largest moment not necessarily coincides with the maximum value of φ'_{dyn}. Therefore, a more more thorough verification was conducted for the field moment of bridge S0 and S1: φ'_{dyn} was calculated for each train separately (within the design speed interval 300-420 km/h) and was then combined with the corresponding moment. The results, presented in Appendix E, suggest that the design value can change significantly if this method of verification is adopted. For the bridge S1 with lighter ballast, the design moment is reduced by almost 40 %. However, for the bridge S0, the same train yielded the largest moment and the maximum value of φ'_{dyn}, and therefore the more thorough verification did not change the design values.

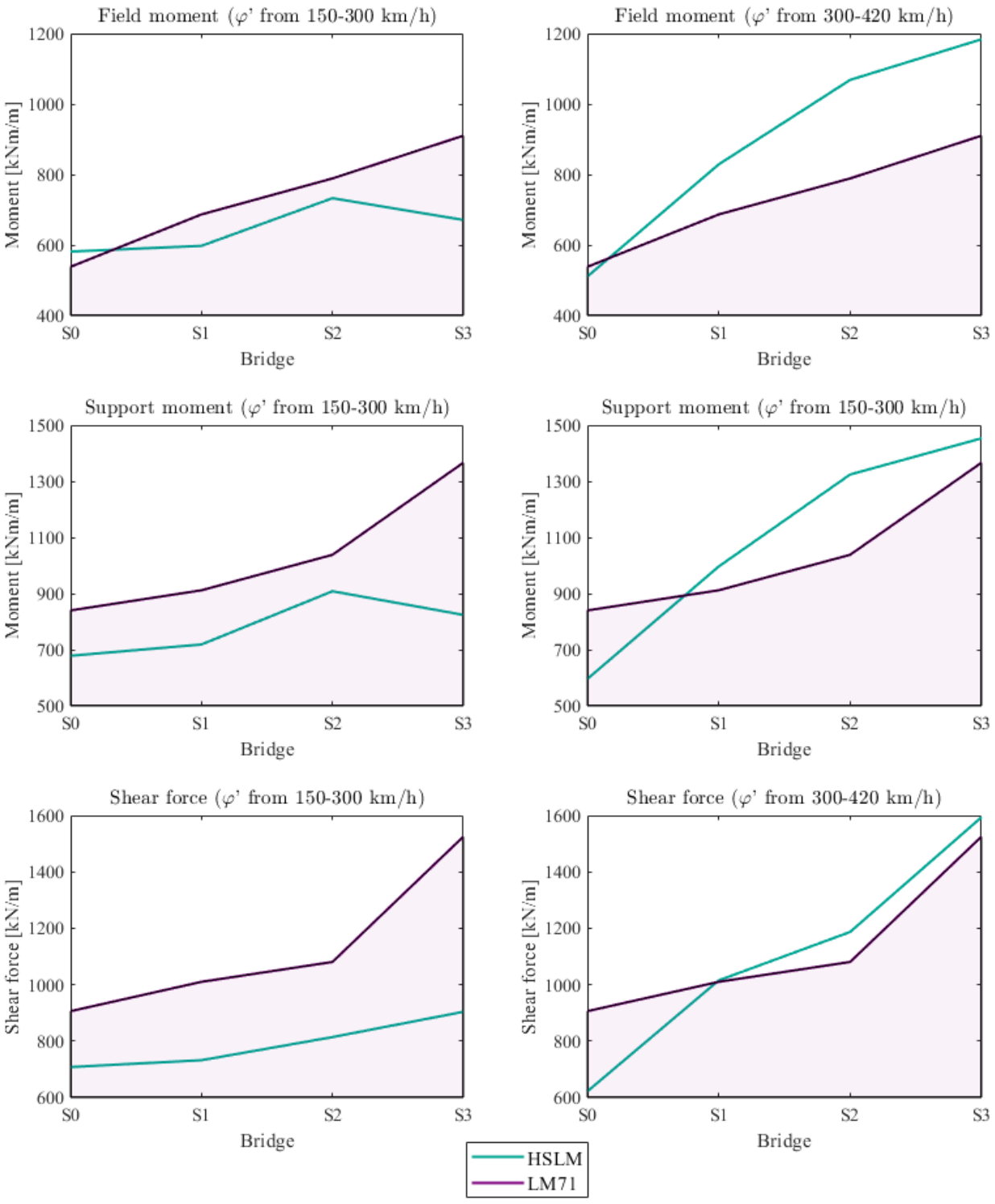

Figure 4.10: Design values of section forces of the slab bridges, obtained from analyses with HSLM and LM71, respectively, with a ballast density of 1700 kg/m^3. The results of the more thorough verification are not implemented in the graphs.

4.1.5 Loading frequencies and size of the output region (viii),(ix)

In Section 3.1, it was suggested that there may be a resemblance between the dominating eigenmodes and the loading frequencies. However, the results, presented in Appendix F, are not very encouraging as there are few cases that confirm the correlation between the frequency of the load and that of the dominating mode(-s). With that in mind, computing loading frequencies of trains with several coaches, different axle spacing, etc., is not a straightforward task. The method used may be an oversimplification, and a possible explanation to the inconsistent results.

Regarding the size of the output region, it was found that the variance in accelerations from an analysis of a wider output region was insignificant compared with that of the smaller strip (why the results of the wider region are not presented). The same applies for the portal frame bridges. This is not surprising, since the torsion modes' contribution to the total response is minor (Appendix A). It should however be noted that this choice might be decisive for other bridge designs. Since the Eurocode does not provide any clear guidelines, it is possible that designers use different approaches. Hence, this could result in more expensive, less competitive solutions with greater cross-section heights or more reinforcement for those who perform analyses on a wider output region.

4.2 Analysis 1B

For the portal frame bridge, the frequency window that needed to be taken into consideration (according to the standards), proved to be insufficient to obtain convergence in number of eigenmodes. In addition, the fundamental bending modes were not as decisive for the response as they were for the slab bridge; instead, several other modes were necessary to accurately describe the behaviour of the bridge at resonance. To reach convergence for the frame bridge S0, 100 modes corresponding to a frequency range up to 250 Hz, were required. Two consequences arose: all eigenmodes were included in the analysis; and the analysis of the loading frequencies lost its purpose. The maximum accelerations were found both at midspan and at a region close to the support (Figure 4.11). Since the behavior of the bridge is not the same in field and at support, the results are presented separately for region 1 and region 2.

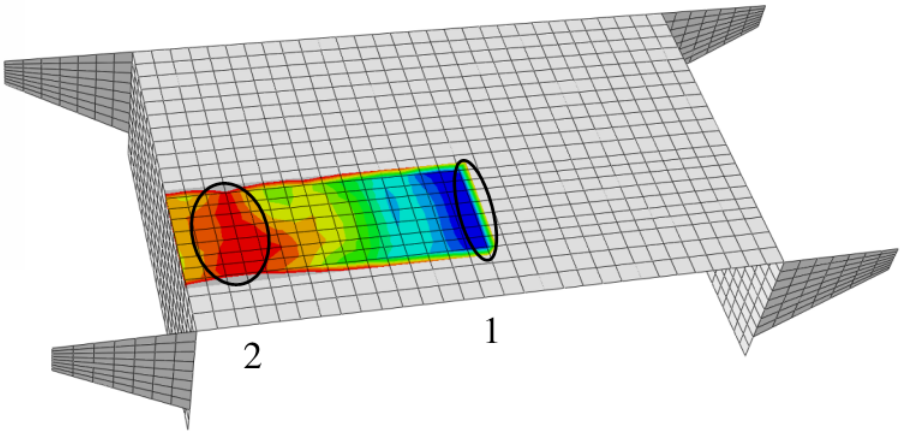

Figure 4.11: Region 1 and 2 where data was extracted.

4.2.1 Parameter study of span length (i)

Figure 4.12 plots the maximum accelerations as a function of the increase in span length according to Table 3.11. As shown in the figure, region 2 is critical for the shortest spans, whereas region 1 is critical for all other spans, when subjected to loading within the lower speed interval. Intuitively, it seems rather bizarre that the amplitude of the oscillation is greater at the support section rather than at midspan; however, this might be due to the greater stiffness of the shorter bridges. Although the location of the maximum acceleration was shifted to midspan when replacing the fixed vertical DOF with a vertical spring, the acceleration at the support section still exceeded 3.5 m/s^2. For the higher speed interval, region 1 is exclusively decisive for the response. Another surprising aspect of the data is that the response decreases with the span length for speeds of 150-300 km/h (up to bridge S3). Further, for the speed window of 300-420 km/h, there is a drastic increase in response between bridge S1 and S2. This demonstrates that the portal frame bridge is very sensitive to changes in span length, and that it is hard to predict whether the intended change will yield more favourable or unfavourable results. Hence, a linear variation between the data points might not be an appropriate choice. Additional data points between the existing points are also necessary to determine the exact breaking point of the graph. In accordance with the results of the slab bridges, the density of the ballast only has a minor impact.

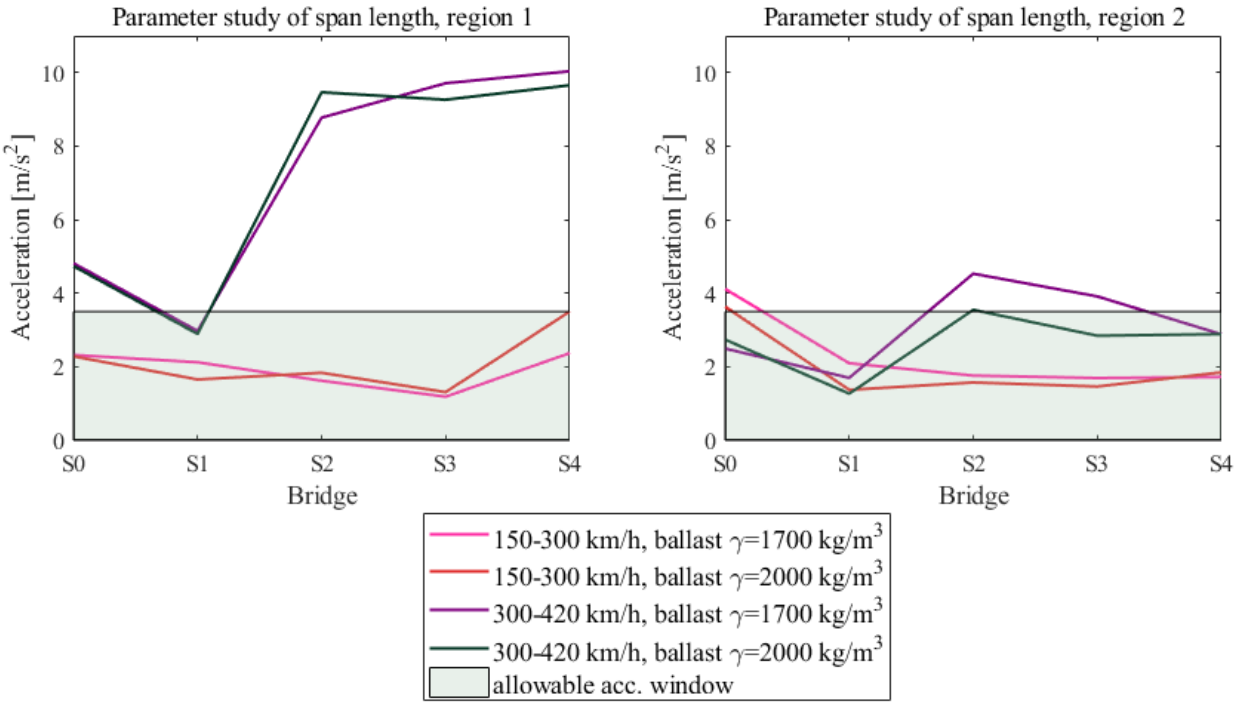

Figure 4.12: Maximum accelerations of the portal frame bridges with different span lengths.

The variance in maximum acceleration over the speed window for region 1 and 2 are provided in Figures 4.13 and 4.14, respectively. In agreement with the results of the slab bridges, the critical speed seems to decrease with increasing span length. It it also clear that the longer bridges, S2 and S3-S4, cannot be used for track speeds above 300 and 250 km/h, respectively. In contrast, the bridge S1 does not exceed the acceleration limit at any speed level. For the shortest bridge (S0), the limit is already exceeded at design speeds of 240 km/h at the support section, correspondent to a track speed of 200 km/h. In other words, either this span length is not an appropriate choice or the model is unable to describe the true behaviour of the bridge. Since the bridge S0 already exists in reality, the former seems unlikely. If the material model of the portal frame bridge is inadequate, all associated results should be interpreted with great caution. However, the large accelerations at the support section were only encountered for the bridge S0, which indicates that the modeling deficiency only has an apparent effect on the shortest bridge and not on all frame bridges. The modeling deficiency may concern the boundary conditions at the soil-structure interface, since the accelerations at support were reduced when a vertical spring was inserted. According to Section 2.4.1, SSI has a greater impact on short and stiff bridges, which further justifies that the results for all frame bridges except for S0 can still be considered reliable.

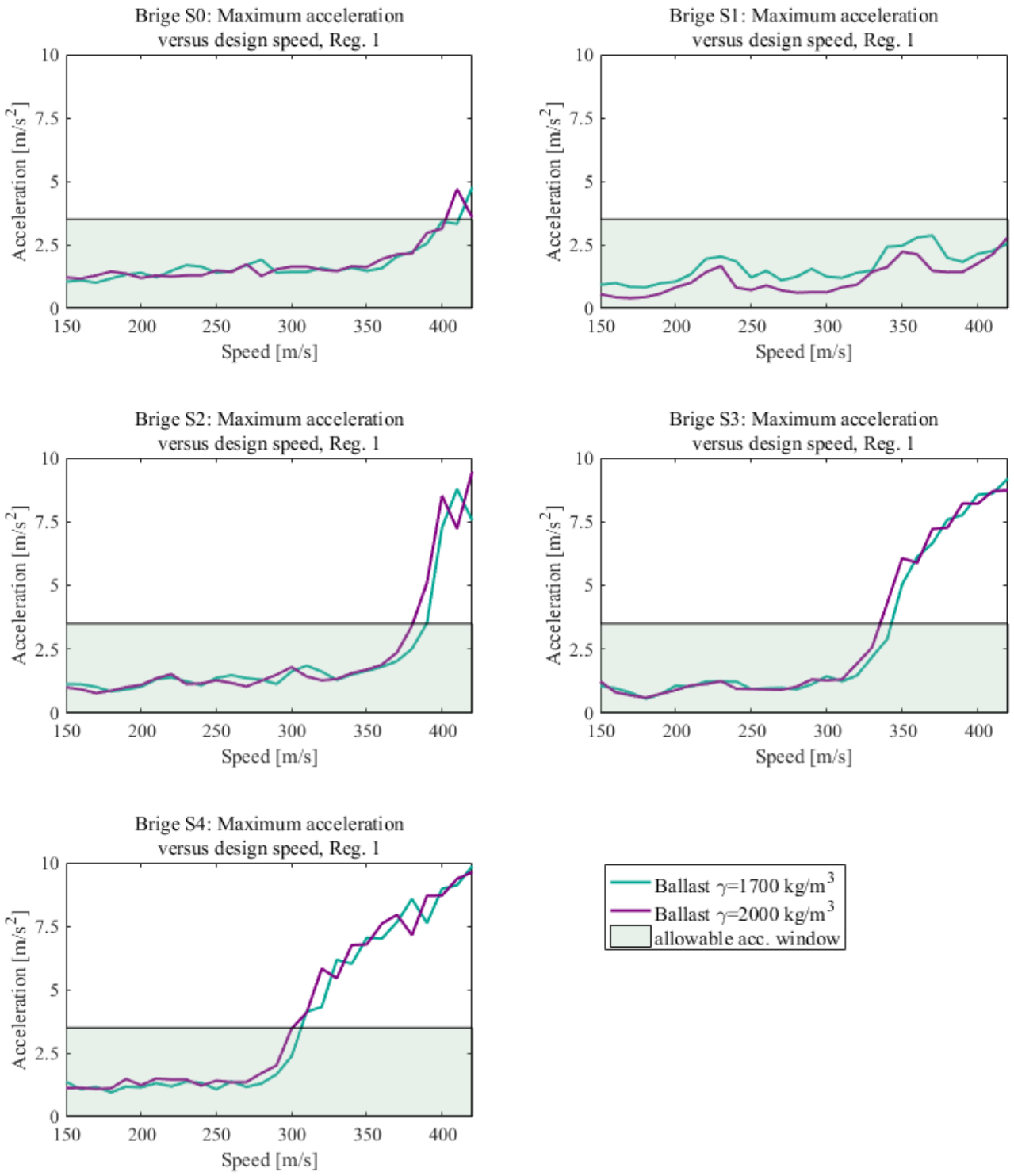

Figure 4.13: Maximum vertical acceleration of the bridge deck as a function of the speed for the portal frame bridges in region 1.

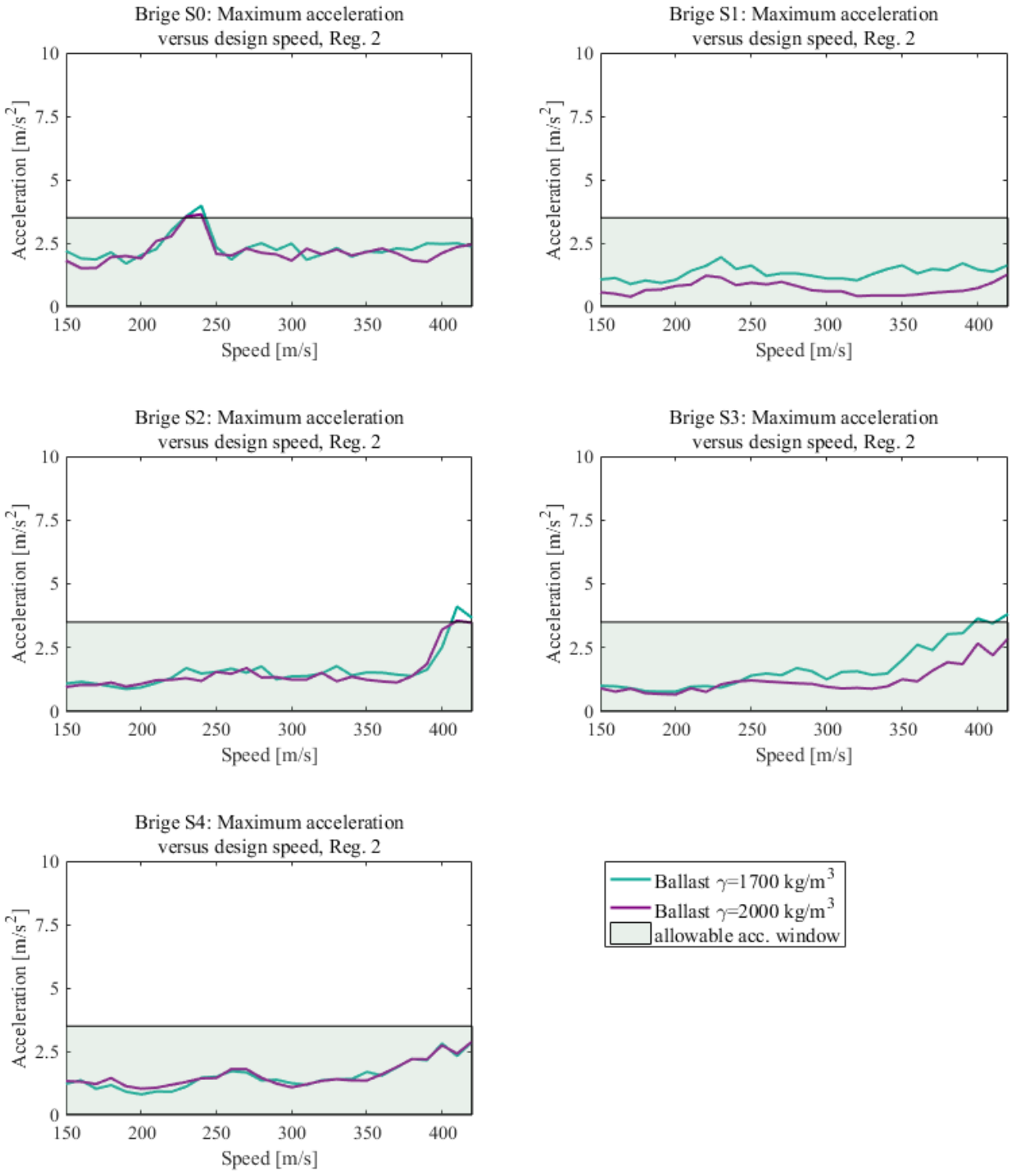

Figure 4.14: Maximum vertical acceleration of the bridge deck as a function of the speed for the portal frame bridges in region 2.

4.2.2 Parameter study of thickness (iii)

The results of the parameter study of the thickness, performed on the bridges that did not meet the design requirements, are displayed in Figure 4.15. In contrast to the results of the slab bridges, the necessary thickness enlargement appears to be rather proportional to the increase in span length (compared with the measures of bridge S0). This becomes even more evident in Figure 4.16, where the thickness almost increases linearly with the span length.

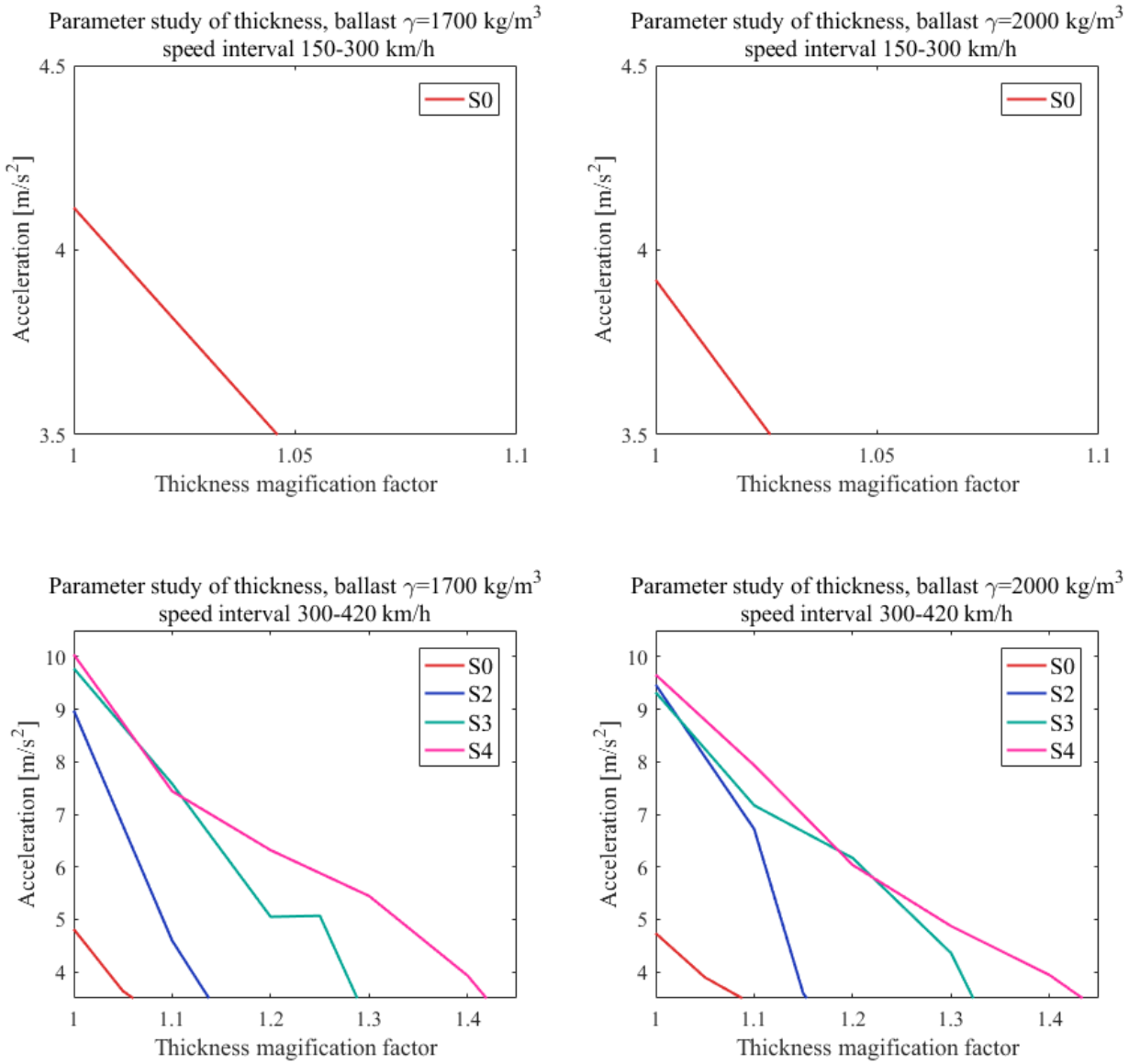

Figure 4.15: Maximum vertical acceleration of the bridge deck as a function of the thickness for the portal frame bridges.

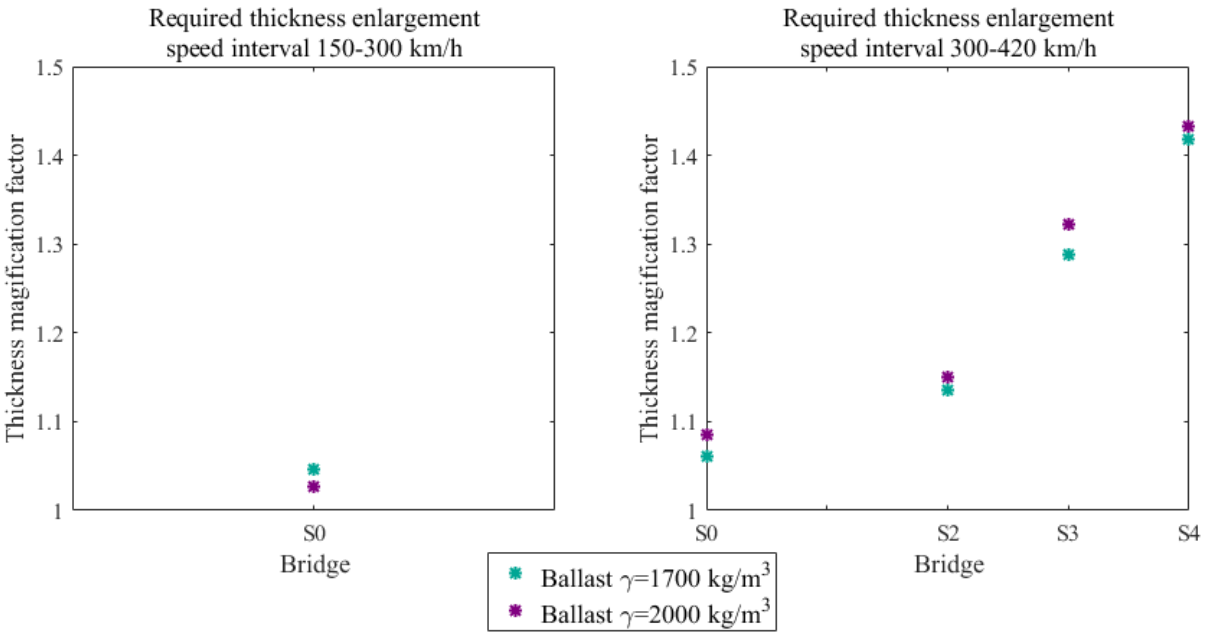

Figure 4.16: Required thickness enlargement for the portal frame bridges with different span lengths.

4.2.3 Deformation and torsion (iv,v)

The deformation at midspan and the maximum relative torsion of the portal frame bridges with different span lengths, are provided in Figures 4.17 and 4.18. Note that the rotation at bearings is not applicable for the frame bridges. The same observations as for the slab bridges can be made: the responses are well below the threshold values. More detailed information about the findings can be found in Appendix E.

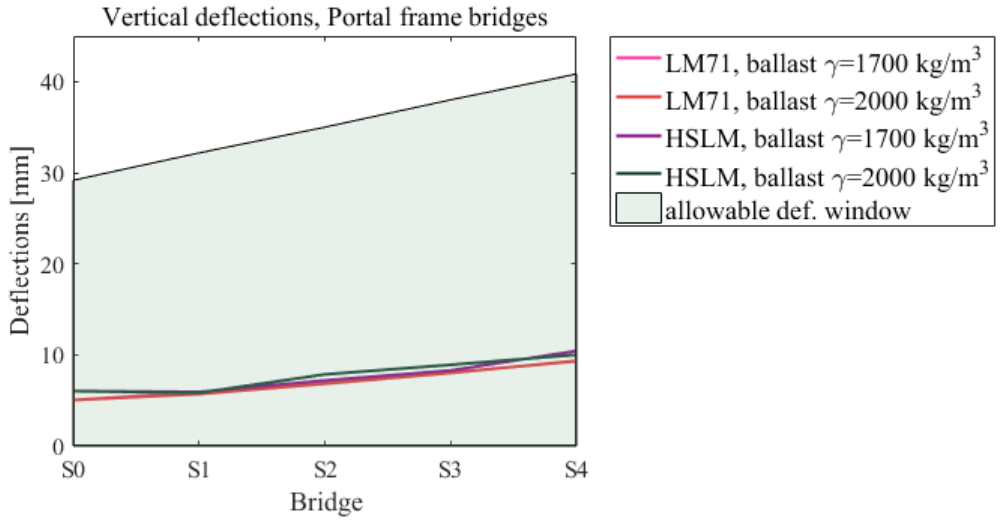

Figure 4.17: Deflection of the portal frame bridges with different span lengths.

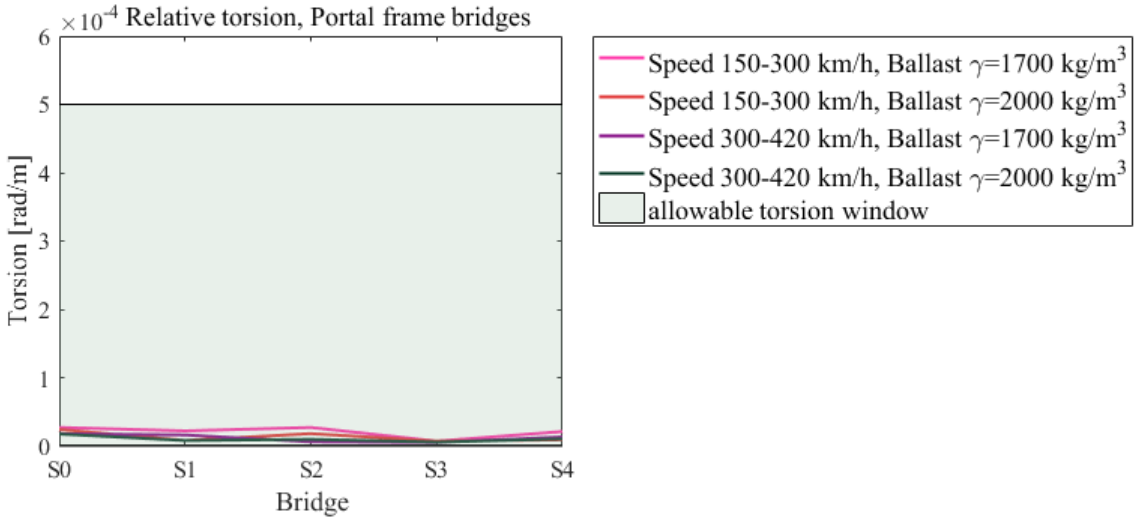

Figure 4.18: Maximum relative torsion of the portal frame bridges with different span lengths.

4.2.4 Section forces (vii)

The design moments and shear forces of the portal frame bridges with a ballast density of 1700 kg/m^3 are shown in Figure 4.19. The same information that was presented for the slab bridges (page 59) applies for the frame bridges. From the graphs it can be concluded that the shortest bridges, S0 and S1, exceed the acceptable limit when φ'_{dyn} of the lower speed interval is used. However, these bridges are well below the threshold values for the case with φ'_{dyn} taken from the higher speed interval. To investigate whether the suspiciously high values of the lower speed interval were due to an overestimation of the dynamic amplification of the section forces, a more thorough verification was performed analogous to that of the slab bridges. Since the same train yielded the largest section forces and the maximum value of φ'_{dyn}, this verification did not change the design values.

As described in Section 3, industry practice is often to design the bridge from static analyses using LM71, SW/0, or any other equivalent load model, where the dynamic magnification is accounted for by the factor ϕ. If the dynamic analysis with HSLM-trains then generates greater responses, as for the case with the bridges S0 and S1, the bridge-dimensions and the amount of reinforcement have to be modified to meet the dynamic requirements. Subsequently, the original static analysis must be redone with the new dimensions, which increases the amount of work for the designer. In other words, the load factor ϕ has underestimated the dynamic magnification. However, this study is not comprehensive enough to draw any general conclusions on whether this is a real deficiency in the standards or if it is simply due to modeling errors.

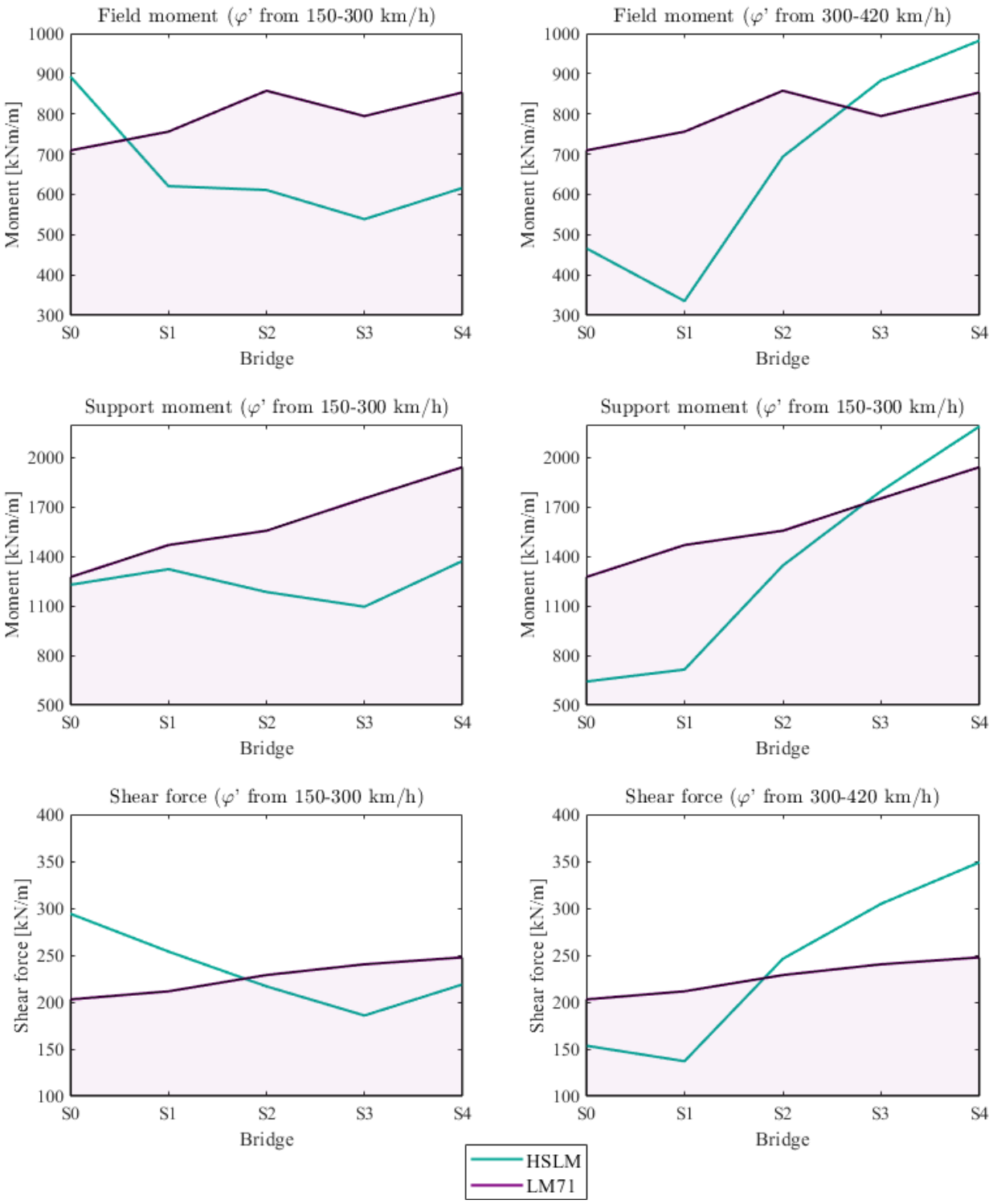

Figure 4.19: Design values of section forces of the portal frame bridges, obtained from analyses with HSLM and LM71, respectively, with a ballast density of 1700 kg/m^3. The results of the more thorough verification are not implemented in the graphs.

4.3 Analysis 2

Tables 4.1 and 4.2 show the results of analyses performed with modifications of the models used in Analysis 1: (a) an increased elastic modulus of the soil (three times greater than the value specified in Table 3.3); (b) a replacement of the fixed vertical DOF with an linear elastic spring; and (c) the combination of (a) and (b). The slab bridge S0 and the portal frame bridge S0 were investigated, and the accelerations were then related to those of the Analysis 1. The data are not consistent; yet it suggests that the acceleration decreases when the strength of the soil is increased for the frame bridge. Further, the vertical spring, implying a reduction in vertical stiffness, yields higher accelerations. However, for the case with both an increased Young's modulus and a vertical spring, no conclusions can be drawn. For the slab bridge, no trends could be identified for any of the scenarios.

Table 4.1: Case study of different boundary conditions for the slab bridge S0. The accelerations are related to those of Analysis 1A (Appendix G), which is referred to as the deviation. The scenarios that yielded a lower acceleration than that of the reference case are highlighted in green.

Ballast density $[kg/m^3]$	Speed interval [km/h]		Increased E-modulus		Vertical spring		Both	
			Acc $[m/s^2]$	Deviation [%]	Acc $[m/s^2]$	Deviation [%]	Acc $[m/s^2]$	Deviation [%]
1700	150-300	Max	2.736	-5	2.398	-17	2.435	-15
		Min	-2.940	-1	-2.543	-14	-2.601	-12
	300-420	Max	4.487	2	4.807	9	4.690	6
		Min	-5.209	-3	-4.492	-17	-4.466	-17
2000	150-300	Max	2.898	1	2.222	-22	2.744	-4
		Min	-3.011	-6	-2.357	-26	-2.87	-10
	300-420	Max	4.445	0	4.61	4	3.352	-25
		Min	-5.095	-3	-4.477	-15	-3.773	-28

Table 4.2: Case study of different boundary conditions for the portal frame bridge S0. The accelerations are related to those of Analysis 1B (Appendix G), which is referred to as the deviation. The scenarios that yielded a lower acceleration than that of the reference case are highlighted in green.

Ballast density $[kg/m^3]$	Speed interval [km/h]		Increased E-modulus		Vertical spring		Both	
			Acc $[m/s^2]$	Deviation [%]	Acc $[m/s^2]$	Deviation [%]	Acc $[m/s^2]$	Deviation [%]
1700	150-300	Max	2.907	-29	4.349	6	3.284	-20
		Min	-2.507	-11	-4.414	57	-3.451	23
	300-420	Max	4.450	-6	6.641	41	6.917	47
		Min	-5.329	11	-7.364	53	-7.412	54
2000	150-300	Max	3.115	-21	4.736	21	3.635	-7
		Min	-2.525	-10	-4.734	70	-3,199	15
	300-420	Max	4.395	-10	7.156	58	7.209	59
		Min	-5.406	14	-8.108	71	-8.131	72

5 Concluding Remarks

In this thesis, the aim was to investigate how the response of railway bridges, subjected to high-speed train loading, changes when three parameters are varied: span length; track speed; and cross-section height. Through dynamic analyses with universal trains, the vertical acceleration of the bridge deck, as well as the deflection, the torsion, the rotation at bearings the section forces, were evaluated. The work has also emphasized some of the modeling issues that bridge designers are facing, in particular the representation of the boundary between the foundation and the subsoil. The results of this study may be used in an initial phase to assess the suitability of different bridge designs, and also to indicate whether the existing bridges can withstand higher train speeds.

5.1 Conclusions

The conclusions based on the findings in Section 4 are compiled in the list that follows. Note that these conclusions are based on a small sample of data, and that more comprehensive research is required to validate the results.

- The vertical acceleration of the bridge deck is not always the governing parameter of the design. For the shortest bridges (the slab bridge S0 and the portal frame bridge S0) in the track speed interval 125-250 km/h, the section forces are decisive.

- The critical track speed for the current bridges on the railway network (here here represented by slab bridge S0 and portal frame bridge S0) regarding the vertical acceleration of the bridge deck seems to be 330 km/h. Note that the acceleration at the support section for the frame bridge is ignored.

- The choice of dynamic enhancement factor (φ'_{dyn}) greatly affects the design values of the section forces. For a design speed spectra of 150-420 km/h, the results varies depending on which value of φ'_{dyn} being used: φ'_{dyn} computed from the lower bound (150-300 km/h); φ'_{dyn} computed from the higher bound (300-420 km/h); or φ'_{dyn} taken as the average value of the two intervals.

- The density of the ballast has no significant impact on the response.

- SSI seems to have a great impact on the shortest portal frame bridge. Since the model only includes a very idealized representation of these boundary conditions, the results associated with the frame bridge S0 should be interpreted with caution.

- The response of the slab bridge can, to a reasonable degree of accuracy, be described by the fundamental bending modes. For the portal frame bridge, however, these

modes only represent about 50 % of the total response. To reach convergence in number of eigenmodes, a large number of modes, with a frequency that is much higher than what is stated in the standards, must be included in the analyses.

- The span length is a very sensitive parameter of the design: a change of 10% could increase the acceleration by a factor 2 for the slab bridge and by a factor 3 for the frame bridge. On the contrary, for certain ranges of span length, an increase may result in lower accelerations. The relation between the magnification of the span length and the response is in general not linear.
- A thickness enlargement reduces the value of the maximum acceleration.
- The investigated method for computing loading frequencies, fails to confirm the correlation between these frequencies and those of the dominating eigenmodes.
- An increased elastic modulus of the soil, better resembling the strength of the soil when subjected to loading with short duration, tends to decrease the response.
- For the portal frame bridge, a vertical spring increases the maximum accelerations by up to 70% compared to the case with a fixed vertical DOF. However, the results regarding the SSI should be treated with extreme caution. Several factors that could have a large impact on the response have been neglected, including the overlaying soil masses on the foundation as well as the damping and frictional properties of the soil.
- There is no significant difference in accelerations obtained from an analysis with an output region correspondent to a small strip underneath the track, and that of a wider output region stretching to the longitudinal edge of the bridge deck. It should be noted that this conclusion only applies for bridges of uniform thickness. For other bridge types, such as beam bridges with cantilevered beams, the choice of output region may be critical.

5.2 Proposal for Further Work

As has been stressed multiple times, there is a clear need of further research within the field of high-speed railway bridges and SSI. A natural progression of this work is to perform analyses with HSLM-trains on a full-scale FE-model, including both the bridge structure and the surrounding soil. Perhaps, the increased acceleration due to the non-infinite vertical stiffness of the soil, can be partially compensative by the retaining soil masses above the foundations and on the sides of the bridge. The results could be used as a basis for establishing actual guidelines of how and when SSI should be included in an analysis, to obtain moderately conservative results. Obviously, the proposed method has to be computationally cheap, in order to be implemented by designers in practice. Furthermore, a comprehensive study of the section forces, and in particular the choice of dynamic magnification factors, is necessary to validate the results of this study. If the same conclusions is obtained from such a study, the formula of ϕ (Equation 2.26) should be revised to more accurately account for the dynamic amplification. Another area that would be interesting to investigate further, is the potential relationship between the loading frequency and the dominating eigenmodes. If such a link could be established, the analysis time could drastically be reduced. For this study, a more sophisticated way of determining the frequency of the trains would be required.

References

[1] M. Zacher, M. Baeβle (2009), *Dynamic behaviour of ballast on railway bridges, In: Dynamics of High-Speed Railway Bridge*, Taylor & Francis Group, London, pp. 99-112.

[2] Trafikverket (2016), *Krav Brobyggande*, Document: TDOK 2016:0204.

[3] Trafikverket (2018), *Ostlänken*, https://www.trafikverket.se/nara-dig/projekt-i-flera-lan/Ostlanken/, Online; accessed 2019-02-20.

[4] Nytt från Öresund (2016), *Tre skånska stopp för nytt snabbtåg*, 1 februari, http://nfo.nu/?p=139935.

[5] SS-EN 1991-2 (2003), *Eurokod 1: Laster på bärverk - Del 2: Trafiklast på broar*, Swedish Standards Institute.

[6] Ottosen, N. & Petersson, H. (1992), *Introduction to the Finite Element Method*, Lunds University, ISBN-13: 978-0-13-473877-2.

[7] Chopra. A (2014), *Dynamics of Structures*, Pearson, ISBN-13: 978-0-273-77424-2.

[8] Sharcnet (n.d.), *Abaqus Analysis User's Manual*, https://www.sharcnet.ca/Software/Abaqus610/Documentation/docs/v6.10/books/usb/default.htm?startat=pt01ch01s01abo01.html.

[9] Diana FEA (2010), *Diana User's Manual 32.4.3 Hilber-Hughes-Taylor*, https://dianafea.com/manuals/d942/Diana.html.

[10] Frýba. L (1996), *Dynamics of railway bridges*, Thomas Telford, ISBN 0 7277 2044 9.

[11] DNV/Risø (2009), *Guidelines for Design of Wind Turbines*.

[12] Ishihara K. (1996), *Soil Behaviour in Earthquake Geotechnics*, Oxford: Oxford University Press.

[13] Zangeneh Kamali, A. (2018), *Dynamic Soil-Structure Interaction Analysis of Railway Bridges: Numerical and Experimental Results*, Licentiate Thesis, Stockholm (Sweden): Royal Institute of Technology.

[14] Gazetas G. (1991), In *Foundation Engineering Handbook* (2nd ed., Chapter 15), New York: Van Nostrand Reinhold.

[15] Ülker-Kaustell M. (2009), *Some aspects of the dynamic soil-structure interaction of a portal frame railway bridge*, Licentiate Thesis 102, Stockholm (Sweden): Royal Institute of Technology.

[16] Andersson A., Battini, J.M., Ülker-Kaustell M. and Östlund, J. (2009), *Considering dynamic soil-structure interaction in design of high-speed railway bridges*, Procedia Engineering vol. 199 page 2384-2389, Elsevier Ltd.

[17] SS-EN 1990 (2002), *Eurokod - Grundläggande dimensioneringsregler för bärverk*, Swedish Standards Institute.

[18] Boverket (2013), *Boverkets författningssamling BFS 2013:10 EKS 9*.

[19] Trafikverket (2011), *TK Geo 11 - Trafikverkets tekniska krav på geokonstuktioner*.

[20] Scanscot Technology (2015), *BRIGADE/Standard Theory manual*.

[21] Trafikverket (2016), *Råd Brobyggande*, Document: TDOK 2016:0203.

Appendix A - Convergence Studies

In the following figures, convergence studies associated with Analysis 1 are shown. The value of the element size, the time step and the number of eigenmodes that were considered sufficient to fulfill convergence, are specified in the caption of the figures. For convergence in element size and number of eigenmodes, a tolerance of 1% was adopted. For convergence in time step and number of eigenmodes, only the negative maximal vertical acceleration is presented in the graphs; however, the results of the positive acceleration were essentially identical.

Convergence in element size

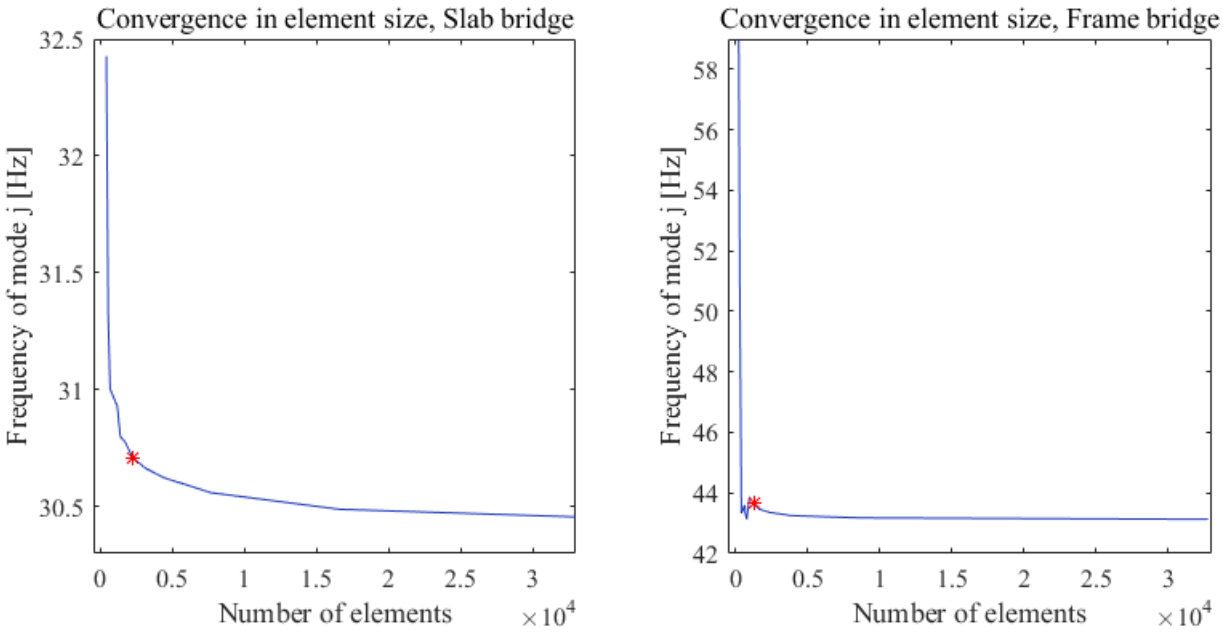

Figure A.1: An element size of $0.6x0.6m^2$ was chosen. This value corresponds to 2252 elements for the slab bridge S0, and 1278 elements for the portal frame bridge S0, respectively, highlighted with red dots in the graphs. Mode j is the highest mode considered in the analysis.

Convergence in time step

To obtain enough resolution in the graphs, a time window of 0.25 s was used. The results of the speed interval 150-300 km/h were similar to those of the speed interval 300-420 km/h; hence, only the results of the lower speed interval are provided.

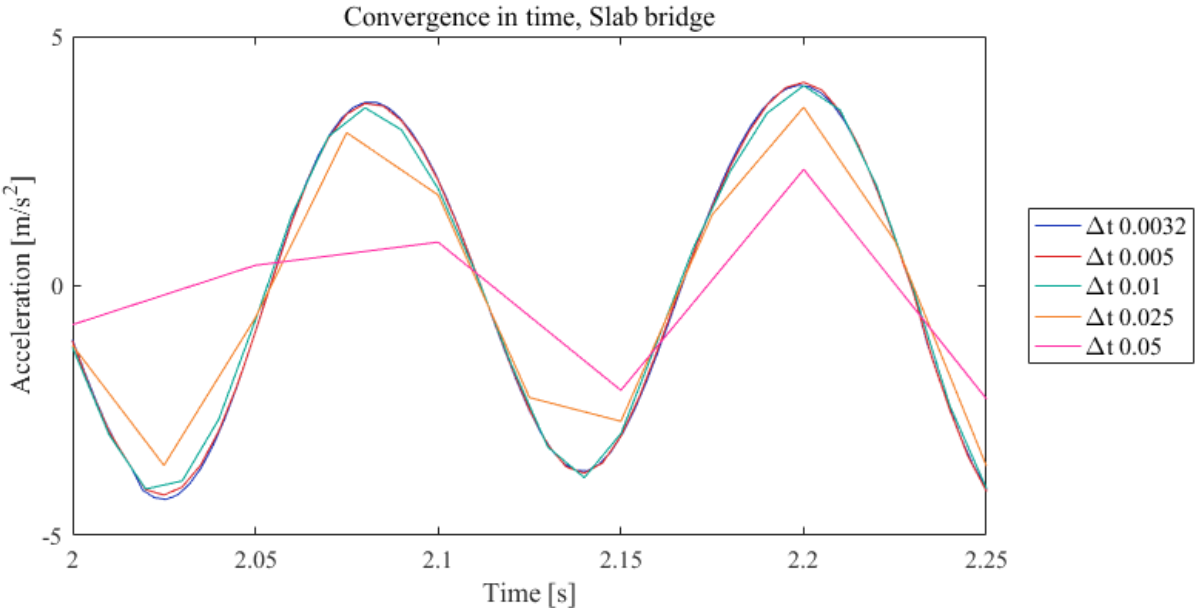

Figure A.2: The time step $\Delta t = 0.01$ was chosen for the slab bridges.

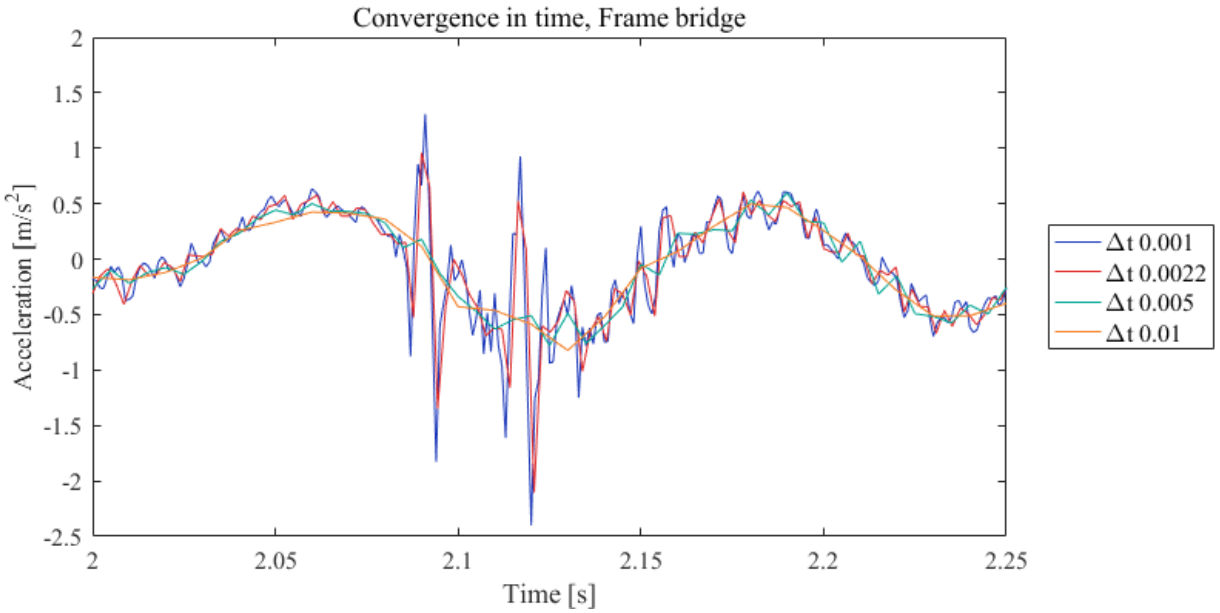

Figure A.3: The time step $\Delta t = 0.0022$ was chosen for the portal frame bridges.

Convergence in number of eigenmodes

Only the results of the slab bridges are shown in the tables and graphs below. For the portal frame bridges, a massive amount of modes proved to be necessary to reach convergence in element size (e.g. 100 modes for frame bridge S0), and therefore, these results are not provided.

Table A.1: Convergence study of the slab bridges with a ballast density of 1700 kg/m^3. The two modes that gave the greatest contribution to the total response for each bridge are specified in terms of frequency and percental contribution to the total response (compared to the case where all modes were included).

Bridge	Speed interval [m/s]	Eigenmodes required for convergence	Dominating modes (% of response & Frequency)
S0	150-300	1-8	1:st bending mode (80 %), 6.78 Hz 3:rd bending mode (12 %), 10.93 Hz
	300-420	1-8	1:st bending mode (19 %), 6.78 Hz 2:nd bending mode (77 %), 8.54 Hz
S1	150-300	1-16	1:st bending mode (34 %), 5.70 Hz 2:nd bending mode (61 %), 7.29 Hz
	300-420	1-18	1:st bending mode (85 %), 5.70 Hz 3:rd bending mode (8 %), 9.31 Hz
S2	150-300	1-9	1:st bending mode (86 %), 4.96 Hz 3:rd bending mode (10 %), 8.09 Hz
	300-420	1-5	1:st bending mode (86 %), 4.96 Hz 3:rd bending mode (10 %), 8.09 Hz
S3	150-300	1-24	1:st bending mode (23 %), 4.94 Hz 2:nd bending mode (57 %), 5.74 Hz
	300-420	1-5	1:st bending mode (12 %), 4.94 Hz 2:nd bending mode (91 %), 5.74 Hz

Table A.2: Convergence study of the slab bridges with a ballast density of 2000 kg/m^3. The two modes that gave the greatest contribution to the total response for each bridge are specified in terms of frequency and percental contribution to the total response (compared to the case where all modes were included).

Bridge	Speed interval [m/s]	Eigenmodes required for convergence	Dominating modes (% of response & Frequency)
S0	150-300	1-15	1:st bending mode (21 %), 6.62 Hz 3:rd bending mode (75 %), 8.36 Hz
	300-420	1-9	1:st bending mode (21 %), 6.62 Hz 2:nd bending mode (75 %), 8.36 Hz
S1	150-300	1-20	1:st bending mode (86 %), 5.57 Hz 3:nd bending mode (8 %), 9.10 Hz
	300-420	1-18	1:st bending mode (87 %), 5.57 Hz 3:rd bending mode (7 %), 9.10 Hz
S2	150-300	1-5	1:st bending mode (18 %), 4.84 Hz 2:rd bending mode (79 %), 6.21 Hz
	300-420	1-5	1:st bending mode (88 %), 4.84 Hz 3:rd bending mode (8 %), 7.90 Hz
S3	150-300	1-22	1:st translation mode (15 %), 1.89 Hz 2:nd bending mode (59 %), 5.61 Hz
	300-420	1-7	1:st bending mode (11 %), 4.82 Hz 2:nd bending mode (90 %), 5.61 Hz

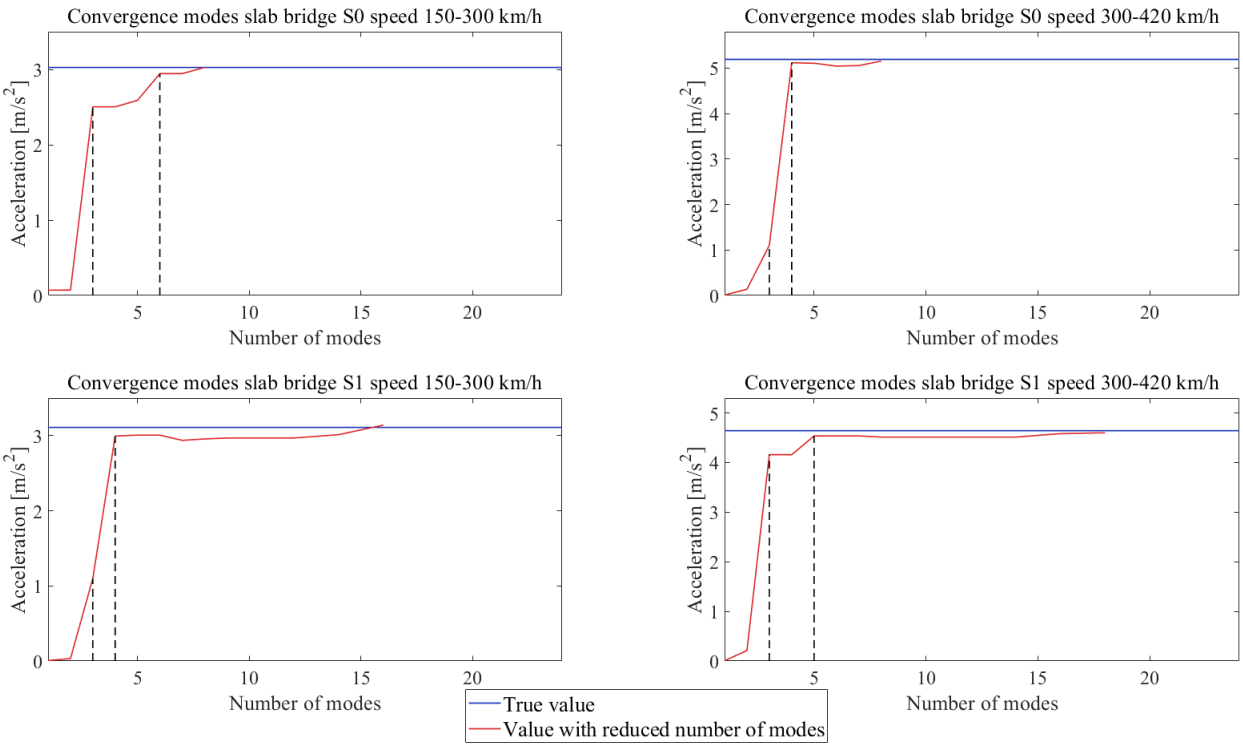

Figure A.4: Visualization of each modes contribution to the total response for the slab bridges S0 and S1 with a ballast density of $1700 kg/m^3$ (red line). The blue line represents the acceleration obtained from a dynamic analysis including all eigenmodes. The frequencies of the dominating eigenmodes are highlighted with dashed lines.

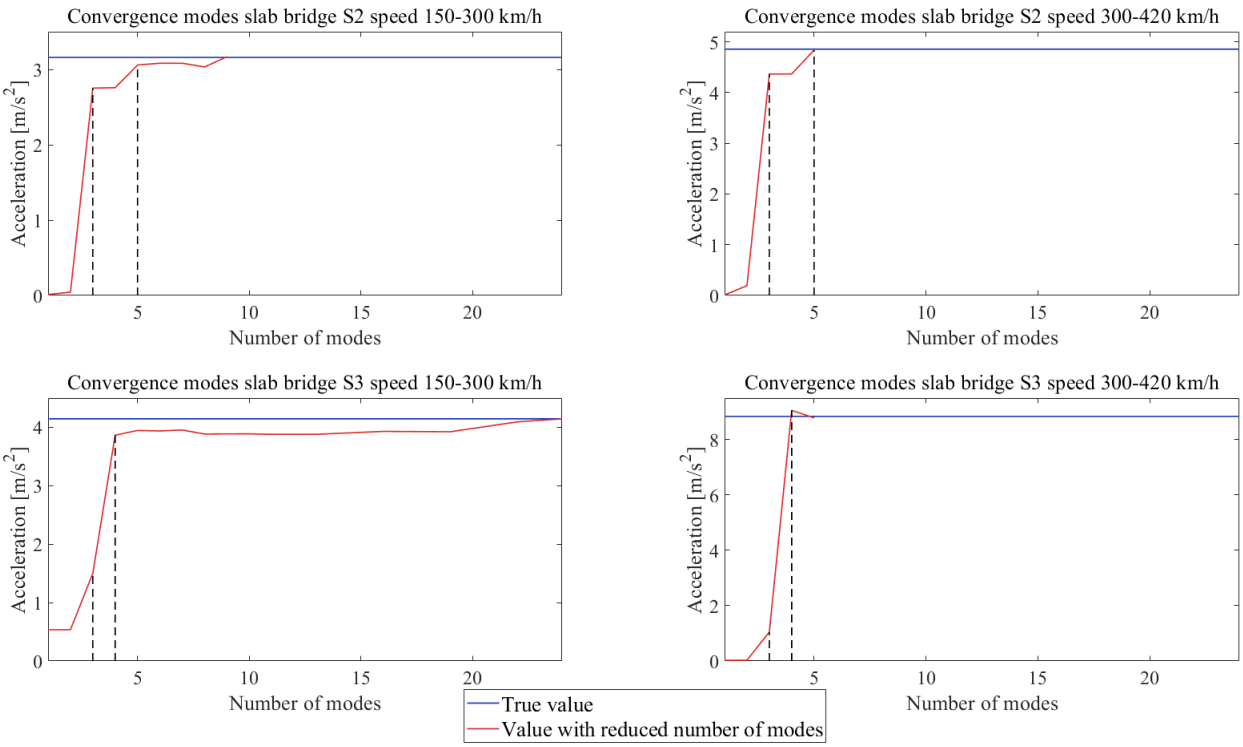

Figure A.5: Visualization of each modes contribution to the total response for the slab bridges S2 and S3 with a ballast density of $1700 kg/m^3$ (red line). The blue line represents the acceleration obtained from a dynamic analysis including all eigenmodes. The frequencies of the dominating eigenmodes are highlighted with dashed lines.

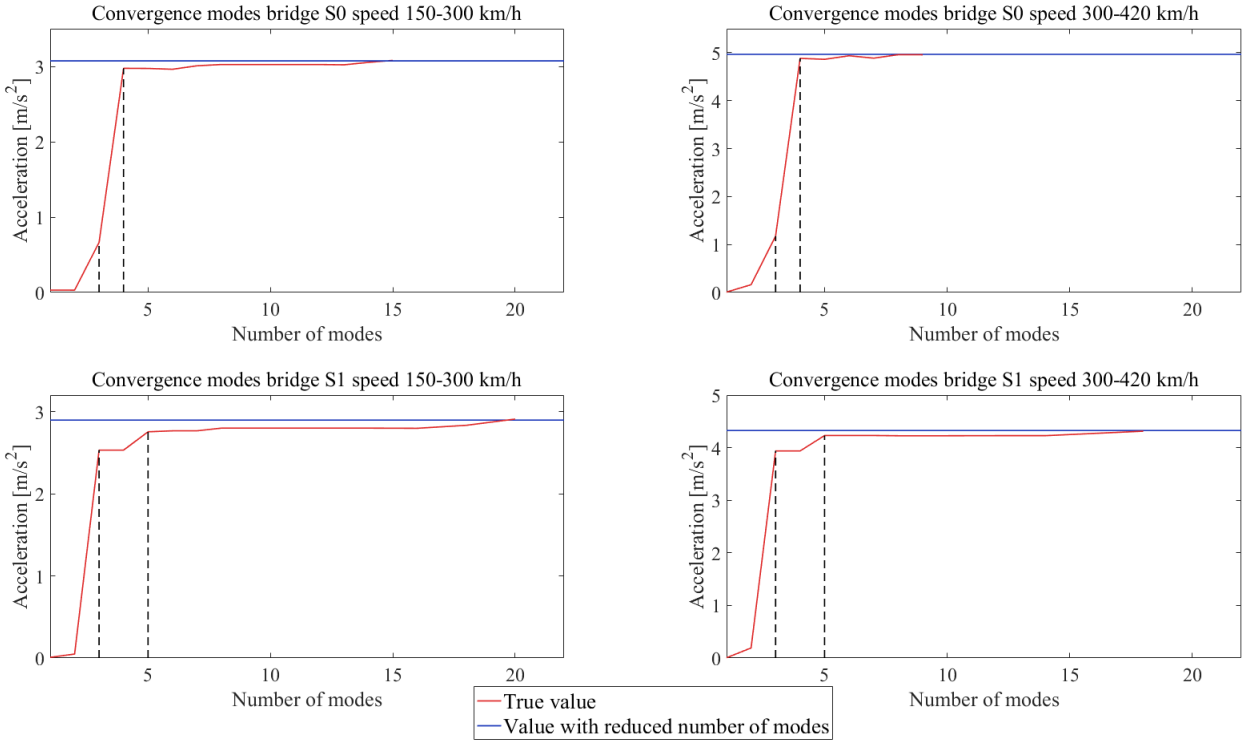

Figure A.6: Visualization of each modes contribution to the total response for the slab bridges S0 and S1 with a ballast density of $2000 kg/m^3$ (red line). The blue line represents the acceleration obtained from a dynamic analysis including all eigenmodes. The frequencies of the dominating eigenmodes are highlighted with dashed lines.

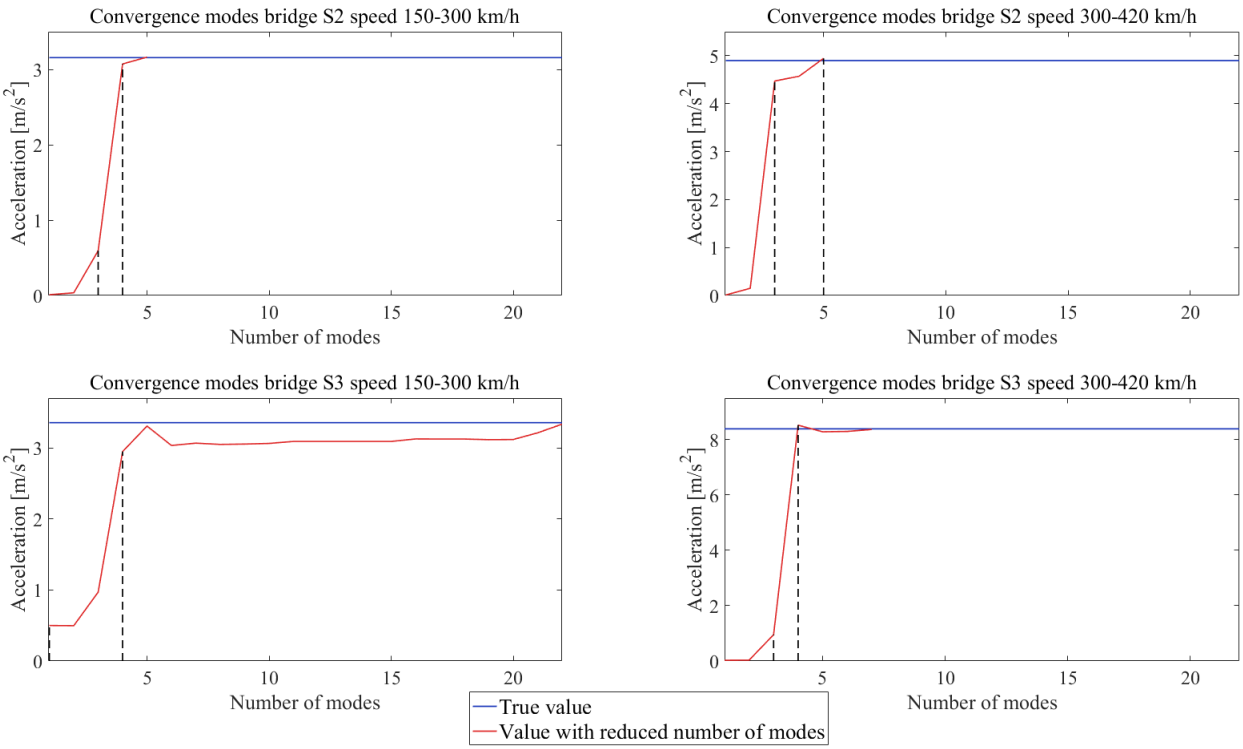

Figure A.7: Visualization of each modes contribution to the total response for the slab bridges S2 and S3 with a ballast density of $2000 kg/m^3$ (red line). The blue line represents the acceleration obtained from a dynamic analysis including all eigenmodes. The frequencies of the dominating eigenmodes are highlighted with dashed lines.

Appendix B - Calculations Associated with Analysis 1A

Calculations of non-structural mass acting on the bridge deck

The loads modelled as non-structural mass in BRIGADE/Plus are listed below.

(a) Components acting on the bridge deck:

- Dead weight of ballast

(b) Components acting on a small strip at the ends of the bridge deck:

- Dead weight of the link plates
- Dead weight of the filling soil that is overlaying the link plate
- Dead weight of the ballast that is overlaying the link plate

The traffic load acting on the link plate only needs to be considered in the actual design of the plate since it does not induce any additional loading on the bridge's superstructure.

(a) By multiplying the density by the thickness, the ballast-load was expressed in the unit kg/m^2. An average value of the thickness was used, calculated as the ballast area divided by the width of the bridge. Only half of the cross-section was considered due to symmetry. The measures are presented in Figure B.1.

$$t = \frac{3.2}{5.35} = 0.6\ m$$

$$m = \rho \cdot t$$

$$m_{\rho=1700kg/m^3} = 1020kg/m^2$$

$$m_{\rho=2000kg/m^3} = 1200kg/m^2$$

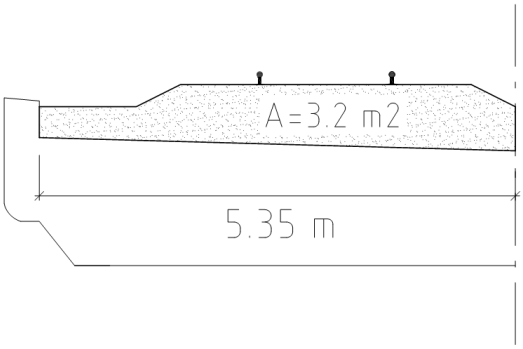

Figure B.1: Half of the cross-section of the bridge deck of the slab bridges.

(b) As can be seen in an extraction of the edge of the bridge (Figure B.2), the link plate is resting on a wedge. Further, the loads acting on the link plate along with relevant dimensions are visualized in Figure B.3. By combining the information in Figures B.2 and B.3, a calculation model was formed (Figure B.4). In accordance with industry practice, the link plate was represented by a simply supported beam, with an overhang of 0.2 times the length of the link plate, at the side that is not attached to the wedge.

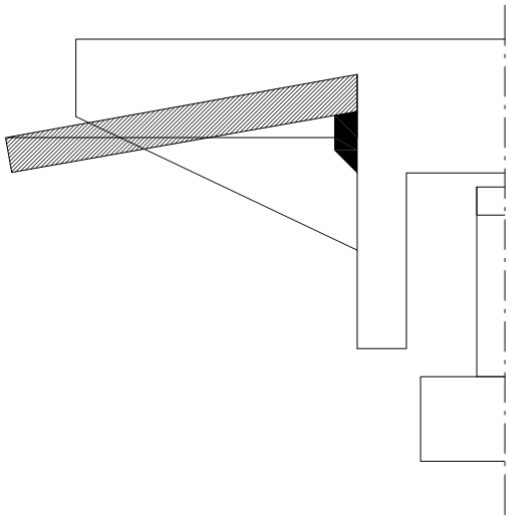

Figure B.2: Principle drawing of the connection between the link plate and the wedge that is attached to the superstructure of the bridge.

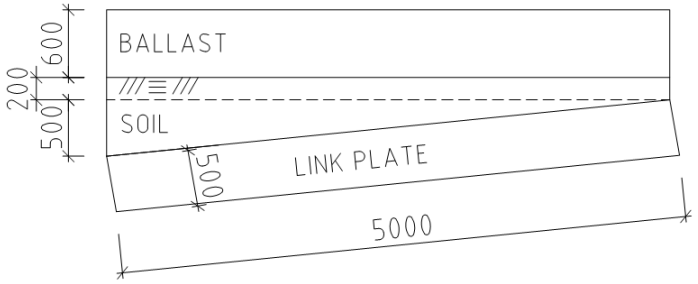

Figure B.3: Loads acting on the link plate. The width of the plate is 10.6 m.

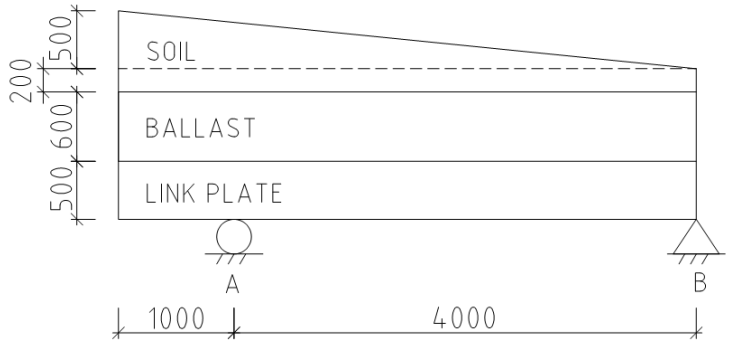

Figure B.4: Calculation model of the link plate.

To estimate how much of the total load that is acting on the wedge, and thus also on the bridge structure, the reaction forces were calculated from a simplified loading case with an evenly distributed load (Figure B.5). This is a conservative assumption, since the triangular load increases the reaction force at support A.

Moment equilibrium around A yields the vertical reaction force at support B.

$$-R_B \cdot 4 + q \cdot 5 \cdot (4 - 2.5) = 0$$

$$R_B = 1.875q \approx 1.9q \ \rightarrow 1.9 \ m$$

This implies that the load up to a distance 1.9 m from the support B acts on the wedge.

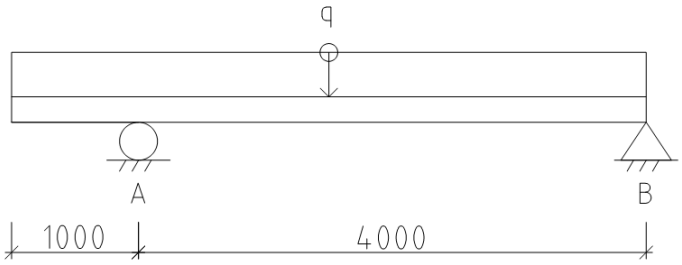

Figure B.5: Calculation model of reaction forces. Support A represents the surrounding soil and support B represents the wedge.

Below, the total mass of each component acting on the wedge is provided, calculated with dimensions according to Figure B.4, and densities and weights from Section 3.1.1. The mass is then distributed over an area of $11.5 \cdot 0.1\ m^2$ at the ends of the bridge deck (Figure 3.3).

$$m_{linkplate} = 2500 \cdot 0.5 \cdot 1.9 \cdot 10.6 = 25175\ kg$$

$$m_{soil,1} = \frac{22 \cdot 10^3}{9.81} \cdot 0.2 \cdot 1.9 \cdot 10.6 = 9033\ kg$$

$$m_{soil,2} = \frac{22 \cdot 10^3}{9.81} \cdot \frac{0.25}{2} \cdot 1.9 \cdot 10.6 = 5646\ kg$$

$$m_{ballast,\ \rho=1700kg/m^3} = 1700 \cdot 0.6 \cdot 1.9 \cdot 10.6 = 20543\ kg$$

$$m_{ballast,\ \rho=2000kg/m^3} = 2000 \cdot 0.6 \cdot 1.9 \cdot 10.6 = 24168\ kg$$

$$q_{tot,\ \rho=1700kg/m^3} = (25175 + 9033 + 5646 + 20543)/(11.5 \cdot 0.1) = 52519\ kg/m^2$$

$$q_{tot,\ \rho=2000kg/m^3} = (25175 + 9033 + 5646 + 24168)/(11.5 \cdot 0.1) = 55671\ kg/m^2$$

Calculation of rotational spring stiffness

The stiffness of the slab foundations were represented by rotational springs. The rotational stiffness depends on the dimensions of the slab foundations, and was derived from Equation 5.2 and 5.1 (Appendix 107 in [21]). As described in Section 3.1.2, the foundations were assumed to be unable to rotate around the z-axis.

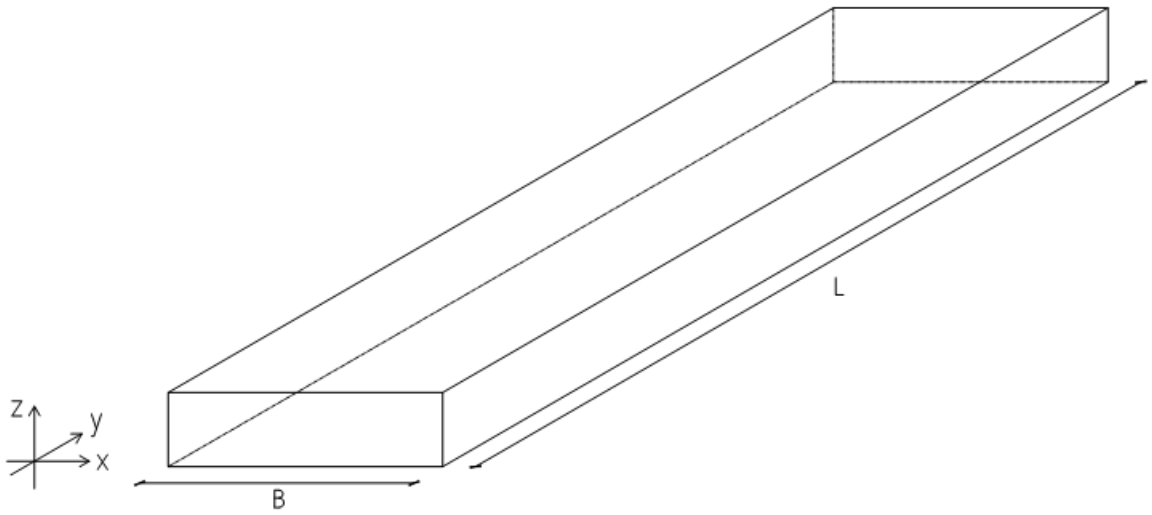

Figure B.6: Definition of directions and measures of the slab foundations, attached to the bottom of the columns.

$$k_{\theta x} = \frac{E_k L^2 B}{5} \qquad \text{In the slab's strong direction (around the x-axis)} \qquad (5.1)$$

$$k_{\theta y} = \frac{E_k B^2 L}{5} \qquad \text{In the slab's weak direction (around the y-axis)} \qquad (5.2)$$

where:
E_k is the characteristic value of the soil's Young's modulus (Section 3.1.1)
B is the width of the slab
L is the length of the slab

Insertion in Equation 5.2 and 5.1 yields the stiffnesses of the rotational springs.

$$k_{\theta x} = \frac{30 \cdot 10^6 \cdot 14^2 \cdot 5}{5} = 5.88 \cdot 10^9 \ N/m/rad$$

$$k_{\theta y} = \frac{30 \cdot 10^6 \cdot 5^2 \cdot 14}{5} = 2.10 \cdot 10^9 \ N/m/rad$$

Appendix C - Calculations Associated with Analysis 1B

Calculation of rotational spring stiffness

The rotational spring stiffnesses of the foundations of the portal frame bridges were computed analogous with Appendix B.

$$k_{\theta x} = \frac{30 \cdot 10^6 \cdot 13^2 \cdot 4}{5} = 4.06 \cdot 10^9 \ N/m/rad$$

$$k_{\theta y} = \frac{30 \cdot 10^6 \cdot 4^2 \cdot 13}{5} = 1.25 \cdot 10^9 \ N/m/rad$$

Appendix D - Calculations Associated with Analysis 2

Calculation of vertical spring stiffness

The vertical spring stiffness, k_z, was calculated according to [20].

$$k_z = 0.5\left(\frac{k_{\theta x}}{I_x} + \frac{k_{\theta y}}{I_y}\right)A$$

where:
$k_{\theta x}$ and $k_{\theta x}$ are the rotational springs (computed in Appendix B and C)
A is the bottom area of the slab
I_x and I_y are the moments of inertia in the x- and y-directions according to

$$I_x = \frac{BL^3}{12}\ , \quad I_y = \frac{LB^3}{12}.$$

The vertical spring stiffnesses of the slab bridges and the portal frame bridges are displayed in Table D.1.

Table D.1: Vertical spring stiffnesses of the slab bridges and the portal frame bridges.

Bridge type	A $[m^2]$	I_x $[m^4]$	I_y $[m^4]$	k_z $[N/(m \cdot rad)]$
Slab bridge	70	1143.33	145.83	$0.68 \cdot 10^9$
Frame bridge	52	732.33	69.33	$0.61 \cdot 10^9$

Appendix E - Supplementary Results of Studies (iv), (v), (vi) & (vii)

In this Appendix, the dynamic response is evaluated in terms of deflection, torsion, rotation at supports, and section forces. The design values of these quantities for all bridges are provided in Section 4; however, the calculation procedures and more detailed information about the data are presented here. As mentioned in Section 2.5.1, load model SW/0 is only applicable for the slab bridges. Therefore, to be able to compare the results of the two different bridge types, LM71 is soley used. Values of φ', φ'' and ϕ, derived from the equations in Section 2.5.1 and used in verifications of deflections and section forces, are displayed in the section below.

Deflections

The vertical deflection was computed from static analyses of load model LM71 and HSLM, multiplied by sets of dynamic amplification factors according to Equations 2.26 and 2.28. The results were then related to the standard value of the maximum allowable deflection specified in [17]: L/600 (where L is the span length). The deflection of the bridge deck was evaluated at location 1 and location i for the slab bridge and the portal frame bridge, respectively (Figures G.1 and G.2). In Tables E.1-E.3 the total dynamic magnification of the static response for the two load models, are followed by calculations of each factor.

Table E.1: The total dynamic magnification factor for LM71 (Equation 2.26) and for HSLM (Equation 2.28), respectively.

Slab bridges				
Name of bridge	Ballast density $[kg/m^3]$	Design speed interval $[m/s]$	$LM71$ [-]	$HSLM$ [-]
S0	1700	150-300	1.16	2.51
		300-420		2.20
	2000	150-300		2.19
		300-420		1.99
S1	1700	150-300	1.15	2.33
		300-420		3.23
	2000	150-300		2.46
		300-420		3.32
S2	1700	150-300	1.12	2.55
		300-420		3.72
	2000	150-300		2.33
		300-420		3.84
S3	1700	150-300	1.12	2.04
		300-420		3.59
	2000	150-300		1.71
		300-420		3.53

Portal frame bridges				
Name of bridge	Ballast density $[kg/m^3]$	Design speed interval $[m/s]$	$LM71$ [-]	$HSLM$ [-]
S0	1700	150-300	1.26	4.46
		300-420		2.33
	2000	150-300		4.43
		300-420		2.35

Name of bridge	Ballast density $[kg/m^3]$	Design speed interval $[m/s]$	$LM71$ [-]	$HSLM$ [-]
S1	1700	150-300	1.25	3.78
		300-420		2.04
	2000	150-300		3.61
		300-420		2.01
S2	1700	150-300	1.22	2.88
		300-420		3.27
	2000	150-300		2.87
		300-420		3.85
S3	1700	150-300	1.22	2.33
		300-420		3.83
	2000	150-300		2.60
		300-420		3.97
S4	1700	150-300	1.21	2.58
		300-420		4.12
	2000	150-300		2.18
		300-420		4.23

Table E.2: Calculation of φ' according to Equation 2.29.

Slab bridges					
Name of bridge	Ballast density $[kg/m^3]$	Design speed interval $[m/s]$	u_{dyn} $[mm]$	$u_{static,HSLM}$ $[mm]$	φ' [-]
S0	1700	150-300	2.03	0.89	1.29
		300-420	1.66		0.87
	2000	150-300	1.93	1.00	0.94
		300-420	1.64		0.65
S1	1700	150-300	2.80	1.30	1.16
		300-420	3.88		1.99
	2000	150-300	2.96	1.29	1.30
		300-420	3.99		2.10

Name of bridge	Ballast density $[kg/m^3]$	Design speed interval $[m/s]$	u_{dyn} $[mm]$	$u_{static,HSLM}$ $[mm]$	φ' [-]
S2	1700	150-300	3.89	1.60	1.44
		300-420	5.69		2.56
	2000	150-300	3.55	1.60	1.22
		300-420	5.89		2.69
S3	1700	150-300	3.30	1.71	0.93
		300-420	5.89		2.44
	2000	150-300	2.77	1.72	0.61
		300-420	5.82		2.39

Portal frame bridges					
Name of bridge	Ballast density $[kg/m^3]$	Design speed interval $[m/s]$	u_{dyn} $[mm]$	$u_{static,HSLM}$ $[mm]$	φ' [-]
S0	1700	150-300	7.14	1.77	3.02
		300-420	3.04		0.71
	2000	150-300	7.12	1.77	3.01
		300-420	3.13		0.76
S1	1700	150-300	7.06	2.04	2.47
		300-420	3.26		0.60
	2000	150-300	6.80	2.05	2.31
		300-420	3.28		0.60
S2	1700	150-300	6.26	2.34	1.67
		300-420	6.98		1.98
	2000	150-300	6.25	2.34	1.67
		300-420	8.36		2.57
S3	1700	150-300	5.93	2.69	1.20
		300-420	9.81		2.65
	2000	150-300	6.74	2.71	1.48
		300-420	10.33		2.81
S4	1700	150-300	7.85	3.11	1.52
		300-420	12.55		3.10
	2000	150-300	6.65	3.12	1.13
		300-420	12.99		3.16

Table E.3: Calculation of ϕ and φ'' according to Equations 2.27 and 2.30.

Slab bridges							
Name of bridge	Ballast density $[kg/m^3]$	Design speed interval $[km/h]$	α [-]	L_Φ $[m]$	ϕ [-]	n_0 $[Hz]$	φ'' [-]
S0	1700	150-300	3.79	19.41	1.16	6.75	0.52
		300-420	5.30				0.73
	2000	150-300	3.79			6.59	0.49
		300-420	5.30				0.69
S1	1700	150-300	3.79	21.36	1.15	5.72	0.34
		300-420	5.30				0.48
	2000	150-300	3.79			5.58	0.32
		300-420	5.30				0.45
S2	1700	150-300	3.79	23.14	1.13	4.98	0.23
		300-420	5.30				0.32
	2000	150-300	3.79			4.86	0.21
		300-420	5.30				0.30
S3	1700	150-300	3.79	25.48	1.12	4.94	0.22
		300-420	5.30				0.30
	2000	150-300	3.79			4.82	0.20
		300-420	5.30				0.28

Portal frame bridges							
Name of bridge	Ballast density $[kg/m^3]$	Design speed interval $[km/h]$	α [-]	L_Φ $[m]$	ϕ [-]	n_0 $[Hz]$	φ'' [-]
S0	1700	150-300	3.79	12.09	1.26	8.58	0.88
		300-420	5.30				1.24
	2000	150-300	3.79			8.38	0.84
		300-420	5.30				1.18

Name of bridge	Ballast density $[kg/m^3]$	Design speed interval $[km/h]$	α [-]	L_Φ $[m]$	ϕ [-]	n_0 $[Hz]$	φ'' [-]
S1	1700	150-300	3.79	12.87	1.25	7.32	0.63
		300-420	5.30				0.88
	2000	150-300	3.79			7.14	0.59
		300-420	5.30				0.83
S2	1700	150-300	3.79	13.61	1.23	6.31	0.42
		300-420	5.30				0.59
	2000	150-300	3.79			6.16	0.39
		300-420	5.30				0.54
S3	1700	150-300	3.79	14.39	1.22	5.51	0.26
		300-420	5.30				0.36
	2000	150-300	3.79			5.37	0.23
		300-420	5.30				0.32
S4	1700	150-300	3.79	15.12	1.21	4.84	0.12
		300-420	5.30				0.17
	2000	150-300	3.79			4.72	0.10
		300-420	5.30				0.14

Torsion

In the standards, the requirements are specified for the difference in torsion over the the track width, referred to as relative torsion. Since the bridge is symmetric in two planes, a quarter of the deck was sufficient to capture the torsion. The relative torsion was calculated as the difference in output from dynamic analyses with HSLM along the two paths highlighted in Figures E.1 and E.2 respectively, and compared with the threshold value of 1.5 $mm/3\ m$ ($5 \cdot 10^{-4}\ rad/m$), valid for speeds of 200 km/h or more in Appendix A2 in [17]. Examples of the variance in torsion over the path (absolute torsion) are shown in Figures E.3-E.6.

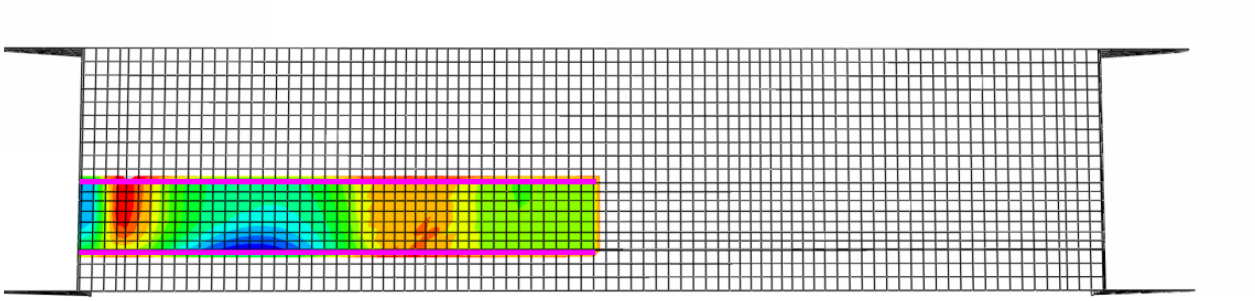

Figure E.1: Output path of the slab bridges, highlighted in magenta.

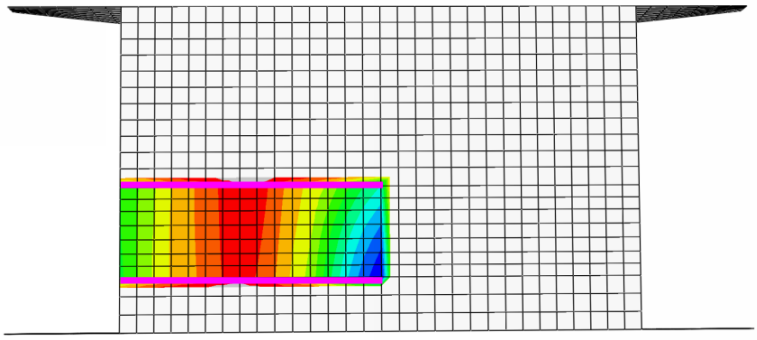

Figure E.2: Output path of the portal frame bridges, highlighted in magenta.

Slab bridge S0

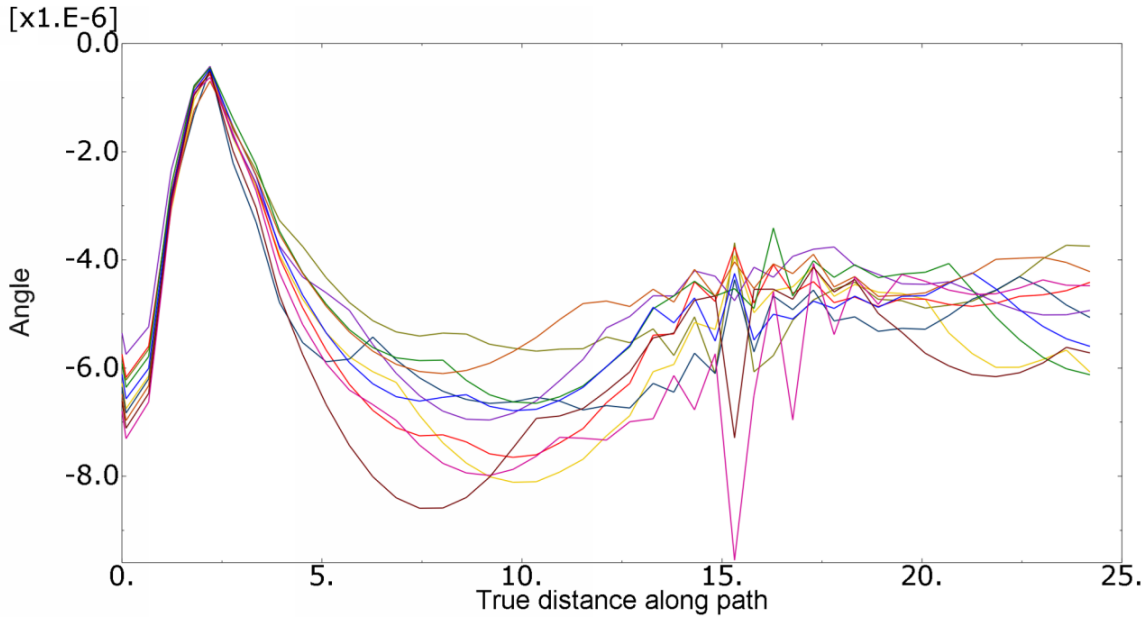

Figure E.3: Negative (absolute) torsion in rad/m along the upper path in Figure E.1 for the slab bridge S0.

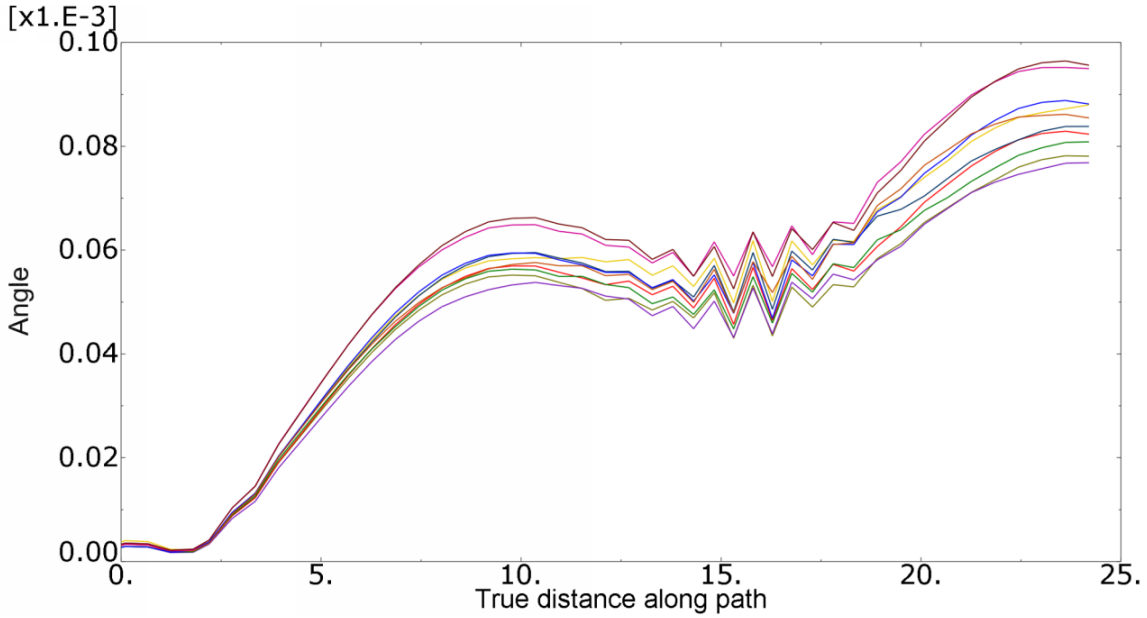

Figure E.4: Positive (absolute) torsion in rad/m along the upper path in Figure E.1 for the slab bridge S0.

Portal frame bridge S0

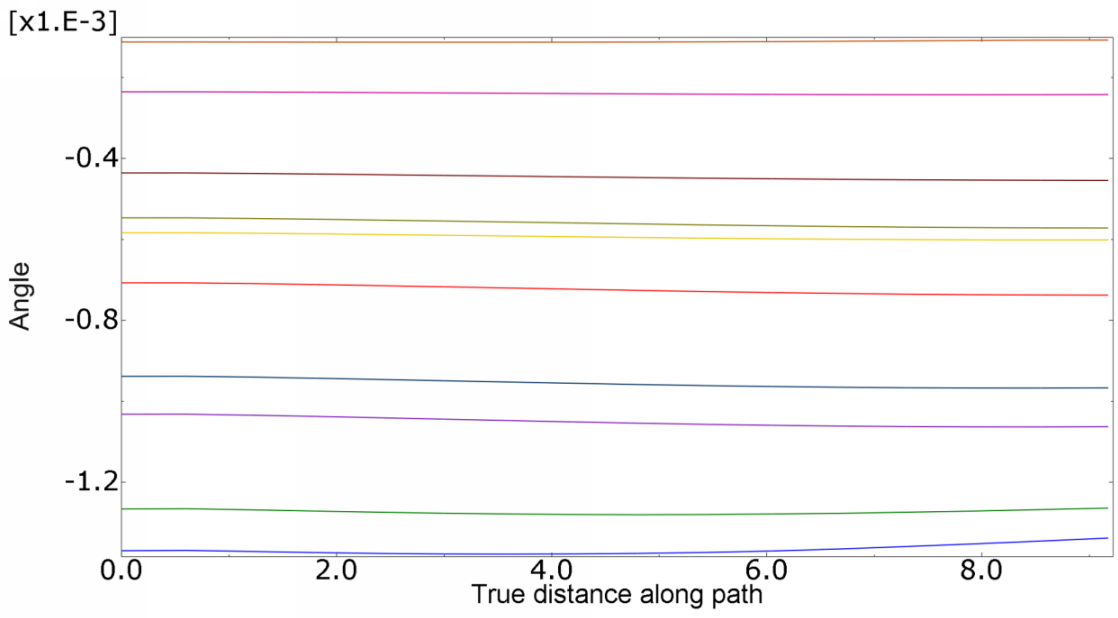

Figure E.5: Negative (absolute) torsion in rad/m along the upper path in Figure E.2 for the portal frame bridge S0.

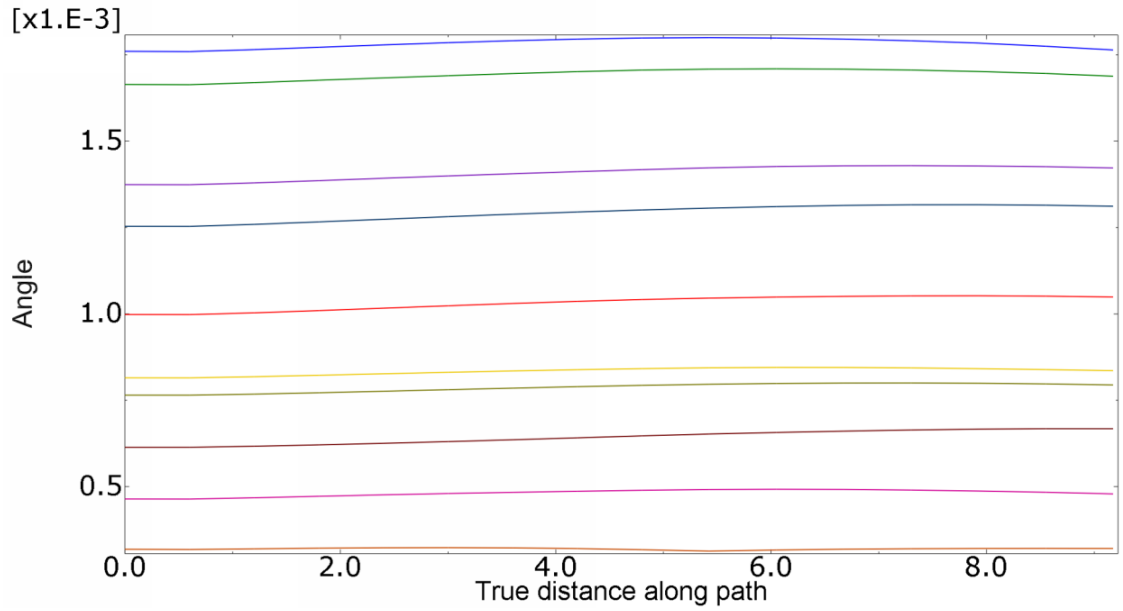

Figure E.6: Positive (absolute) torsion in rad/m along the upper path in Figure E.2 for the portal frame bridge S0.

Rotation at bearings

The rotation at bearings was computed from dynamic analyses with HSLM trains along a path visualized in figure E.7. The maximum values were then related to the threshold value specified in Section B.2.3 in [2]:

$$\theta = \frac{2 \cdot 10^{-3}}{h_{(m)}} \quad [rad]$$

where $h_{(m)}$ is the distance between the upper edge of the rails and the rotation center of the bearings. Since the portal frame bridges are not supported by bearings, only the slab bridges were included in this analysis. The value of θ for the slab bridges is provided in Table E.4.

Table E.4: Maximum allowable value of the rotation angle for the slab bridges. The distance between the top of the rail and the ballast was assumed to be 0.25 m.

Bridge type	$h_{(m)}$ $[m]$	θ $[rad]$
Slab bridge	2.2	$9.09 \cdot 10^{-4}$

Excerpts of the variance in rotation angle along the path are presented in Figures E.8-E.9.

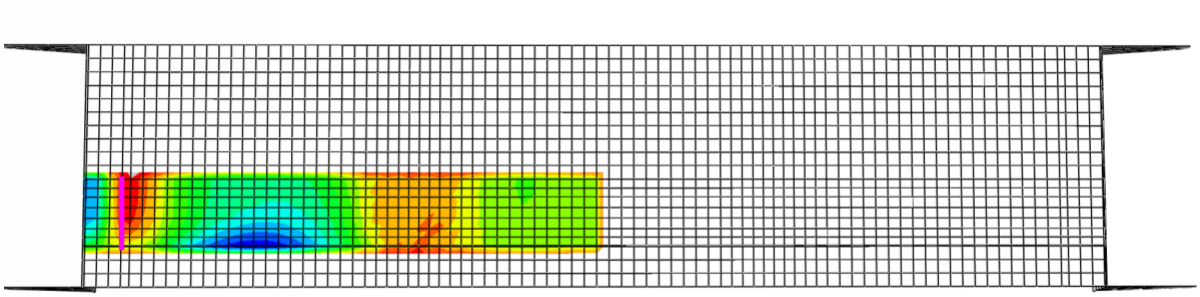

Figure E.7: Output path of the slab bridges, highlighted in magenta.

Slab bridge S0

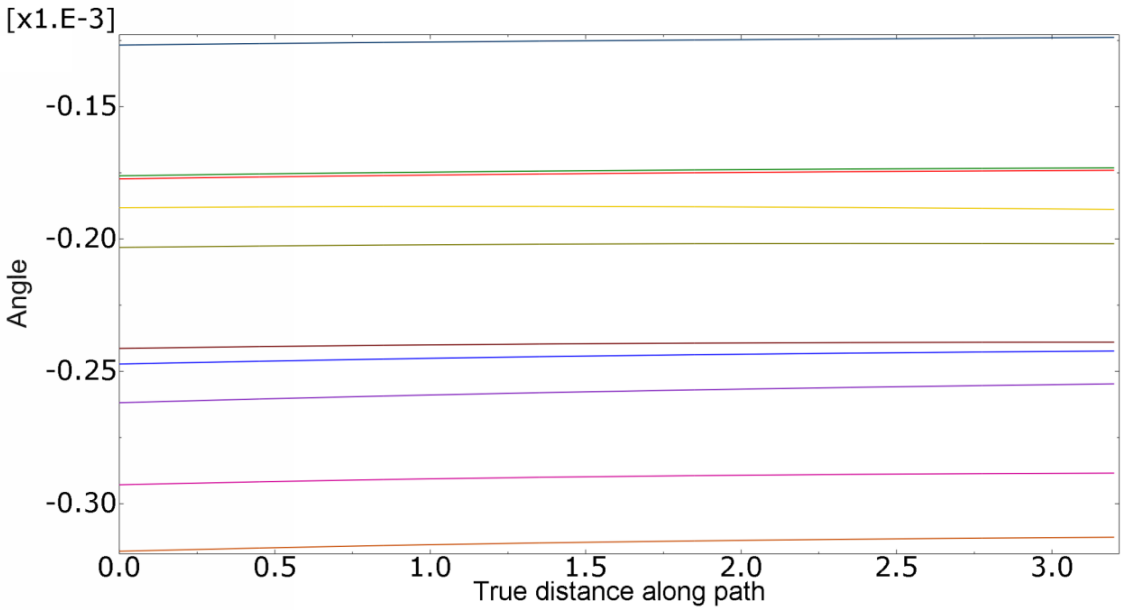

Figure E.8: Negative rotation at supports in rad/m for the slab bridge S0.

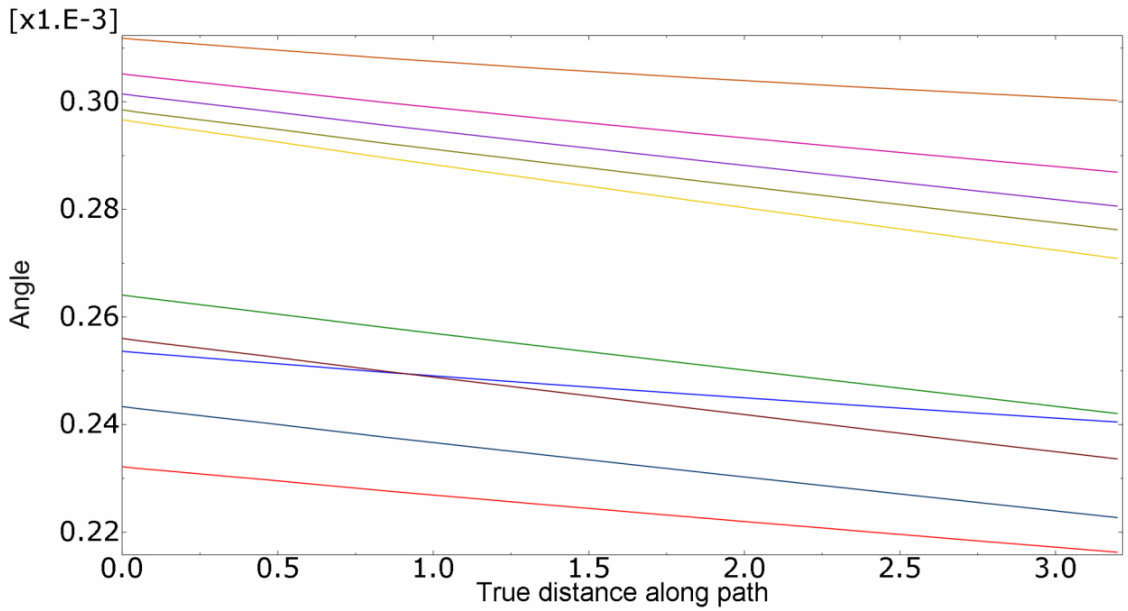

Figure E.9: Positive rotation at supports in rad/m for the slab bridge S0.

Section forces

Section moments and shear forces were computed analogously to the deflections, i.e. from static analyses of LM71 and HSLM multiplied by certain factors to account for the dynamic amplification. Note that the response of the HSLM-trains could alternatively be taken directly from the dynamic analysis; however, the static results were used here. The dynamic enhancement factor, φ' , can be obtained from Table E.2. The value of the section force was considered as acceptable if the value of the HSLM loading was less than that of the LM71 loading. The principal appearance of the moment- and shear force distribution proved to be similar for the different span lengths; therefore, only the distributions of the slab bridge S0 and the portal frame bridge S0 (both with ballast density 1700 kg/m^3) are provided (Figures E.14-E.29). Note that the moment only includes the bending moment and that no dynamic magnification factors have been applied. In reality, the moment design values are a sum of the bending moment and the absolute value of the corresponding twisting moment.

These design values for each bridge are shown in Figures E.10 and E.11 with a ballast density of 2000 kg/m^3 (Bridges with a ballast density of 1700 kg/m^3 is already presented in Section 4). Some design values needed to be verified more thoroughly; these verifications can be obtained from Tables E.5 and E.6.

The section forces, except for the shear force for the slab bridges, are extracted along a path at the longitudinal edge of the bridges. For the slab bridges, the shear force is evaluated at the support sections, i.e. at the locations of the bearings and where the columns are attached to the bridge deck. The different output paths are visualized in Figures E.12 and E.13.

When the element size is very small, the value of the section forces at the section of the supports approaches infinity (instead of converging towards the true value). Therefore, the design values of the shear force were taken as the mean value of the three elements closest to each support. The graphs do not however display these smoothed values, which means that the peaks are larger and sharper than in reality.

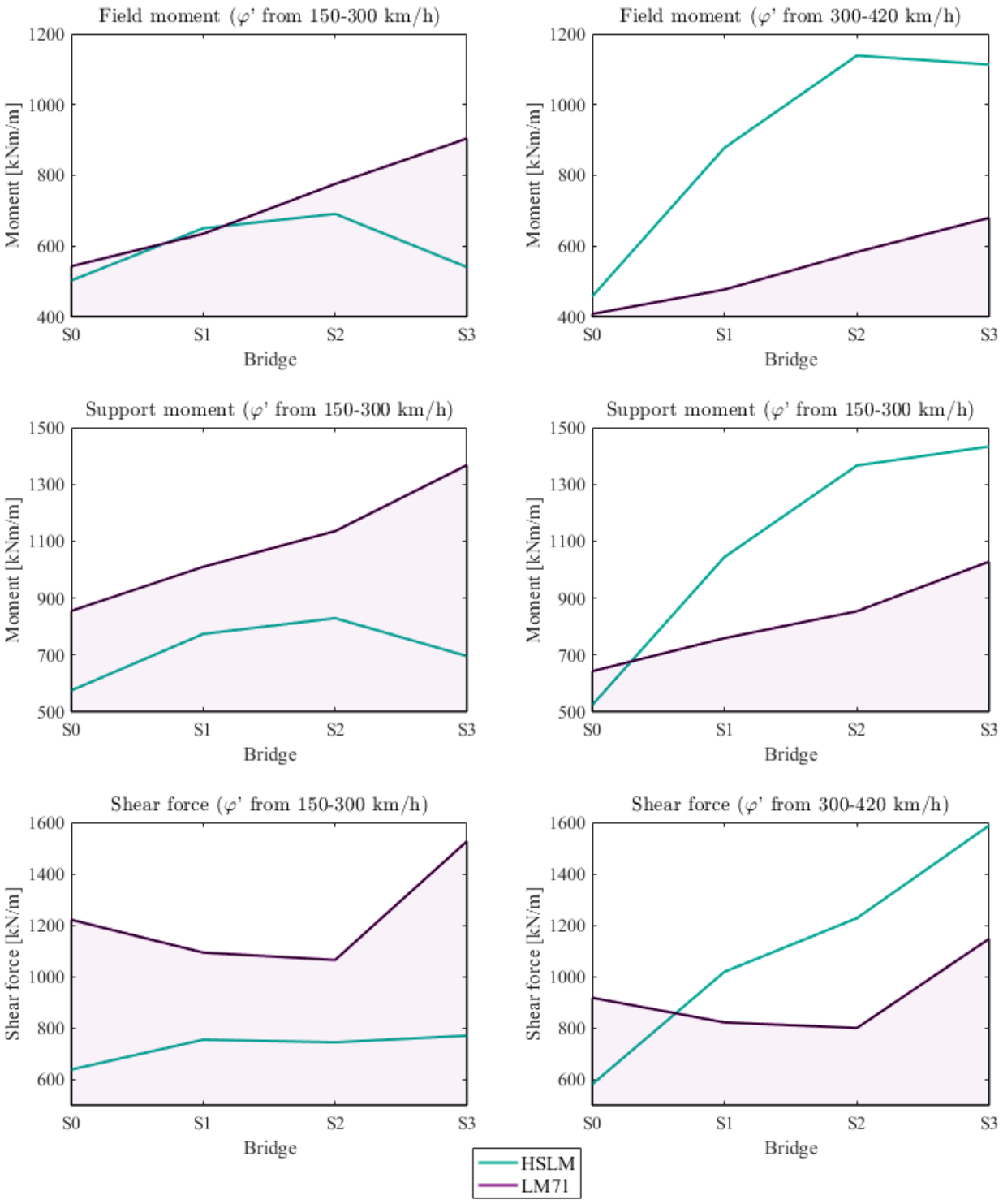

Figure E.10: Design values of section forces of the slab bridges obtained from analyses with HSLM and LM71, respectively, with a ballast density of 2000 kg/m^3.

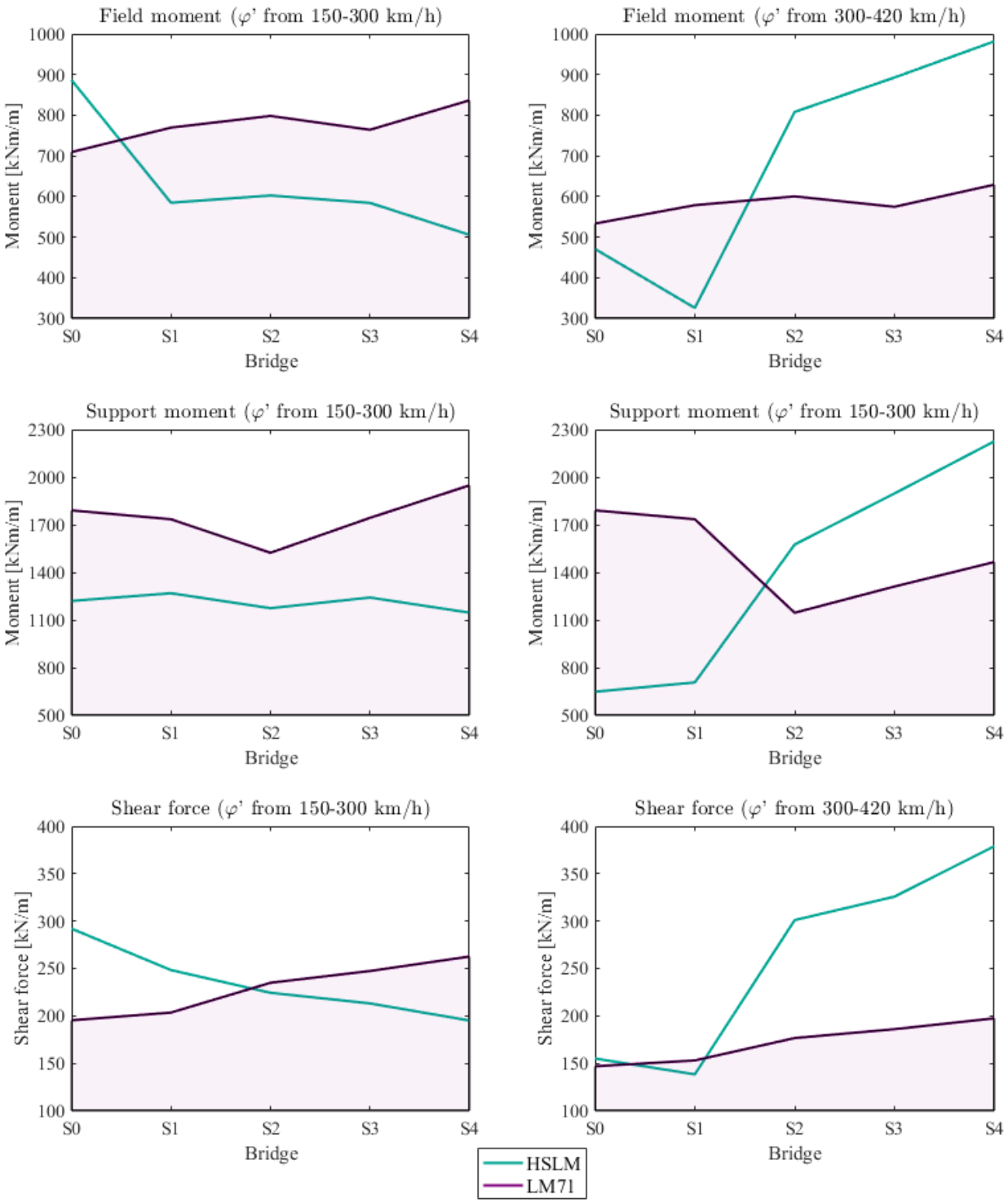

Figure E.11: Design values of section forces of the portal frame bridges obtained from analyses with HSLM and LM71, respectively, with a ballast density of 2000 kg/m^3.

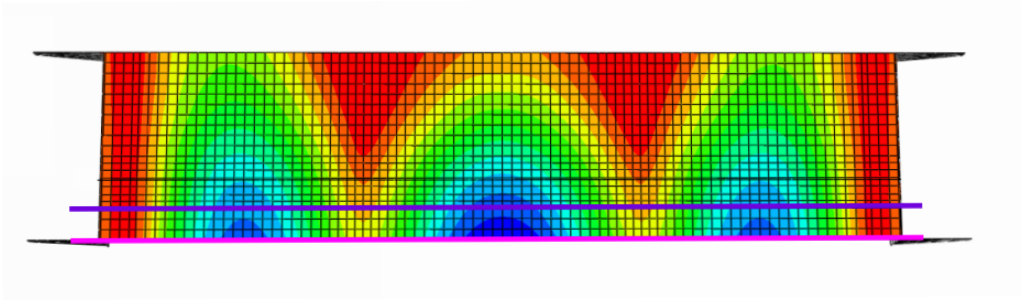

Figure E.12: Output paths of the slab bridges. The path along which the moment was extracted is highlighted in magenta, and that of the shear force is highlighted in purple.

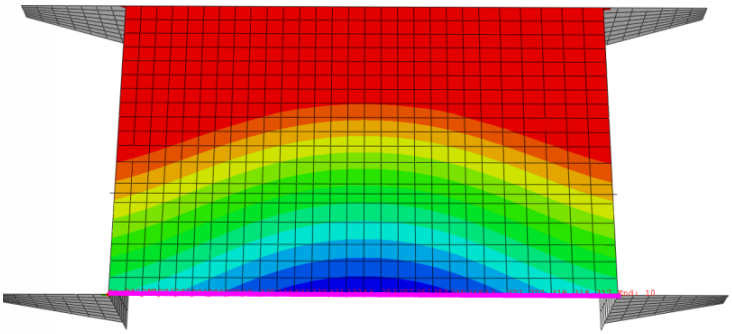

Figure E.13: Output path of the portal frame bridges, highlighted in magenta.

Table E.5: Design values of section forces for bridges that needed to be verified more thoroughly, for the case with a ballast density of 1700 kg/m^3. The largest value of each column is highlighted in yellow.

Field moment for slab bridge S0					
HSLM train	M $[kNm]$	u_{dyn} $[mm]$	u_{stat} $[mm]$	Total dynamic factor [-]	M_{dim} $[kNm]$
A1	168	1.24	0.63	2.32	390
A2	177	1.32	0.71	2.23	394
A3	181	1.30	0.71	2.20	398
A4	179	1.40	0.73	2.28	411
A5	184	1.22	0.71	2.10	387
A6	196	1.30	0.76	2.07	405
A7	208	1.37	0.81	2.05	427
A8	195	1.67	0.79	2.48	485
A9	231	1.55	0.90	2.09	482
A10	232	1.66	0.89	2.23	517

Field moment for slab bridge S1					
HSLM train	M $[kNm]$	u_{dyn} $[mm]$	u_{stat} $[mm]$	Total dynamic factor [-]	M_{dim} $[kNm]$
A1	120	3.88	0.89	4.60	567
A2	126	2.86	0.99	3.13	409
A3	142	1.79	0.98	2.07	311
A4	140	2.02	1.01	2.25	332
A5	125	1.93	0.97	2.22	294
A6	137	2.09	1.06	2.21	321
A7	150	2.36	1.15	2.30	362
A8	166	2.52	1.13	2.47	429
A9	173	2.04	1.28	1.83	337
A10	175	2.04	1.29	1.82	341

Field moment for portal frame bridge S0					
HSLM train	M $[kNm]$	u_{dyn} $[mm]$	u_{stat} $[mm]$	Total dynamic factor [-]	M_{dim} $[kNm]$
A1	162	1.77	1.44	1.67	271
A2	180	2.28	1.63	1.83	330
A3	171	2.91	1.52	2.35	403
A4	176	3.35	1.57	2.58	455
A5	162	3.50	1.44	2.88	466
A6	171	4.55	1.52	3.43	589
A7	181	5.55	1.61	3.90	705
A8	177	5.90	1.59	4.16	736
A9	200	6.89	1.77	4.32	865
A10	200	7.09	1.77	4.44	888

Shear force for portal frame bridge S0			
HSLM train	V $[kN]$	Total dynamic factor [-]	V_{dyn} $[kN]$
A1	52	1.67	87
A2	57	1.83	104
A3	55	2.35	129
A4	55	2.58	141
A5	52	2.88	149
A6	55	3.43	189
A7	58	3.90	226
A8	56	4.16	235
A9	64	4.32	277
A10	64	4.44	284

Table E.6: Design values of section forces for bridges that needed to be verified more thoroughly, for the case with a ballast density of 2000 kg/m^3. The largest value of each column is highlighted in yellow.

Field moment for slab bridge S0					
HSLM train	M $[kNm]$	u_{dyn} $[mm]$	u_{stat} $[mm]$	Total dynamic factor [-]	M_{dim} $[kNm]$
A1	182	0.71	1.29	2.17	394
A2	176	0.79	1.38	2.08	366
A3	192	7.92	1.36	2.06	396
A4	179	0.82	1.41	2.07	371
A5	193	0.79	1.41	2.13	410
A6	195	0.85	1.35	1.93	376
A7	207	0.91	1.43	1.91	395
A8	193	0.89	1.40	1.92	371
A9	230	1.01	1.58	1.90	437
A10	230	1.00	1.64	1.99	458

Field moment for slab bridge S1					
HSLM train	M $[kNm]$	u_{dyn} $[mm]$	u_{stat} $[mm]$	Total dynamic factor [-]	M_{dim} $[kNm]$
A1	204	0.88	3.78	4.50	917
A2	206	0.94	2.75	3.17	652
A3	219	0.97	1.80	2.07	453
A4	217	1.00	2.34	2.56	554
A5	210	0.97	2.26	2.56	536
A6	223	1.05	2.36	2.46	549
A7	237	1.14	2.43	2.34	556
A8	229	1.13	2.56	2.49	570
A9	264	1.27	2.28	2.01	532
A10	265	1.29	2.06	1.82	483

Field moment for portal frame bridge S0					
HSLM train	M $[kNm]$	u_{dyn} $[mm]$	u_{stat} $[mm]$	Total dynamic factor [-]	M_{dim} $[kNm]$
A1	162	1.43	1.77	1.65	267
A2	180	1.63	2.02	1.66	298
A3	172	1.52	2.73	2.22	380
A4	176	1.57	3.68	2.77	488
A5	162	1.44	4.22	3.36	544
A6	172	1.52	50.0	3.71	636
A7	181	1.61	5.68	3.96	717
A8	177	1.59	5.66	3.99	705
A9	200	1.77	6.34	3.99	799
A10	200	1.77	6.67	4.18	836

Shear force for portal frame bridge S0			
HSLM train	V $[kN]$	Total dynamic factor [-]	V_{dyn} $[kN]$
A1	52	1.65	86
A2	57	1.66	94
A3	55	2.22	122
A4	55	2.77	151
A5	52	3.36	174
A6	55	3.71	204
A7	58	3.96	229
A8	56	3.99	225
A9	64	3.99	256
A10	64	4.18	268

Slab bridge S0 - LM71

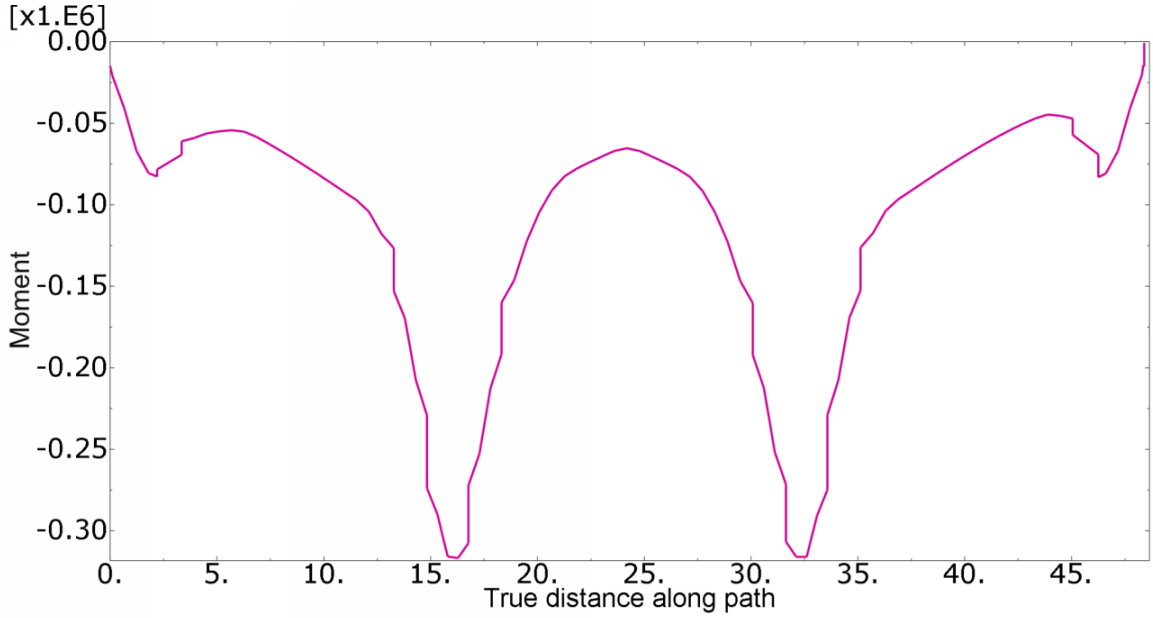

Figure E.14: Negative bending moment distribution over the span length for the slab bridge S0, load model LM71 (ballast density 1700 kg/m^3). The largest negative value is found at the section where the columns are placed.

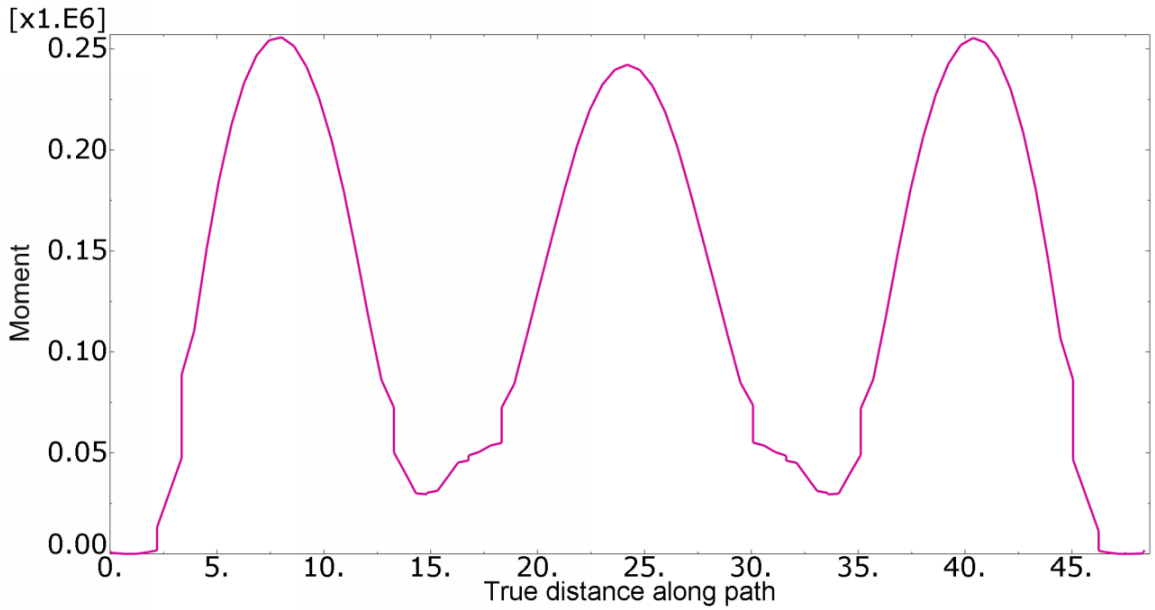

Figure E.15: Positive bending moment distribution over the span length for the slab bridge S0, load model LM71 (ballast density 1700 kg/m^3). The largest positive value is found at the midsection of each span.

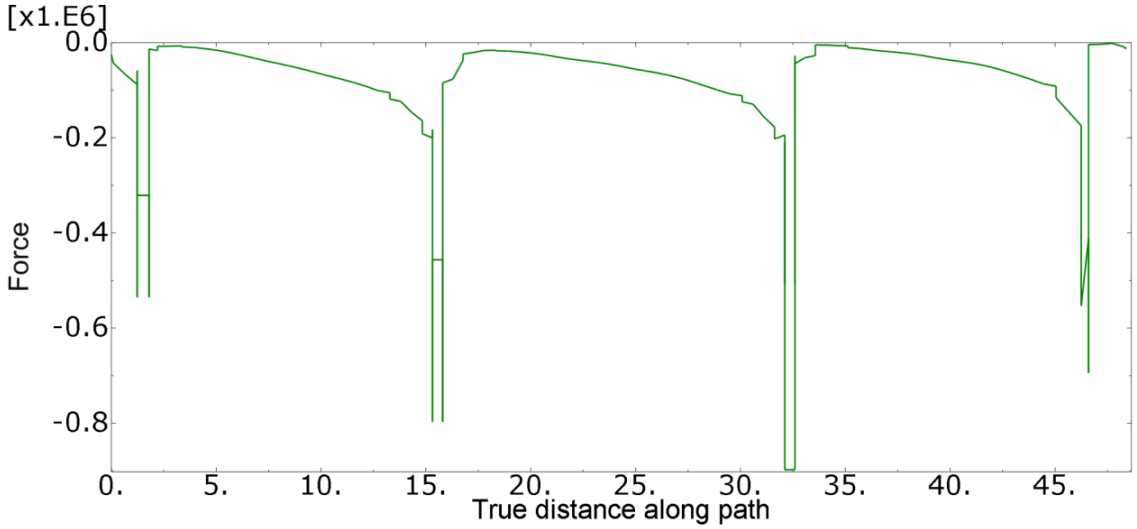

Figure E.16: Negative shear force distribution over the span length for the slab bridge S0, load model LM71 (ballast density 1700 kg/m^3. The largest negative value is retrieved at the section of the columns.

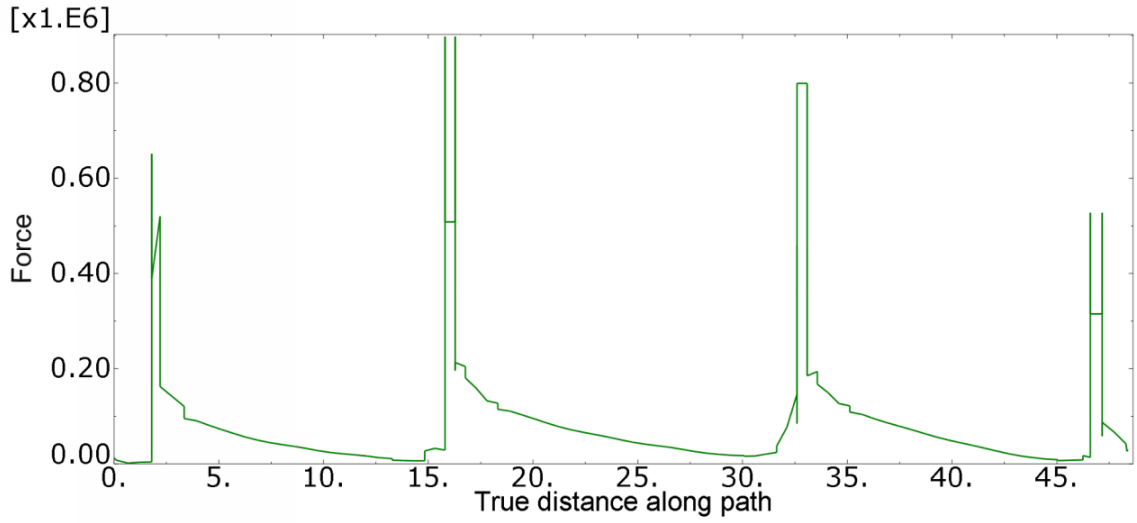

Figure E.17: Positive shear force distribution over the span length for the slab bridge S0, load model LM71 (ballast density 1700 kg/m^3). The largest positive value is retrieved at the section of the columns. Note that the positive shear force distribution is a mirror reflection of the negative shear force distribution.

Slab bridge S0 - HSLM. The different lines in the graphs corresponds to the universal trains A1-A10

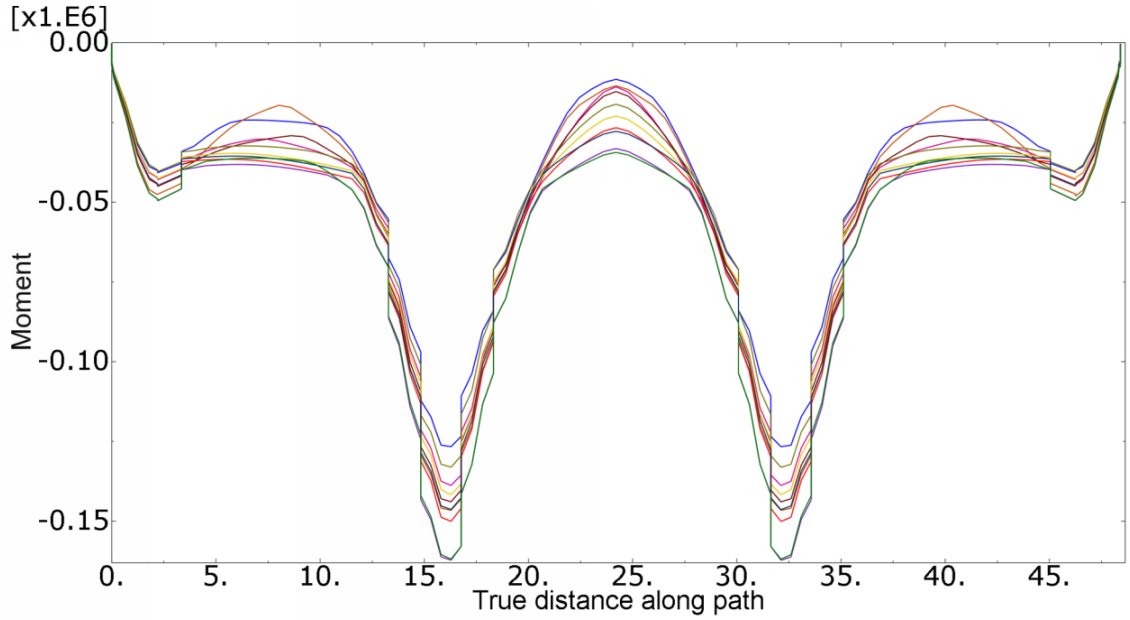

Figure E.18: Negative bending moment distribution over the span length for the slab bridge S0, load model HSLM (ballast density 1700 kg/m^3). The largest negative value is found at the section where the columns are placed.

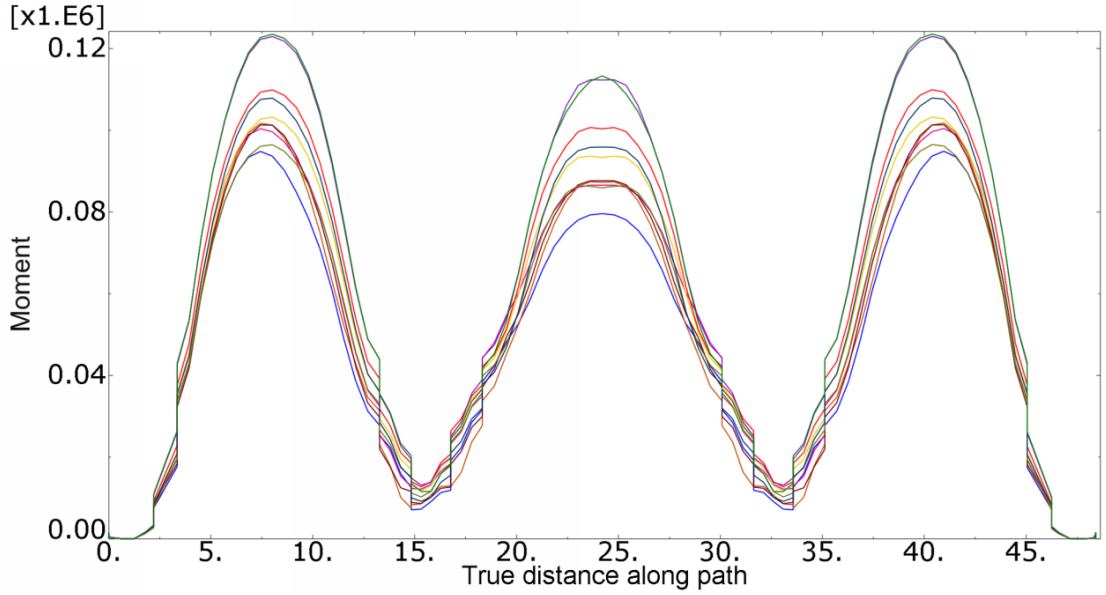

Figure E.19: Positive bending moment distribution over span length for slab bridge S0, load model HSLM (ballast density 1700 kg/m^3). The largest positive value is found at the midsection of each span.

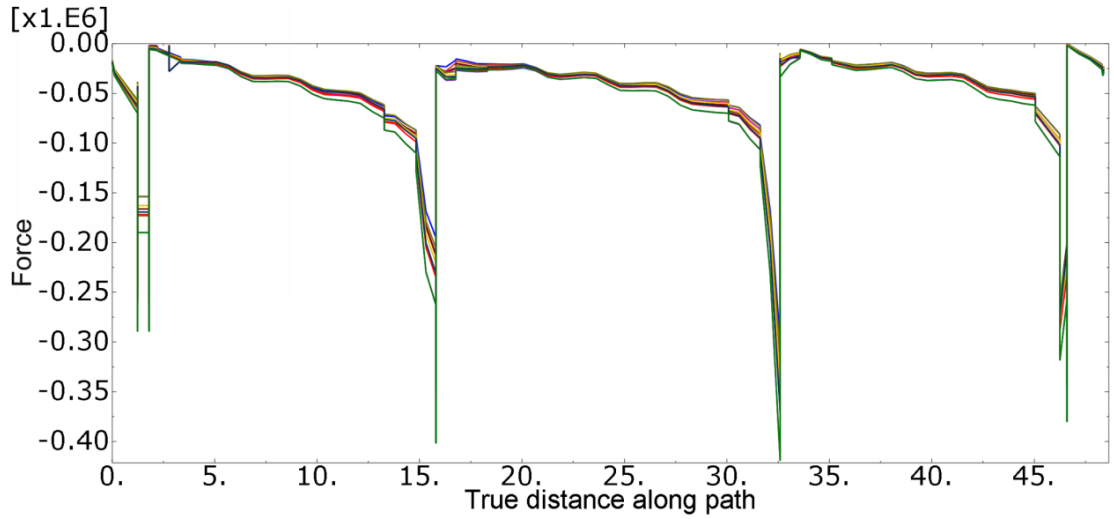

Figure E.20: Negative shear force distribution over the span length for the slab bridge S0, load model HSLM (ballast density 1700 kg/m^3). The largest negative value is retrieved at the section of the columns.

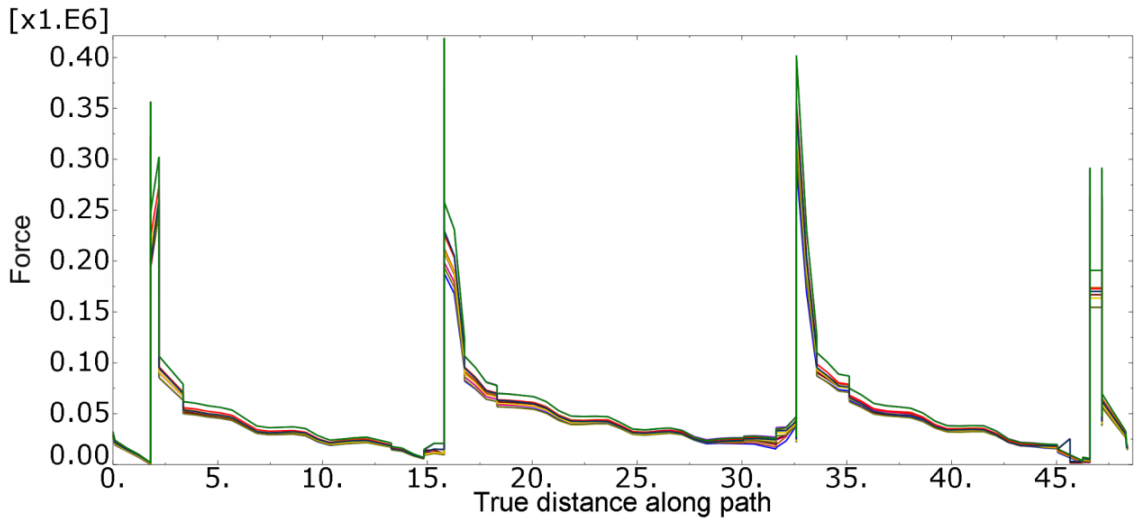

Figure E.21: Positive shear force distribution over the span length for the slab bridge S0, load model HSLM (ballast density 1700 kg/m^3). The largest positive value is retrieved at the section of the columns. Note that the positive shear force distribution is a mirror reflection of the negative shear force distribution.

Portal frame bridge S0 - LM71

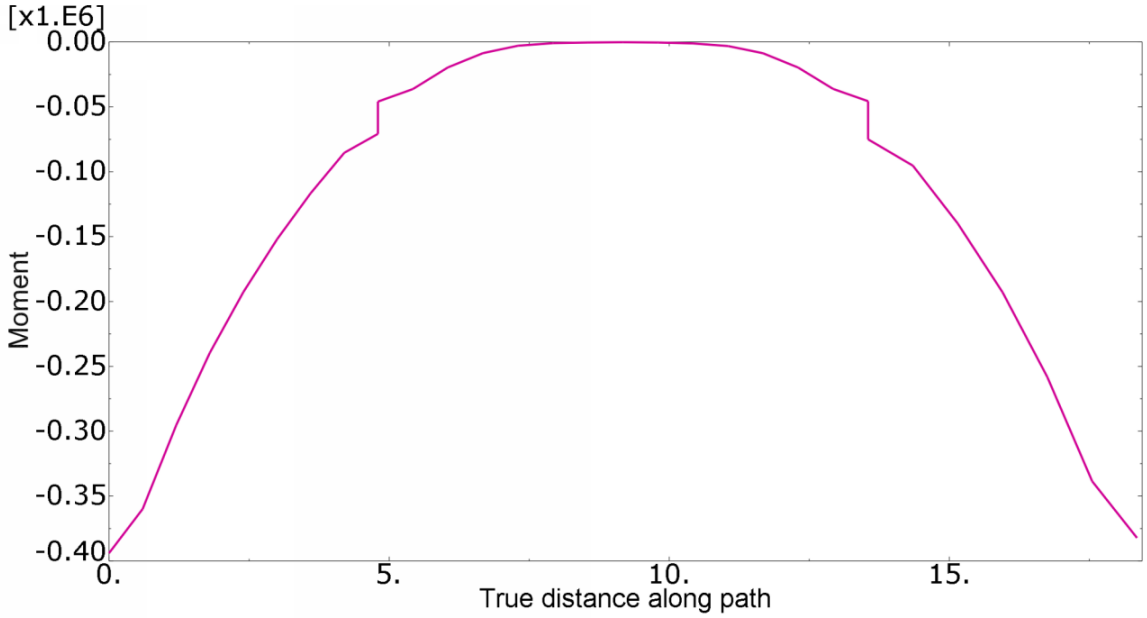

Figure E.22: Negative bending moment distribution over the span length for the portal frame bridge S0, load model LM71 (ballast density 1700 kg/m^3). The largest negative value is found at the section where the columns are placed.

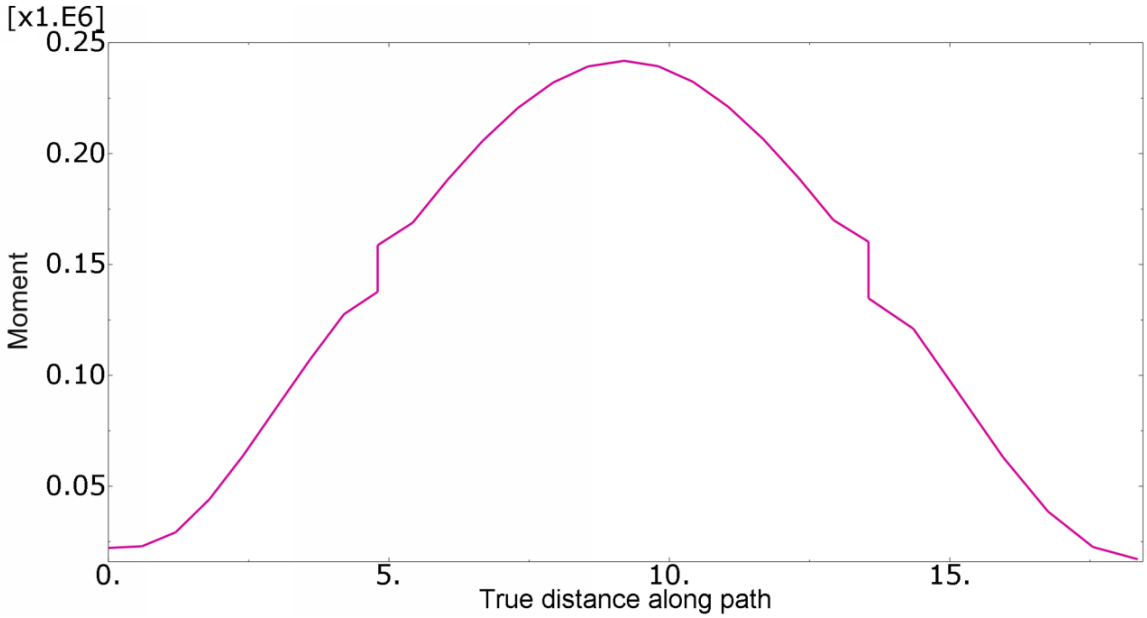

Figure E.23: Positive bending moment distribution over the span length for the portal frame bridge S0, load model LM71 (ballast density 1700 kg/m^3). The largest positive value is found at the midsection of each span.

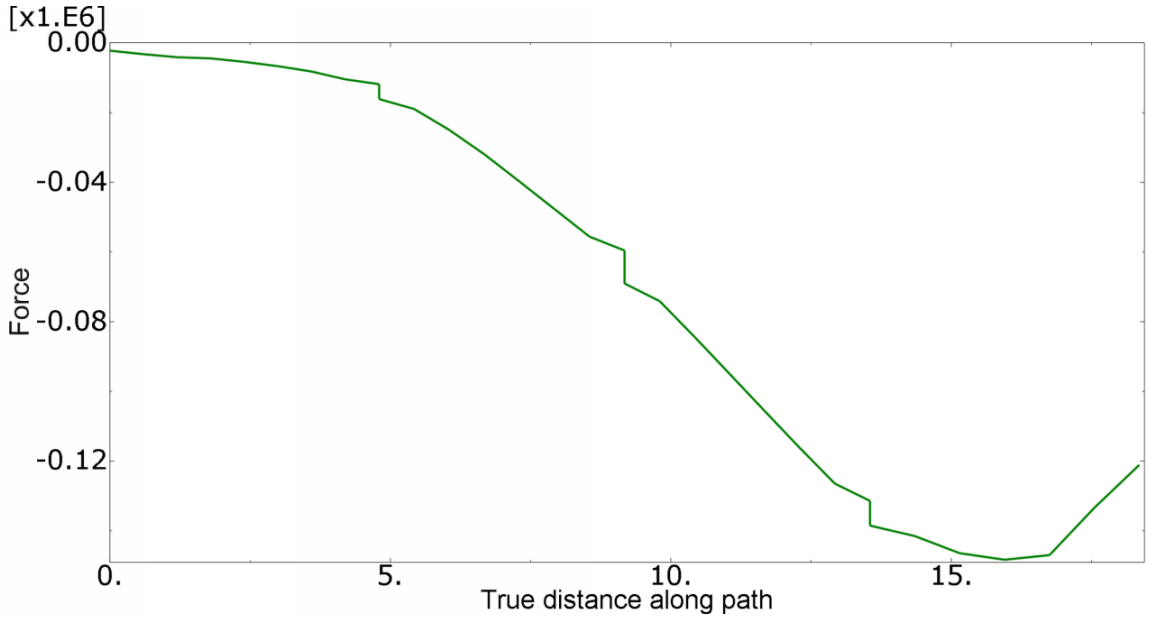

Figure E.24: Negative shear force distribution over the span length for the portal frame bridge S0, load model LM71 (ballast density 1700 kg/m^3. The largest negative value is retrieved at the support section.

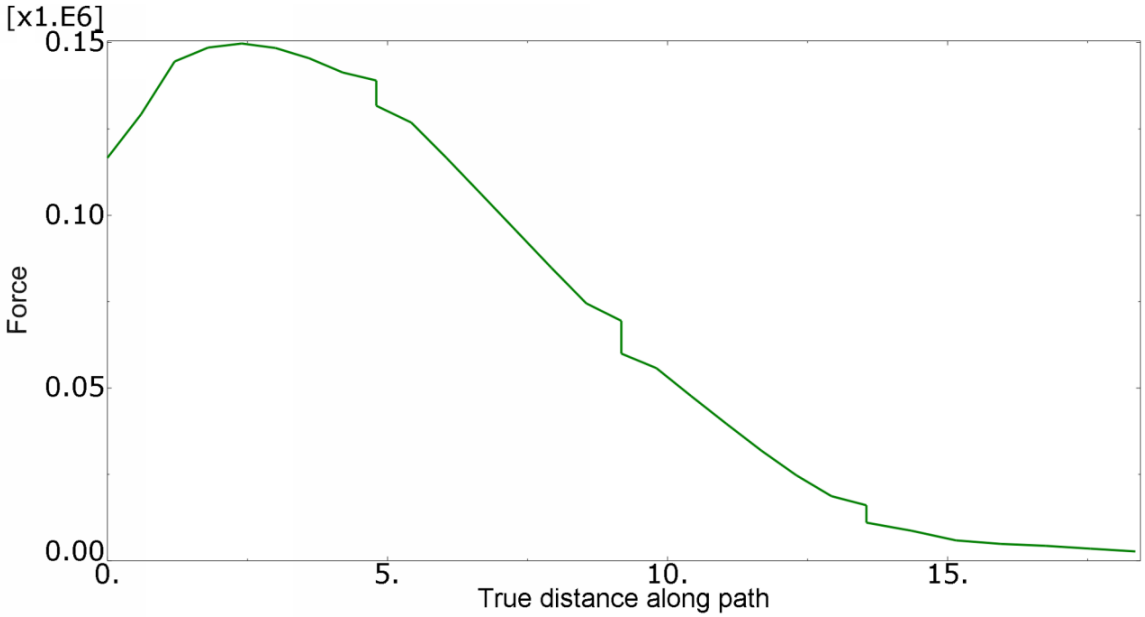

Figure E.25: Positive shear force distribution over the span length for the portal frame bridge S0, load model LM71 (ballast density 1700 kg/m^3). The largest positive value is retrieved at the support section. Note that the positive shear force distribution is a mirror reflection of the negative shear force distribution.

Portal frame bridge S0 - HSLM. The different lines in the graphs corresponds to the universal trains A1-A10

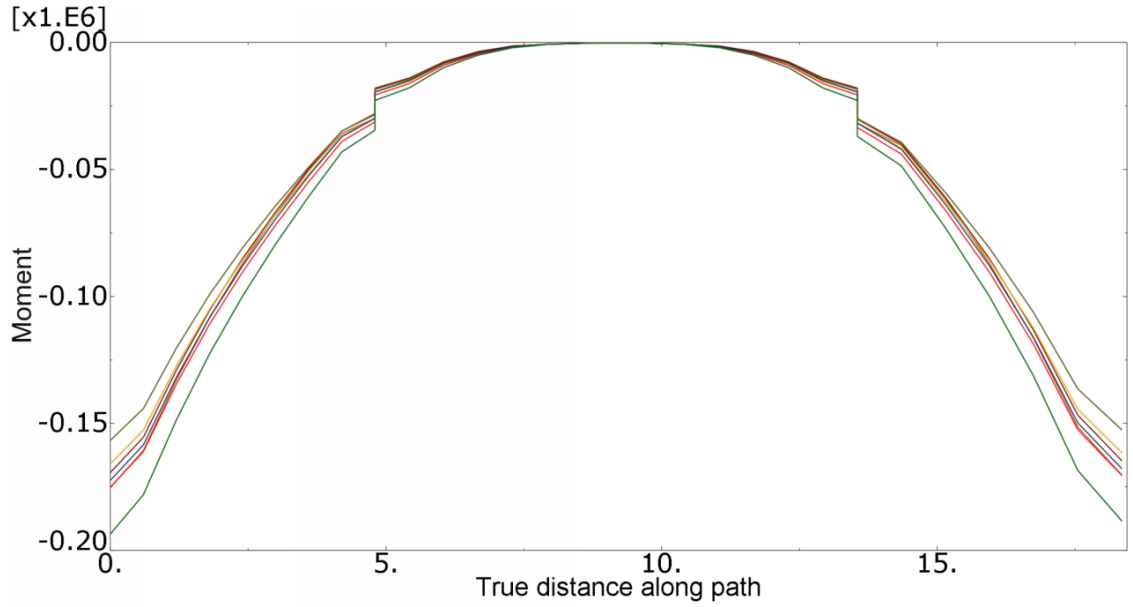

Figure E.26: Negative bending moment distribution over the span length for the portal frame bridge S0, load model HSLM (ballast density 1700 kg/m^3).The largest negative value is found at the corners of the frame.

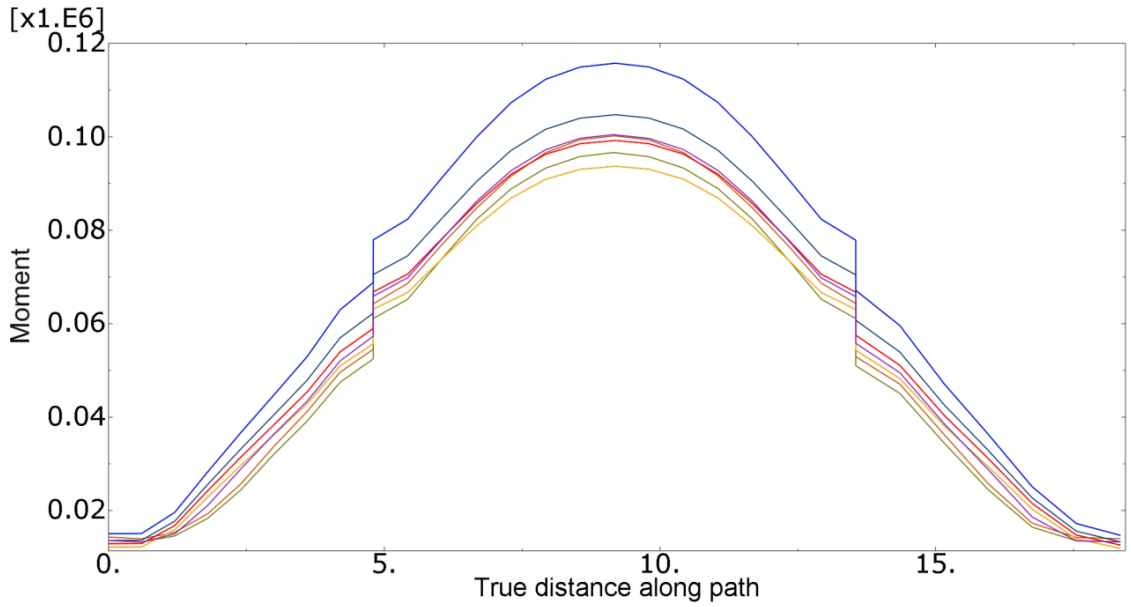

Figure E.27: Positive bending moment distribution over the span length for the portal frame bridge S0, load model HSLM (ballast density 1700 kg/m^3). The largest positive value is found at midspan.

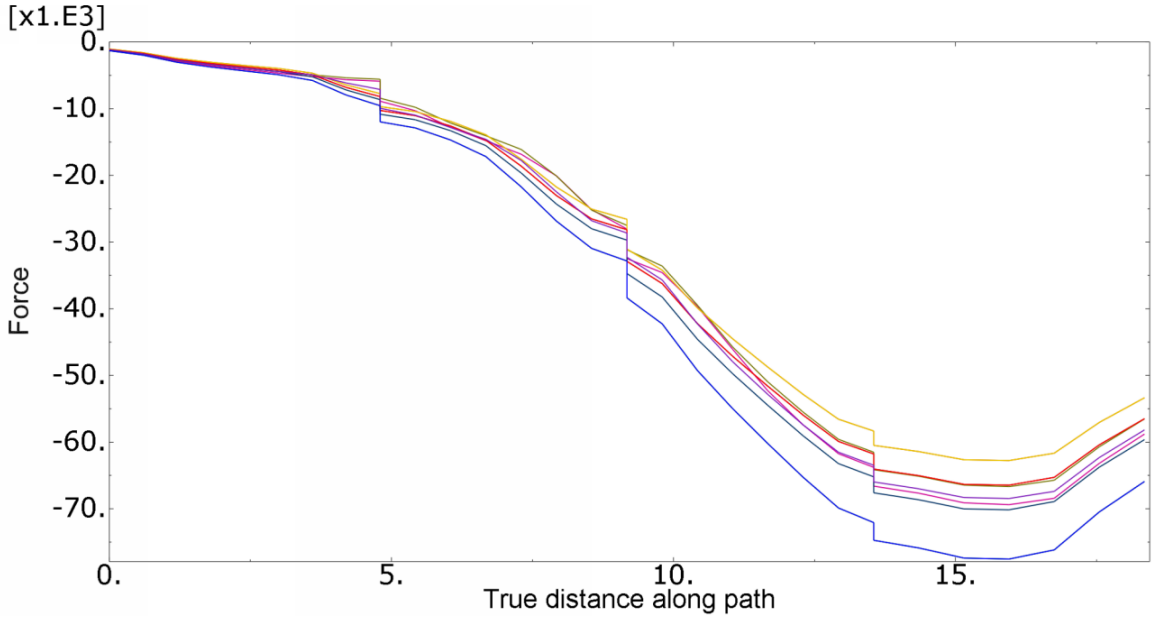

Figure E.28: Negative shear force distribution over the span length for the portal frame bridge S0, load model HSLM (ballast density 1700 kg/m^3). The largest negative value is found at the right corner of the frame.

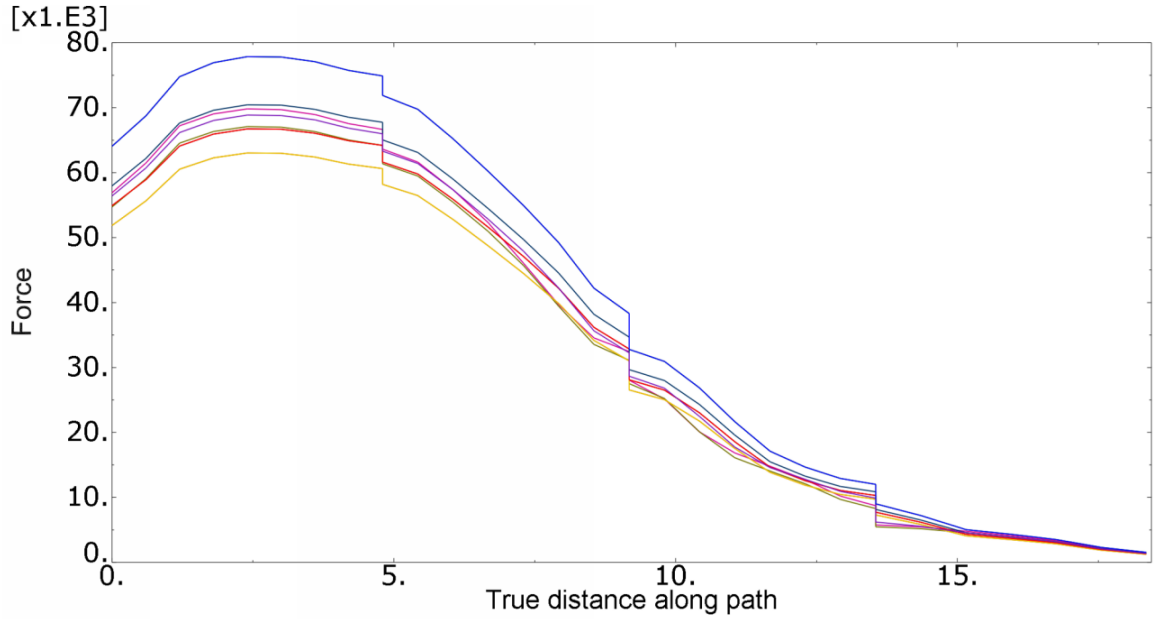

Figure E.29: Positive shear force distribution over the span length for the portal frame bridge S0, load model HSLM (ballast density 1700 kg/m^3). The largest positive value is found at the left corner of the frame. Note that the positive shear force distribution is a mirror reflection of the negative shear force distribution.

Appendix F - Loading frequencies

The loading frequencies of the design trains and those of the dominating eigenmodes are presented in Tables F.1 and F.2. A description of the different quantities displayed in the tables, are provided in the list below. The cells correspondent to a deviation of less than 10% are highlighted in green.

- The distance L and coach lengths D are defined in Section 3.1.
- The design speed, v_{design}, is the speed at which the maximum acceleration occurs.
- The loading frequency, $f_{loading}$, was determined from the design speed and the coach length.
- The frequency of the dominating modes, f_{modes}, are obtained from Tables A.1 and A.2 in Appendix D.
- The deviation describes how much the loading frequency differs from the frequency of the dominating modes.

Table F.1: Loading frequencies and dominating eigenmodes, ballast $\gamma = 1700\ kg/m^3$.

Name of bridge	L [m]	Closest D [m]	Speed interval	v_{design} [km/h]	$f_{loading}$ [Hz]	f_{modes} [Hz]	deviation [%]
S0	15.3	18	150-300	280	4.32	6.62	34
						8.36	48
			300-420	400	6.17	6.62	7
						8.36	26
S1	17.4	18	150-300	300	4.63	5.57	17
						9.10	49
			300-420	370	5.71	5.57	-3
						9.10	37
S2	18.8	19	150-300	240	3.51	4.84	27
						6.21	43
			300-420	340	4.97	4.84	-3
						7.90	37
S3	21.0	21	150-300	280	3.70	1.89	-95
						5.61	34
			300-420	370	4.89	4.82	-1
						5.61	13

Table F.2: Loading frequencies and dominating eigenmodes, ballast $\gamma = 2000\ kg/m^3$.

Name of bridge	L [m]	Closest D [m]	Speed interval	v_{design} [km/h]	$f_{loading}$ [Hz]	f_{modes} [Hz]	deviation [%]
S0	16.5	18	150-300	300	4.63	6.62	30
						8.36	45
			300-420	410	6.33	6.62	4
						8.36	24
S1	17.4	18	150-300	260	4.01	5.56	28
						9.10	56
			300-420	360	5.56	5.56	0
						9.10	39
S2	18.8	19	150-300	270	3.95	4.84	18
						6.21	36
			300-420	420	6.14	4.84	-27
						7.90	1
S3	21.0	21	150-300	270	3.57	1.89	-89
						5.61	36
			300-420	360	4.76	4.82	1
						5.61	15

Appendix G - Design Trains and Speeds

In the tables below, information about the design trains and critical speeds of the different bridges in each parameter study, is provided.

Slab bridge: Parametric study of span length

The different locations of the peak acceleration values are displayed in Figure G.1.

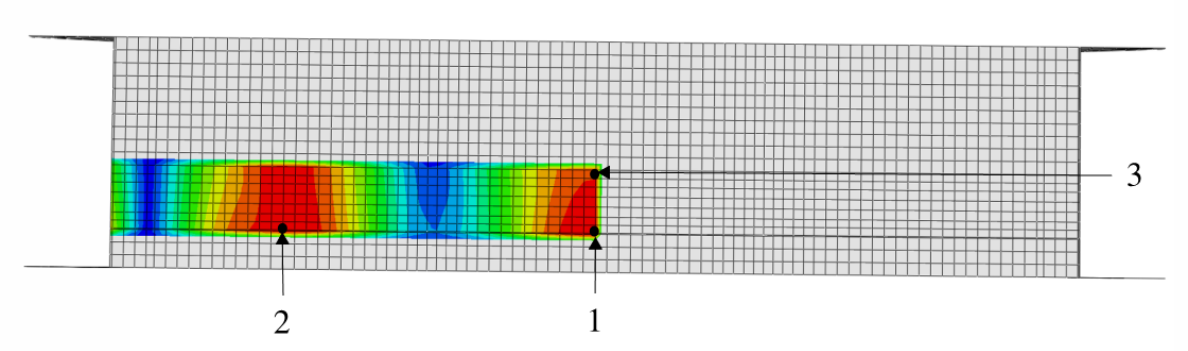

Figure G.1: Critical locations for the slab bridge.

Table G.1: Results from parametric study of span length for the slab bridges with ballast density 1700 kg/m^3. The cases where the acceleration exceeds the design requirements are highlighted in yellow.

Name of bridge	Speed interval	Acceleration $[m/s^2]$		HSLM Train	Design speed [km/h]	Location
S0	150-300	max	2.879	A6	280	i
		min	-2.961	A6	280	i
	300-420	max	4.454	A9	397.5	ii
		min	-5.388	A9	400	ii
S1	150-300	max	3.365	A9	267.5	i
		min	-3.260	A9	267.5	i
	300-420	max	4.446	A1	372.5	i
		min	-4.942	A1	372.5	i
S2	150-300	max	3.105	A10	242.5	i
		min	-3.178	A10	242.5	i
	300-420	max	4.924	A2	342.5	i
		min	-4.973	A2	342.5	i
S3	150-300	max	3.764	A10	280	ii
		min	-4.143	A10	280	ii
	300-420	max	8.817	A1	370	ii
		min	-8.860	A1	370	ii

Table G.2: Results from parametric study of span length for the slab bridges with ballast density 2000 kg/m^3. The cases where the acceleration exceeds the design requirements are highlighted in yellow.

Name of bridge	Speed interval	Acceleration $[m/s^2]$		HSLM Train	Design speed [km/h]	Location
S0	150-300	max	2.863	A3	300	ii
		min	-3.193	A3	300	ii
	300-420	max	4.448	A10	405	ii
		min	-5.264	A9	392.5	ii
S1	150-300	max	3.106	A9	262.5	i
		min	-3.040	A9	262.5	i
	300-420	max	4.230	A1	365	i
		min	-4.334	A1	362.5	i
S2	150-300	max	2.963	A7	267.5	iii
		min	-3.395	A7	267.5	ii
	300-420	max	4.855	A7	420	ii
		min	-4.778	A7	420	i
S3	150-300	max	3.535	A9	262.5	ii
		min	-3.871	A9	262.5	ii
	300-420	max	8.435	A1	362.5	ii
		min	-8.386	A1	360	ii

Slab bridge: Parametric study of thickness

Only the bridges that did not meet the design requirements in the parameter study of the span length are covered in the analysis of the thickness. The thicknesses necessary to keep the acceleration within allowable limits are highlighted in green.

Table G.3: Results from parametric study of thickness for the slab bridges with ballast density 1700 kg/m^3.

Speed interval 150-300 km/h						
Name of bridge	Thickness magnification	Acceleration $[m/s^2]$		HSLM Train	Design speed [km/h]	Location
S3	1.0	max	3.764	A10	280	ii
		min	-4.143	A10	280	ii
	1.1	max	3.309	A9	300	ii
		min	-3.550	A9	300	ii
	1.15	max	2.002	A8	300	ii
		min	-2.028	A8	300	ii

Speed interval 300-420 km/h						
Name of bridge	Thickness magnification	Acceleration $[m/s^2]$		HSLM Train	Design speed [km/h]	Location
S0	1.0	max	4.454	A9	397.5	ii
		min	-5.388	A9	400	ii
	1.05	max	4.263	A9	420	ii
		min	-4.872	A9	420	ii
	1.1	max	2.754	A8	420	ii
		min	-2.947	A3	340	ii
S1	1.0	max	4.446	A1	372.5	i
		min	-4.650	A1	372.5	i
	1.1	max	3.908	A1	410	i
		min	-3.77272	A1	420	i
	1.15	max	3.850	A1	420	i
		min	-3.946	A1	420	i
	1.2	max	2.642	A10	420	ii
		min	-2.605	A6	360	ii

Name of bridge	Thickness magnification	Acceleration $[m/s^2]$		HSLM Train	Design speed [km/h]	Location
S2	1.0	max	4.924	A2	342.5	i
		min	-4.973	A2	342.5	i
	1.1	max	4.408	A2	370	i
		min	-4.333	A2	370	iii
	1.2	max	4.206	A2	400	i
		min	-3.919	A2	400	i
	1.3	max	3.497	A1	410	i
		min	-3.500	A1	410	i
S3	1.0	max	8.817	A1	370	ii
		min	-8.860	A1	370	ii
	1.1	max	7.678	A1	410	ii
		min	-7.497	A1	410	ii
	1.15	max	5.240	A1	420	ii
		min	-5.580	A1	420	ii
	1.2	max	3.422	A3	420	ii
		min	-3.338	A3	420	ii

Table G.4: Results from parametric study of thickness for the slab bridges with ballast density 2000 kg/m^3.

Speed interval 150-300 km/h						
Name of bridge	Thickness magnification	Acceleration $[m/s^2]$		HSLM Train	Design speed [km/h]	Location
S3	1.0	max	3.535	A9	262.5	ii
		min	-3.871	A9	262.5	ii
	1.05	max	3.32	A10	290	ii
		min	-3.541	A10	290	ii
	1.1	max	3.022	A9	290	ii
		min	-3.050	A9	290	ii

Speed interval 300-420 km/h						
Name of bridge	Thickness magnification	Acceleration $[m/s^2]$		HSLM Train	Design speed [km/h]	Location
S0	1.0	max	4.448	A10	405	ii
		min	-5.264	A9	392.5	ii
	1.1	max	2.883	A9	420	ii
		min	-3.925	A8	420	ii
	1.15	max	2.252	A7	420	ii
		min	-2.386	A7	420	ii
S1	1.0	max	4.230	A1	365	i
		min	-4.334	A1	362.5	i
	1.1	max	3.700	A1	400	i
		min	-3.637	A1	400	i
	1.15	max	3.725	A1	410	i
		min	-3.791	A1	410	i
	1.2	max	3.110	A1	420	i
		min	-3.269	A10	420	i

Name of bridge	Thickness magnification	Acceleration $[m/s^2]$		HSLM Train	Design speed [km/h]	Location
S2	1.0	max	4.855	A7	420	ii
		min	-4.778	A7	420	i
	1.1	max	3.979	A2	360	i
		min	-4.175	A2	360	i
	1.2	max	3.904	A2	390	i
		min	-3.936	A2	390	i
	1.3	max	3.612	A2	420	i
		min	-3.548	A2	420	i
	1.35	max	3.394	A1	410	i
		min	-3.357	A1	410	i
S3	1.0	max	8.435	A1	362.5	ii
		min	-8.386	A1	360	ii
	1.1	max	6.993	A1	400	ii
		min	-7.021	A1	400	ii
	1.2	max	3.982	A3	420	i
		min	-3.811	A3	420	i
	1.25	max	2.92	A10	350	ii
		min	-2.967	A10	350	ii

Portal frame bridge: Parametric study of span length

The different locations of the peak acceleration values are displayed in Figure G.2.

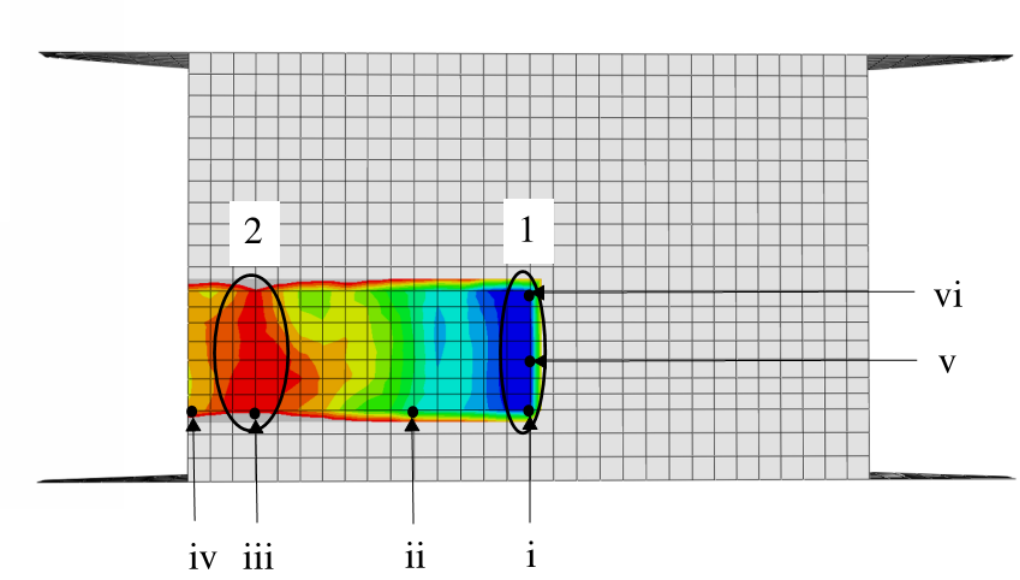

Figure G.2: Critical locations for the portal frame bridge, denoted by roman numbers. In Section 4, location i, v, and vi are denoted region 1 and location iii is denoted region 2.

Table G.5: Results from parametric study of span length for the portal frame bridges with ballast density 1700 kg/m^3. The cases where the acceleration exceeds the design requirements are highlighted in yellow.

Name of bridge	Speed interval	Acceleration $[m/s^2]$		HSLM Train	Design speed [km/h]	Location
S0	150-300	max	4.115	A10	242.5	iii
		min	-2.817	A10	242.5	i
	300-420	max	4.712	A10	420	v
		min	-4.814	A10	417.5	v
S1	150-300	max	2.095	A10	227.5	iii
		min	-2.143	A10	235	i
	300-420	max	2.969	A10	357.5	i
		min	-2.947	A10	357.5	i
S2	150-300	max	1.773	A7	280	iii
		min	-1.670	A3	225	i
	300-420	max	8.276	A1	412.5	i
		min	-8.997	A1	407.5	i
S3	150-300	max	1.510	A7	260	iii
		min	-1.719	A9	280	ii
	300-420	max	9.778	A4	415	i
		min	-8.707	A4	417.5	vi
S4	150-300	max	2.339	A1	300	i
		min	-2.339	A1	300	i
	300-420	max	10.040	A7	417.5	i
		min	-10.040	A7	415	i

Table G.6: Results from parametric study of span length for the portal frame bridges with ballast density 2000 kg/m^3. The cases where the acceleration exceeds the design requirements are highlighted in yellow.

Name of bridge	Speed interval	Acceleration $[m/s^2]$		HSLM Train	Design speed [km/h]	Location
S0	150-300	max	3.919	A10	240	iii
		min	-2.792	A10	237.5	ii
	300-420	max	4.540	A10	407.5	i
		min	-4.735	A10	407.5	vi
S1	150-300	max	1.453	A10	227.5	i
		min	-1.653	A10	230	i
	300-420	max	2.332	A1	420	i
		min	-2.892	A1	420	i
S2	150-300	max	1.835	A10	300	i
		min	-1.607	A3	220	i
	300-420	max	8.949	A2	420	i
		min	-9.466	A2	420	i
S3	150-300	max	1.463	A1	287.5	ii
		min	-1.627	A1	290	ii
	300-420	max	9.320	A4	405	i
		min	-8.282	A4	407.5	vi
S4	150-300	max	3.420	A1	300	i
		min	-3.501	A1	300	i
	300-420	max	9.626	A8	420	i
		min	-9.656	A7	405	i

Portal frame bridge: Parametric study of thickness

Only the bridges that did not meet the design requirements in the parametric study of the span length are covered in the analysis of the thickness. The thicknesses necessary to keep the acceleration within allowable limits are highlighted in green.

Table G.7: Results from parametric study of thickness for the portal frame bridges with ballast density 1700 kg/m^3.

Speed interval 150-300 km/h						
Name of bridge	Thickness magnification	Acceleration $[m/s^2]$		HSLM Train	Design speed [km/h]	Location
S0	1.0	max	4.115	A10	242.5	iii
		min	-2.817	A10	242.5	i
	1.05	max	3.446	A10	240	iii
		min	-2.333	A10	240	ii

Speed interval 300-420 km/h						
Name of bridge	Thickness magnification	Acceleration $[m/s^2]$		HSLM Train	Design speed [km/h]	Location
S0	1.0	max	4.712	A10	420	v
		min	-4.814	A10	417.5	v
	1.05	max	3.635	A9	420	i
		min	-3.443	A9	420	v
	1.1	max	2.998	A9	330	iv
		min	-2.547	A9	350	iv
S2	1.0	max	8.276	A1	412.5	i
		min	-8.997	A1	407.5	i
	1.1	max	3.548	A1	420	vi
		min	-4.594	A1	420	i
	1.15	max	2.009	A2	420	i
		min	-3.127	A9	330	iii

Name of bridge	Thickness magnification	Acceleration $[m/s^2]$		HSLM Train	Design speed [km/h]	Location
S3	1.0	max	9.778	A4	415	i
		min	-8.707	A4	417.5	vi
	1.1	max	7.579	A3	420	i
		min	-7.099	A4	420	i
	1.2	max	5.049	A1	410	i
		min	-4.858	A1	410	i
	1.25	max	5.069	A1	410	i
		min	-4.887	A1	410	i
	1.3	max	2.871	A1	420	i
		min	-3.001	A1	420	i
S4	1.0	max	10.040	A7	417.5	i
		min	-10.040	A7	415	i
	1.1	max	7.439	A5	410	i
		min	-7.057	A5	410	i
	1.2	max	6.317	A4	420	i
		min	-6.132	A4	420	i
	1.3	max	5.445	A3	420	i
		min	-5.006	A3	420	i
	1.4	max	3.929	A2	420	i
		min	-3.612	A2	420	i
	1.45	max	2.766	A1	410	i
		min	-2.805	A1	410	i

Table G.8: Results from parametric study of thickness for the portal frame bridges with ballast density 2000 kg/m^3.

Speed interval 150-300 km/h						
Name of bridge	Thickness magnification	Acceleration $[m/s^2]$		HSLM Train	Design speed [km/h]	Location
S0	1.0	max	3.919	A10	240	iii
		min	-2.792	A10	237.5	ii
	1.05	max	3.109	A10	230	iii
		min	-2.528	A10	230	i

Speed interval 300-420 km/h						
Name of bridge	Thickness magnification	Acceleration $[m/s^2]$		HSLM Train	Design speed [km/h]	Location
S0	1.0	max	4.540	A10	407.5	i
		min	-4.735	A10	407.5	vi
	1.05	max	3.896	A10	420	i
		min	-3.802	A10	420	v
	1.1	max	3.372	A9	420	i
		min	-3.066	A9	420	i
S2	1.0	max	8.946	A2	420	i
		min	-9.466	A2	420	i
	1.1	max	5.420	A1	420	vi
		min	-6.719	A1	420	i
	1.15	max	2.821	A1	420	i
		min	-3.584	A1	420	i
	1.2	max	1.835	A1	420	vi
		min	-2.350	A1	420	i

Name of bridge	Thickness magnification	Acceleration $[m/s^2]$		HSLM Train	Design speed [km/h]	Location
S3	1.0	max	9.320	A4	405	i
		min	-8.282	A4	407.5	vi
	1.1	max	7.170	A3	420	i
		min	-6.784	A3	410	i
	1.2	max	6.168	A2	420	i
		min	-6.098	A2	420	i
	1.3	max	4.357	A1	420	i
		min	-4.153	A1	420	i
	1.35	max	2.267	A1	420	i
		min	-2.45	A1	420	i
S4	1.0	max	9.626	A8	420	i
		min	-9.656	A7	405	i
	1.1	max	7.933	A6	420	i
		min	-7.407	A6	420	i
	1.2	max	6.036	A4	410	i
		min	-5.842	A4	420	i
	1.3	max	4.872	A3	410	i
		min	-4.702	A3	410	i
	1.4	max	3.905	A2	420	i
		min	-3.940	A2	420	i
	1.45	max	3.281	A2	420	i
		min	-3.148	A2	420	i